UNIVERSITY OF CALIFORNIA,

IRVINE

Tissue Engineering and Biosensing, Towards Cure and Control of Diabetes

DISSERTATION

Submitted in partial satisfaction of the requirements
for the degree of

DOCTOR OF PHILOSOPHY

in Materials Science and Engineering

by

Avid Najdahmadi

Dissertation Committee
Professor Elliot L. Botvinick, Chair
Associate Professor Wendy Liu,
Professor Bernard Choi

2018

DEDICATION

To my mother, who cherished my first steps and taught me how to walk

To my father, who trained me to think and enjoy the road

To my sister, who travels the path with me

TABLE OF CONTENTS

LIST OF FIGURES

LIST OF TABLES

ACKNOWLEDGMENTS

Sentences, paragraphs or pages of words cannot truly express the level of my gratitude for my mentor Professor Elliot Botvinick. Over the past few years he provided advice and academic training, the likes of which I have never seen. He encouraged me to explore, think and implement and allowed me to work on the most intriguing projects. Joining Elliot's laboratory and finding a second family so far away from home is a priceless gift that I will always cherish. Thank you Elliot.

I would like to also thank my committee members Professors Wendy Liu and Bernard Choi, for their time as well as being examples of inspirational scientists. Additionally, a sincere thank you to Professor Jonathan Lakey for providing great help in different collaborative studies.

A very special thanks to Dr. John Weidling for his excellent guidance and support and for teaching me how to keep calm, think and solve. Thanks for allowing me to brainstorm with you for hours at a time. I also would like thank Dr. Samir Shreim and Dr. Sean White for all their intelligent feedback and teachings and for being true inspirations. I would like to extend my thanks to Dr. Bhupinder Shergill for all the helpful discussions on my research projects. I thank Rachel Gurlin for all her critical feedback and also her work on histology, immunostaining and vessel count of PDMS devices. In addition a big thank you to all of my BEAMs lab friends who made the journey exceptional and fun.

I would like to thank Professor Paul de Vos and Dr. Alexandra M. Smink for their help and their work on the collaborative study of H_2S administration and vessel morphology of PDLLCL devices. A special thank you to Tomas Walker and Justin Macklin at Dexom, for providing me with an opportunity to wear a continues glucose monitor for a ten day trial. I also thank my dear friend Dr. Kenta Ohtaki for helping me with scanning electron microscopy.

I thank Materials Research Society and SPIE for giving permission to use copyright materials in chapter 2. Some contents of Chapter 3 is under review at journal of Cell Transplantation, aimed for open access publication. Financial support for the different projects in this dissertation has been provided by Juvenile Diabetes Research Foundation (JDRF), Air Force Office of Scientific Research/DoD (United States Department of Defense), National Institute of Health (NIH) and Leona M. and Harry B. Helmsley Charitable Trust.

CURRICULUM VITAE

Education:

Ph.D. in Materials Sciences and Engineering, University of California, Irvine 2015-12/2018

Advisor: Professor Elliot Bovinick

M.S. in Materials Sciences and Engineering, University of California, Irvine 2013-2014

Advisor: Professor Elliot Bovinick

B.Sc. in Metallurgy and Materials Science, University of Tehran 2008-2013

Advisor: Professor Abbas Zareri-Hanzaki

Notable Awards & Achievements:

- UCI School of Medicine Business Plan Competition Award: $10,000. 2016

Competition sponsored by the *UC Irvine Paul Merage School of Business.*
Role: Student Entrepreneur and Material Scientist.

Memberships:

- ADA(American Diabetes Association) 2018
- BMES (Biomedical Engineering Society) 2015-2018
- SFB (Society for Biomaterials) 2017-2018
- SPIE (Society of Photo-Optical Instrumentation Engineers) 2017-2018
- MRS (Materials Research Society) 2018
- Materials Advantage Program (ASM ,TMS, AIST, ACerS) 2018

Work Experience

- Graduate Research Assistant, University of California at Irvine 2013-2018
  Bio-Engineering of Advanced Mechanical Systems (BEAMS) Laboratory
- Graduate Teaching Assistant, University of California at Irvine
  Design Failure Investigation (CBEMS175), Department of Materials Science and Engineering 2015
- Undergraduate Research Assistant, University of Tehran 2011-2013
  The Hot Deformation and Thermo-Mechanical Processing Laboratory (HDTPL) 2012
- Summer Intern, Razi Metallurgical Research Center 2011
- Summer Intern, North Melt Industries Company

Research Experiences:

- Developing a heat treatment strategy to increase fatigue life of biocompatible titanium alloy (TNTZ)

  B.Sc. Research

  ➢ Applying different heat treatment process to increase mechanical strength of TNTZ.

  ➢ Structural analysis of different phase formation after heat treatment using XRD and microscopic imaging.

  ➢ Mechanical shear punch and hardness test to measure the changes in mechanical properties.

  ➢ Concluding that liquid nitrogen quenching provides a lower young's modulus and higher mechanical strength.

- Advancing pancreatic islet alginate encapsulation, a method to reverse type 1 diabetes:

  M.S. Research

  ➢ Leading a comprehensive study of alginate crosslinking process and modifications to characterize changes in polymerization time and temperature.

  ➢ Study of physiological effects on changes in alginate volume and mechanical stability and permeability.

  ➢ Characterization of alginate after *in vivo* implantation in CD1 mice.

  ➢ Study of alginate degradation after incubation in a physiological environment.

  ➢ Calculating polymer diffusion constant in alginate through controlled diffusion experiments using fluorescent dextran dyes.

  ➢ Designing and building a novel, low-cost pancreatic islet alginate micro encapsulator for laboratory use.

  ➢ *Project funding provided by:*

  ❖ Juvenile Diabetes Research Foundation (JDRF*),*

- Developing novel pre-vascularized medical device for subcutaneous pancreatic islet transplantation, a method to reverse type 1 diabetes. (Bioartificial pancreas):

  Ph.D. Research

  ➢ Developing a method to reshape the pancreatic islets to decrease the diffusional distance of oxygen and nutrients, for preventing hypoxia and subsequent cell death after implantation.

  ➢ Developing new designs for better vascularization of the subcutaneous medical devices, through introducing new geometries and surface features.

  ➢ Advancing the device development through biomaterials selection to improve transport kinetic and ease of islet replacement while providing immunoisolation

  ➢ Fabricating novel phosphorescence biocompatible oxygen sensitive implants for measuring partial pressure of oxygen as well as level of vascularization into devices made of different biomaterials (PDMS and PDLLCL).

  ➢ Developing phase shift optical sensors for detecting intensity and lifetime of the developed photonic implants for non-invasive study of vascularization into the devices.

  ➢ Preforming animal study to track the vascularization of PDMS and PDLLCL devices in more than 50 non-diabetic nude CD1mice. The length of the study is 63 days.

  Project funding provided by:

  ❖ Juvenile Diabetes Research Foundation (JDRF),

- Development of continues glucose lactate monitor for increasing survival in clinically ill patients

Ph.D. Research

- ➢ Changing the enzyme immobilization method to increase the activity of the enzyme
- ➢ Creating a proprietary material for enzyme immobilization and photonic measurements of tissue lactate level.
- ➢ Developing new materials to provide high luminescence signal for detection of lactate.
- ➢ Developing a proprietary new methods for device fabrication to maintain robustness during implantation while maintaining manufacturability.
- ➢ Developing optical phase shift sensor to study lactate level with reduced sampling rates.

Project funding provided by:

- ❖ Air Force Office of Scientific Research/DoD (United States Department of Defense)
- ❖ NIH

- Developing novel multi analyte continues glucose and lactate monitor for better glycemic control in diabetic patients (Artificial Pancreas):

Ph.D. Research

- ➢ Developing new formulations for glucose and lactate sensing.
- ➢ Increasing homogeneity of mixtures for a repeatable manufacturing.
- ➢ Increasing shelf life (13 months so far) and operational life of the multi analyte sensors by material development
- ➢ Innovating a new method to minimize thickness of continuous glucose & lactate sensors (thickness <30 μm)
- ➢ Building automated systems to calibrate 16 glucose & lactate sensors simultaneously.

Project funding provided by:

- ❖ Juvenile Diabetes Research Foundation
- ❖ Leona M. and Harry B. Helmsley Charitable Trust

- Inventing the first colorimetric user-friendly lactose strip

Ph.D. Research

- ➢ Creating an engineered strip capable of housing lactose detecting reagents and color changing dye.
- ➢ Successful macromolecule immobilization into the engineered strips.
- ➢ Inventing an proprietary method to differentiate between lactose and other sugars for improved reliability.
- ➢ Applying a mechanical design for fluid transfer through the lactose strip.
- ➢ Advancing the detection system by having the color change occur within a measurable length, the length can correlate with food lactose level.

Project funding provided by

- ❖ Regents for the University of California

Experiences, Technical Skills & Software

- Knowledge in R&D, biocompatibility, ISO10993, FDA regulations (CFR), Quality System Regulation (QSR), Design of Experiments (DOE), Design for Manufacturing (DFM), and Assembly (DFA)
- Material Science: SEM (scanning electron microscopy), Metal Fabrication (casting, welding, machining), Mechanical Testing (MTS), Plasma Treating, Laser Cutting, Sputter Coating, 3D Printing, Material Characterization, Polymer Processing, Diffusion Simulation, Image Analysis, Fracture Mechanics, Failure Analysis

- Biomedical Engineering: Confocal Microscopy, Fluorescent/Phosphorescent microscopy Spectroscopy, Cell Encapsulation/Immunoisolation, Enzyme Immobilization, Animal Anesthesia, *in vivo* Implantation, ELISA, Cell Viability Assays
- Circuit Board (PCB) Design & Assembly, Signal Processing, Data Analysis, Statistical Analysis, System Automation
- Software: SolidWorks, Matlab, LabVIEW, NI Multisim, ImageJ, Microsoft Office

Presentations:

- Najdahmadi, A., Lakey, J.R.T., Botvinick, E." Structural characteristics and diffusion coefficient of alginate hydrogels used for cell based drug delivery", MRS spring meeting, Phoenix, April 2018.
- Najdahmadi, A., Gurlin, R.E., Weidling, J. White, S., Shergill, B., Lakey, J.R.T, Botvinick, E. "Non invasive study of oxygen tension and vascularization in subcutaneously implanted medical devices", SPIE photonic west, San Fransisco, January 2018.
- Najdahmadi, A., Lakey, J.R.T., Botvinick, E." "Diffusion coefficient of alginate microcapsules used in pancreatic islet transplantation, a method to cure type 1 diabetes", ", SPIE photonic west, San Fransisco, January 2018.
- Najdahmadi, A., Weidling, J., White, S., Ortenzio, F., Radom-Aizik, S., Botvinick, E. "Novel Continuous Lactate Monitor Passes Pilot Clinical Study: One Step Closer to Field-Deployable Early Warnings of Shock and Enablement of Lactate-Guided Therapy", Military Health System Research Symposium, Orlando, August 2017.
- Najdahmadi, A. Gurlin, R., Shergill. B., Sher Biomedical, Fearless in the Fight for Better Diabetes Treatment, September, 2016
- Najdahmadi, A., Krishnan.R, Kummerfeld.C, Lakey. J.R.T., Botvinick.E "Evaluation of alginate structure for superior encapsulation of pancreatic islets" BMES Annual Meeting, Tampa, 2015.
- Najdahmadi, A., Zarei-Hanzaki,A., Farghadani,E. "Microstructural evaluation and mechanical properties of solution treated biomedical TNTZ alloy", 1622-IMES-CONGR-FULL ,Tehran , 2012.

Journal Publications:

- Najdahmadi, A., Smink, A.M., de Vos, P., Lakey, J. R., Elliot Botvinick, E. Non-invasive optical monitoring of oxygen tension and vasculature growth in subcutaneous cellular therapy medical devices. Cell Transplantation, [Under Review]
- Smink A.M. , Najdahmadi, A , Alexander, M. , Krikke, R.R., Li, S., Goor, H. , Hillebrands, J., Botvinick, E., R.T. Lakey., de Vos, P. Hydrogen sulfide improves innervation of subcutaneous polymeric scaffolds applicable for pancreatic islet transplantation. Tissue Engineering and Regenerative Medicine, [Under Review]
- Najdahmadi, A., Lakey, J. R., & Botvinick, E. (2018). Structural Characteristics and Diffusion Coefficient of Alginate Hydrogels Used for Cell Based Drug Delivery. *MRS Advances*, 1-10.
- Najdahmadi, A., Lakey, J. R., & Botvinick, E. (2018, February). Diffusion coefficient of alginate microcapsules used in pancreatic islet transplantation, a method to cure type 1 diabetes. In *Nanoscale Imaging, Sensing, and Actuation for Biomedical Applications XV* (Vol. 10506, p. 105061D). International Society for Optics and Photonics.

- Najdahmadi, A., Zarei-Hanzaki, A., & Farghadani, E. (2014). Mechanical properties enhancement in Ti–29Nb–13Ta–4.6 Zr alloy via heat treatment with no detrimental effect on its biocompatibility. *Materials & Design (1980-2015)*, *54*, 786-791.

Intellectual property:

- A.Najdahmadi, J.Weidling, E.Botvinick "Composite Matrix for Photonic Analyte Biosensors", US Application No. 62719529, *Patent Pending*
- E.Botvinick, A.Najdahmadi, C.Duhay, "Lactose-Detecting Strip", Record of Invention is filed at UCI Applied innovation (Case 2018-069-1)

ABSTRACT OF THE DISSERTATION

Tissue Engineering and Biosensing, Towards Cure and Control of Diabetes

By

Avid Najdahmadi

Doctor of Philosophy in Materials Science and Engineering

University of California, Irvine, 2018

Professor Elliot L. Botvinick, Chair

In Type 1 Diabetes, insulin producing cells are destroyed by the immune system, resulting in unchecked glycemic conditions. Different approaches including tissue engineering and continuous analyte monitoring hold promise in providing insulin independence and glycemic control. Tissue engineering aims to transplant and protect pancreatic islets, cells responsible for secretion of insulin. One strategy is to encapsulate the islets inside alginate hydrogels. The encapsulant provides passage to glucose, nutrients and the secreted insulin, while blocking the passage of antibodies. In this study, confocal microscopy is used to study diffusional characteristics of alginate. This approach can quantitatively analyze the structural changes after exposure to physiological conditions. Using this strategy can potentially tune the structure prior to implantation to account for the upcoming *in vivo* changes. Another approach is to place the islets inside subcutaneous medical devices. Such devices can provide protection to the cells, however due to hypoxic conditions transplanted cells can lose function. In this study vascularization of different types of polymer devices is studied. Oxygen sensitive tubes were fabricated and placed inside devices prior to subcutaneous implantation in nude mice. Using a non-invasive optical technology oxygen partial pressure within the devices is monitored. This

technology aims to create a quantitative metric to assess the state of vascularization and readiness of devices for cell insertion. Another promising technology for diabetes management and achievement of tight glycemic control is continuous analyte monitoring. In this technique, different analytes such as glucose and lactate can be continuously measured. The data collected can be used to create a mathematical algorithm that can predict upcoming glycemic changes and in conjunction with an insulin pump can automatically administer insulin. In this work, a new composite material is invented that can accommodate necessary components to detect and report the changes of analyte levels in physiological conditions. This material can be used to create different types of continuous biosensors. Importantly this composite material shows success in preserving sensitivity and activity of biosensors for long periods of storage, it shows fast responses to changes of analyte concentrations and is manufacturable in very small geometries aimed for painless insertion.

CHAPTER 1: Introduction

1.1 Approaches to provide insulin independence and glycemic control

Diabetes is one of the most prevailing diseases in the world [1]. The number of people diagnosed with diabetes has nearly quadrupled in the past few decades [2]. World Health Organization estimates that diabetes is the seventh cause of death [3]. Type 1 diabetes (T1D) is caused by autoimmune destruction of insulin producing β cells [4, 5]. These cells synthesize and regulate insulin, which is the most important hormone involved in physiological regulation of blood glucose. The current method of treatment is daily injection of insulin, which is not a cure, the glycemic control achieved is imperfect and can cause inevitable secondary conditions and deteriorate the body especially, eyes, kidney, heart and blood vessels [6–8]. Finding an alternative solution to eliminate daily injections and provide perfect glycemic control has been a challenge over the past few decades. In the next few chapters, three promising approaches that can potentially result in insulin independence and better glycemic control in T1D are discussed and explored.

1.1.1 Tissue engineering and cell encapsulation

One promising method to provide insulin to type 1 diabetic patients is transplantation of isolated pancreatic islets, a method introduced in 2000 and named Edmonton protocol [9]. Although this strategy showed short term results in providing insulin independence to patients, its long term success was limited [10]. One main limitation of such approach is the limited supply of donor cells which requires xenotransplantation, ultimately resulting in destruction of the transplanted

islet cells by the recipient's immune system, and therefore necessitating a lifelong of immunosuppression drugs therapy [10]. Different techniques have been used to address this problem. In one strategy, the pancreatic islets are enclosed in microcapsules made of a semipermeable membrane, usually made of hydrogels that can provide immunoprotection while allowing the influx of the nutrients and oxygen to the cell for its survival [11-14]. This method obviates the need for immunosuppressive therapy and pretreatment or culturing of the islets prior to encapsulation [15]. Most techniques use modification of the procedure originated by Lim and Sun during which the encapsulant is suspended in an aqueous solution and extruded by an air jet syringe pump droplet generator into an ionic solution to initiate the gelation [16]. The inability to adjust and maintain microcapsule characteristics such as mechanical strength, size and stability has limited the success of this system [17]. Another important factor that needs characterization is the diffusivity of hydrogel encapsulants, as they are required to provide immunoisolation by blocking the passage of antibodies while simultaneously allowing necessary glucose and nutrients as well as secreted hormones such as insulin to pass. Hydrogel microcapsules have shown to undergo structural changes after exposure to physiological conditions. Therefore it is imperative to study these change *in vitro,* in order to predict the final characteristics of the material *in vivo.* In *Chapter II* the aforementioned changes are studied through exploring the fundamental characteristics of alginate, which is the most commonly used hydrogel for pancreatic islet encapsulation.

1.1.2 Tissue engineering and subcutaneous medical devices

A more advanced alternative to islet encapsulation is to create medical devices that that can act as bioartificial organs [18, 19]. In the case of diabetes, evidence suggests that it is unnecessary to

create the whole organs and only transplantation of pancreatic islets can result in restoration of the endocrine function [9]. In this strategy, devices are engineered to house the pancreatic islets. Such devices need to maintain the functionality of the pancreatic islets through providing safe passage to glucose, nutrients and oxygen as well as secreted insulin. A variety of polymer devices as well as implantation sites have been tested for this approach [9, 20-25]. Literature suggests that the subcutaneous space can be advantageous in this strategy because of ease of access and less invasive surgical procedure [26, 27]. However due to lack of oxygen under the skin hypoxia can occur, resulting in apoptosis and necrosis and ultimately comprising cells functionality [28]. Therefore vascularization of such devices is extremely important, ensuring a supply of oxygen and nutrients at the close proximity of the transplanted cells. Such vascularization can be simulated through use of one or multiple strategies including, use of microporous structures [29], inclusion of angiogenic factors [30], or engineered device that can be implanted for prevascularization prior to transplantation of cells [31]. The strategy to insert the pancreatic cells into already implanted and prevascularized devices can be very advantages, however its success relies on monitoring of the vessel growth and time of cellular tissue insertion. In *Chapter III* a developed non-invasive optical technology to monitor the state of oxygenation and vasculature growth inside implanted medical devices is introduced. In this technology the allocated space for housing pancreatic islets within the devices is initially filled with developed retrievable oxygen sensitive implants that can provide information on vascularization and then be removed prior to cell insertion. This strategy aims to provide a metric to assess the readiness of subcutaneously implanted devices for cell insertion, ultimately increasing the rate of cell survival and maintaining the device functionality.

1.1.3 Analyte biosensors and glycemic control

The previously mentioned approaches to provide insulin independence by transplantation of pancreatic cells show great promise, however their success may be decades away due to regulatory procedures for medical devices [32, 33]. One very different strategy to help with diabetes management is continuous monitoring of glucose levels. A better glycemic control achieved this way, can also help with reducing secondary complications [34]. Continuous stream of data can also lead to creation of mathematical algorithms that can predict the upcoming glycemic changes. Moreover a continuous glucose monitor can be used in conjunction with an insulin pump system to create an Artificial Pancreas (AP) [35]. Mathematical calculations in an AP based on glucose level and food intake aims to predict glycemic changes and automatically administer insulin. However the current state of technology is limited. As an example, factors including physical exercise can affect the direction and rate of glycemic changes [36], therefore there is a need for a new metric that can record and analyze the intensity of a physical activity. *Chapter IV* focuses on creating a new class of material that can be used in creating different analyte biosensors. This material also addresses the current limitations in the analyte sensing technology by providing a fast response to changes, repeatable sensitivity over physiological concentrations, long shelf storage times and easy manufacturing procedure. Important to improving glycemic control in AP, the developed material was used to fabricate glucose and lactate sensors. Lactate measurements can be used as a metric that can identify physical activity and its intensity [37]. Combined continuous measurements of lactate and glucose can lead to more advanced mathematical algorithm and therefore better glycemic prediction and insulin administration.

1.2 Overview of the dissertation

The aforementioned approaches that can potentially provide insulin independence and tight glycemic control, are explored in this dissertation. Each chapter is dedicated to one of the approaches and aims to advance their current state of technology. *Chapter I* focuses on alginate biopolymers used for encapsulation of pancreatic islets, and their structural changes upon exposure to physiological environment. Understanding such changes can help to tune the material properties prior to implantation and increase cell survival. *Chapter II* deals with developing a non-invasive optical technology to monitor the oxygen level within implanted subcutaneous medical devices. This technology aims to provide a metric for determining the readiness of the implanted devices for cell insertion. This technique includes fabrication of oxygen sensitive implants that are placed within devices. These implants can be phonetically excited and their emission can act as an indicator of oxygen level. Two types of polymer devices that contained oxygen sensitive implants are implanted in athymic nude mice for this study. Over period of weeks the rate of vascularization in the implanted devices is monitored through using a developed procedure in which animals inhale different gases with different levels of oxygen and the changes of device oxygenation is monitored throughout the experiment. *Chapter III* explores methods to advance photonic anlayte biosensors. Such sensors work based on biochemical reaction of incorporated enzymes with analytes in interstitial tissue. These chemical reaction results in consumption of oxygen, the rate of which can be measured and correlated to the analyte concentration. In this chapter the invention of a new material that immobilize enzymes in close proximity photonic oxygen indicators, is discussed. This invention increases the storage and operational life of glucose and lactate sensors. In addition it decreases the response time to changes in analyte level and also increases the sensitivity range.

CHAPTER 2: Structural characteristics of alginate hydrogel

2.1 Introduction

The field of biomedical engineering frequently requires different materials with specific and tunable properties for variety of its applications [38, 39]. Tailored hydrogels have been developed for a number of applications, for which the hydrogel serves as a bulking agent [40], tissue engineering scaffold , cell transplantation vehicle [24, 40, 41] and controlled drug delivery systems [42]. One commonly used biocompatible hydrogel for these applications is alginate, a natural polysaccharide polymer derived from brown seaweed [43]. Sodium alginate is soluble in aqueous solutions and forms stable gels in the presence of certain divalent cations such as calcium, barium and strontium [44]. These polymers can absorb large quantities of water due to the hydrophilic groups attached to their backbone and resist dissolution via ionic crosslinks between the network chains [45]. The stored water allows free diffusion of molecules, while the polymer serves as a matrix to hold the structure together [22]. The tunable diffusional characteristics of this polymer can be advantages in sustained and localized drug delivery applications. The classical approach to drug delivery, oral administration or injection, may lead to unacceptably high concentrations and poor targeting that can result in side effects and low efficiency [46]. The release kinetics of drugs encapsulated in this hydrogel can be modified by tuning the alginate characteristics and drug/alginate interactions, for example Methotrexate an anionic drug used mainly as a chemotherapy agent and immune system suppressant, has been incorporated within the pores of alginate and is released by simple diffusion through the alginate network [47]. Another example of this controlled release is encapsulation and release of proteins drugs such as growth factors that can promote or impede cell differentiation, proliferation, tissue

growth and vascularization [48]. However these protein drugs degrade rapidly in the body, requiring use of high doses which can cause severe side effects [49]. Localized delivery of these proteins using polymers may ensure concentrated local exposure over a prolonged time without negative side effects. Alginate hydrogel is also commonly used as cell delivery vehicles in tissue engineering to allow localization of transplanted cells and control over their fate [49, 50]. This approach can provide an alternative treatment to whole organ transplantations, for failing or malfunctioning organs such as liver or pancreas. Examples of this applications include encapsulation and transplantation of chondrocytes for new cartilage formation, calvarial osteoblasts for enhanced bone formation [51], and important to our research, pancreatic islet cells to provide insulin secretion, resulting in glycemic control in type 1 diabetes [52].

Type 1 diabetes is caused by autoimmune destruction of pancreatic Beta cells [5]. These cells normally synthesize and secrete insulin, which is the most important hormone involved in physiological regulation of blood glucose level. The current method of treatment which is daily injection of insulin, is not considered as a cure, the glycemic control achieved is imperfect and furthermore it can cause inevitable secondary complications [52]. Encapsulation of pancreatic islets in alginate is a promising alternative to lifelong insulin therapy is pancreatic islet transplantations [52-54]. Potentially alginate encapsulation can obviate requirements for lifelong pharmaceutical immunosuppression therapy to prevent implant rejection, even for xenografts. Alginate microcapsules must be formulated to provide diffusion passage to necessary nutrients (e.g. glucose and oxygen) and the secreted peptide hormones including insulin and glucagon between the host's blood vessels and the transplanted cells. They must also block the passage of larger sized immunoglobulins, important to immunoisolation [55]. Such diffusional

characteristics between implants and vasculature are important to cellular transplantation and can be studied in vivo using non-invasive optical techniques [56, 57].

This work has studied the volume change of alginate samples after crosslinking at different temperatures, incubation at physiological conditions and *in vivo* implantation. Lastly, a custom-built hydrogel encapsulator was fabricated and diffusion of particles with different molecular weights into spherical microcapsules crosslinked in a solution of 120 mM $CaCl_2$ was studied. Diffusivity of these molecules in the spherical alginate microcapsules is studied following incubation in either the crosslinking solution and/or a model physiological solution. It is hypothesized that incubation of these microcapsules (formed in 120 mM CaCl2) in a physiological condition can change their structure, volume and permeability through an ionic substitution of sodium for calcium ions in the physiological condition. Understanding the effects of this physiological environment on material permeability aids in the prediction of alginate properties *in vivo*. These observations are critically important since a change in diffusivity can alter the kinetics of drug release as well as immunoisolative characteristics of alginate.

2.2 Materials and methods

2.2.1 *In vitro* volume changes of bulk samples

The effect of temperature on gel volume change was measured during crosslinking conditions (exposure to 120 mM $CaCl_2$). Samples of UPLVM alginate with weight concentrations of 1.5% and 2.5% and initial volumes of 0.1 mL were prepared and crosslinked using the multi-well plate technique (Fig. 2.1). Subsequent sample volumes were measured by placing them in a graduated cylinder containing the incubation solution and recording the change in the volume within the cylinder. Average of five samples were used for each experimental condition.

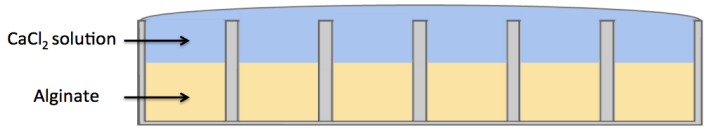

Figure 2.1: The process of cross linking cylindrical samples of alginate in a multi well plate.

2.2.2 *In vivo* assay and volume change of microcapsules

microcapsules of initial concentration 1.5% and 2.5% UPLVM alginate (2000 per concentration) were prepared with average diameter of 400 μm by an air jet syringe pump electrostatic droplet generator (Nisco Inc) at standards settings (Voltage: 9kV, Agitator Speed: 80 rpm, Pressure: 3psi, Needle gauge: 25G, Needle height: 25mm). The liquid spheres are dropped in a stirring bath of 120mM CaCl2 solution and left to crosslink for four hour at room temperature (24° C). They are then placed in culture media solution for 15 hours at 37° C. Microcapsules were implanted in two different sites (intraperitoneal cavity and subcutaneous) of two immunocompetent CD1 mice for seven days. Microcapsules were then excised, incubated overnight in culture media at 37°C. The microcapsules were imaged before and after explanation using EVOS microscope. Pictures were then analyzed using ImageJ with FIJI plugin script to obtain the average diameter.

2.2.3 Custom-Built alginate encapsulator and microcapsule formation

For this study an encapsulator structure is formed from optomechanical hardware (Thorlabs, USA) selected to keep components well aligned (Fig. 2.2). Compressed Nitrogen gas flows into a pressure regulator and is then injected into the top of a glass syringe containing sodium alginate solution (pressure 2-3 PSI). Pro Nova Ultra-Pure Low Viscosity sodium alginate (Novamatrix, Norway) was used to make liquid alginate with concentration of 2.5% (weight/volume). The gas

pressure forces the alginate solution through a 25 gauge stainless steel needle. Using a voltage generator (SUNKEE DC 3V to 7KV) a positive voltage of +7kV is applied to a conductive post that holds the needle in place, thus applying the voltage to the entire needle. Negative -7kV voltage is applied in the same way to another horizontal post directly underneath the needle, this post is connected to a right angle clamp (Thorlabs, USA) with a cylindrical opening of 12.5 mm diameter which is co-aligned to needle tip (distance 10 mm). Both posts that carry voltage are isolated from the system with insulating polymer tapes. Strong electromagnetic force formed between the needle tip and the cylindrical opening underneath, forces the alginate droplets formed at the tip of the needle to detach and fall down, this force results in the formation of small microcapsules. These microcapsules fall into a stirred solution of 120mM $CaCl_2$ for crosslinking (speed 80 rpm). The total travelling distance for microcapsules from the needle tip to the solution surface is 30 mm. The microcapsules are crosslinked in the stirring solution for one hour, followed by another three hours of crosslinking without stirring. The entire microcapsule formation and crosslinking process is performed at room temperature.

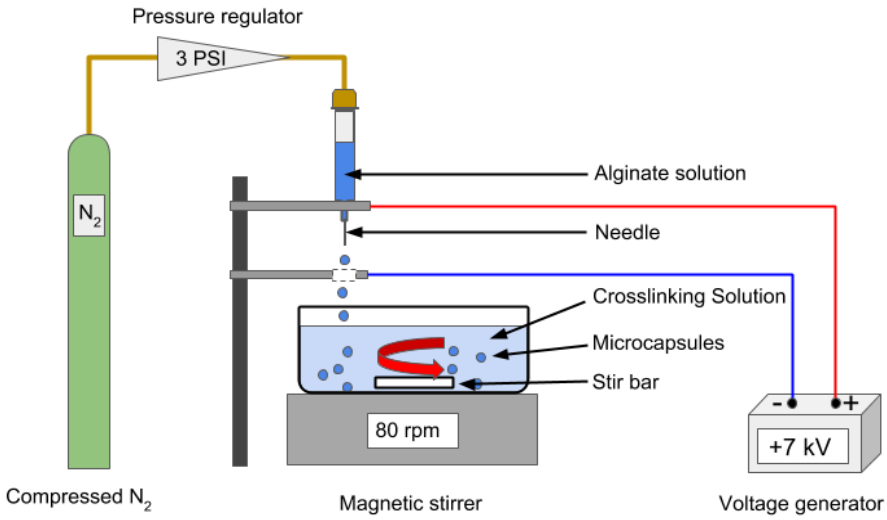

Figure 2.2: Custom-built alginate microencapsulator used to make 2.5% UPLVM microcapsules of around 400 µm diameter.

2.2.4 Diffusion assay

After the initial four hours of crosslinking in 120 mM $CaCl_2$ solution at 24℃ the microcapsules are separated into three different groups. Two groups are kept in crosslinking solution at 120 mM $CaCl_2$ at 24℃ and 37℃. The third group is placed in a developed physiological media at 37℃ with appropriate protein and ion concentrations to mimic the physiological environment. The media contains; 145 mM Na+, 3mM Ca++, 4mM K+, 20 mM HEPES and 3% Albumin (weight/volume). Microcapsules are kept in their incubating conditions for a duration of seven days. After this incubation period the diffusional characteristics of these microcapsules are studied using a Fluoview 3000 confocal microscope (Olympus, Japan). For this experiment microcapsules are placed in a solution of multiple spectrally-distinct fluorescently tagged dextrans each with its own molecular weight (MW) and concentration: 10 kD -Alexa Fluor 647 (Thermo-Fisher, USA) at 0.25mg/ml; 150 kD-FITC (Sigma-Aldrich, USA) at 6 mg/ml; 500 kD-Texas Red (Sigma-Aldrich, USA) at 6 mg/ml. The microcapsules are placed in a glass-bottom well containing dye solution. Confocal fluorescence images were acquired at the microcapsule midplane every 30 seconds for 60 minutes using a 10X NA=0.4 objective (Olympus, Japan). Diffusion coefficients are estimated by fitting fluorescence dynamics to the modified mathematical solution of non steady state diffusion into a sphere [58]. See equation 2.1.

$$\frac{C}{C_0} = \alpha\,(1 + 2\sum_{n=1}^{J}(-1)^n exp(-Dn^2\,\pi^2 t/R^2)\,) \qquad (2.1)$$

where C and C_0 are the concentration of a molecule at the center and boundary of the microcapsule respectively, D is the diffusion coefficient of that molecule in the sphere material, and R is the radius of the sphere. α is a prefactor constant introduced to the model to account for the observation that in a porous structure, the equilibrium condition can lead to $C/C_0<1$ due to

the volume fraction of the solid phase. $J = 5000$ is a constant, at which the value of the argument is near to zero. Fluorescence intensity is assumed to be proportional to fluorophore concentration and represented as I. Values for D and n are estimated from intensity measurements that were fit to this model using a multivariable nonlinear least square regression algorithm in MATLAB (MathWorks, USA). Prior to fitting, the image intensity background (estimated as the intensity value at the center of the sphere at time zero) is subtracted from every intensity value for each time series. (D value is reported as average and standard deviation for n = 4-5).

2.2.5 Image analysis

Confocal images are analyzed by custom code written in MATLAB (MathWorks, USA). As shown in Figure 2.3 the code implements the Hough transform (sensitivity set to 0.87) to locate the circular microcapsules (Fig. 2.3A). Intensity values were then extracted from line scans passing through the center of each circle (Fig. 2.3B). At each timepoint values for I and I_0 were computed as the average of 30 consecutive pixels located at the center and boundary of the circle respectively.

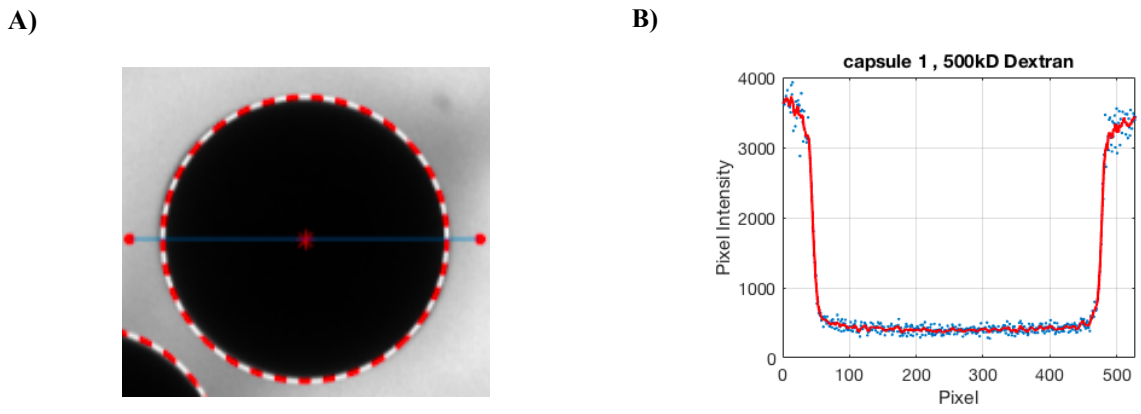

Figure 2.3: (A) Confocal fluorescence image (red channel) of one microcapsules in the fluorescence dextran solution with filters configured to image 500 kD dextran labeled with Texas Red. Microcapsule were detected using the circular Hough transform. For each microcapsule a line is drawn passing its center. (B) Intensity values along the lines drawn in (A).

2.2.6 Statistical analysis

Prism 7 (GraphPad Software, Inc., La Jolla, CA, USA) is used for statistical testing. Data passed tests for normality and samples were compared using one-way ANOVA with Tukey's multiple comparisons test. Tests are determined statistically significant when $p < 0.05$.

2.3 Results

2.3.1 Temperature-environment and structural changes

Alginate samples (1.5% and 2.5% UPLVM) were made and crosslinked (*2.2.1*). The volume changes of these samples were measured at different timepoints during the first ten hours of crosslinking. Volume of five samples is measured at each timepoint. Figure 2.4 shows a decrease of volume over time for both concentrations. A higher level of shrinkage is noted in lower alginate concentration of 1.5%, possibly due to the fact that the structure occupies more free space and therefore is less resistant to the contraction. These changes seem to indicate that crosslinking between Ca++ ions and alginate are exerting an inward force on the structure.

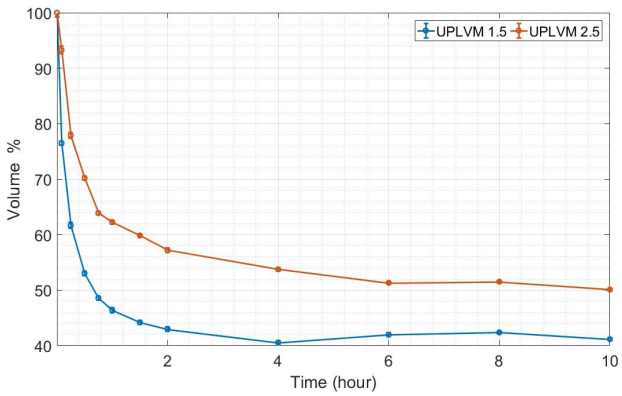

Figure 2.4: Changes in volume during crosslinking alginate samples made with concentration of 1.5% and 2.5%. Values reported at each timepoint are the mean and standard deviation of five unique gels. In total 60 gel samples were analyzed per condition.

To determine if the observed contraction is due to the ON/OFF kinetics of bonds between ions and alginate blocks, volume change experiments are repeated at multiple temperatures of crosslinking. Alginate gels (1.5% and 2.5%) were incubated within 120 mM $CaCl_2$ solutions for 48 hours at either 3°C, 24°C or 37°C, temperatures typical for refrigeration, room and body temperatures respectively. As shown in Figure 2.5 gel contraction (reported as % volume change) increased with incubation temperature. Next, the reversibility of the temperature dependent volume changes was investigated. Following the 48 hour treatment described above, samples were separated into three groups, each further incubated for five days at 3°C, 24°C, or 37°C (experiment illustrated in Fig. 2.5B and Fig. 2.5D). The group first incubated at 3°C continued to contract over the five day period at the increased temperatures. The group first incubated at 24°C exhibited both relative expansion and further contraction at lesser or greater temperatures respectively. This finding speaks to the reversibility of the ionic crosslinking. Interestingly, the group first incubated at 37°C was resilient to further volume changes after incubation at cooler temperatures maintaining its initial reduced volume for both the 1.5% and 2.5% gels. This suggests irreversible crosslinking is not achieved during the following incubations at lower temperatures of 3°C and 24°C temperatures, at least over the observed duration, possibly due to a complete polymerization with higher diffusion and bonding of Ca++ to alginate blocks.

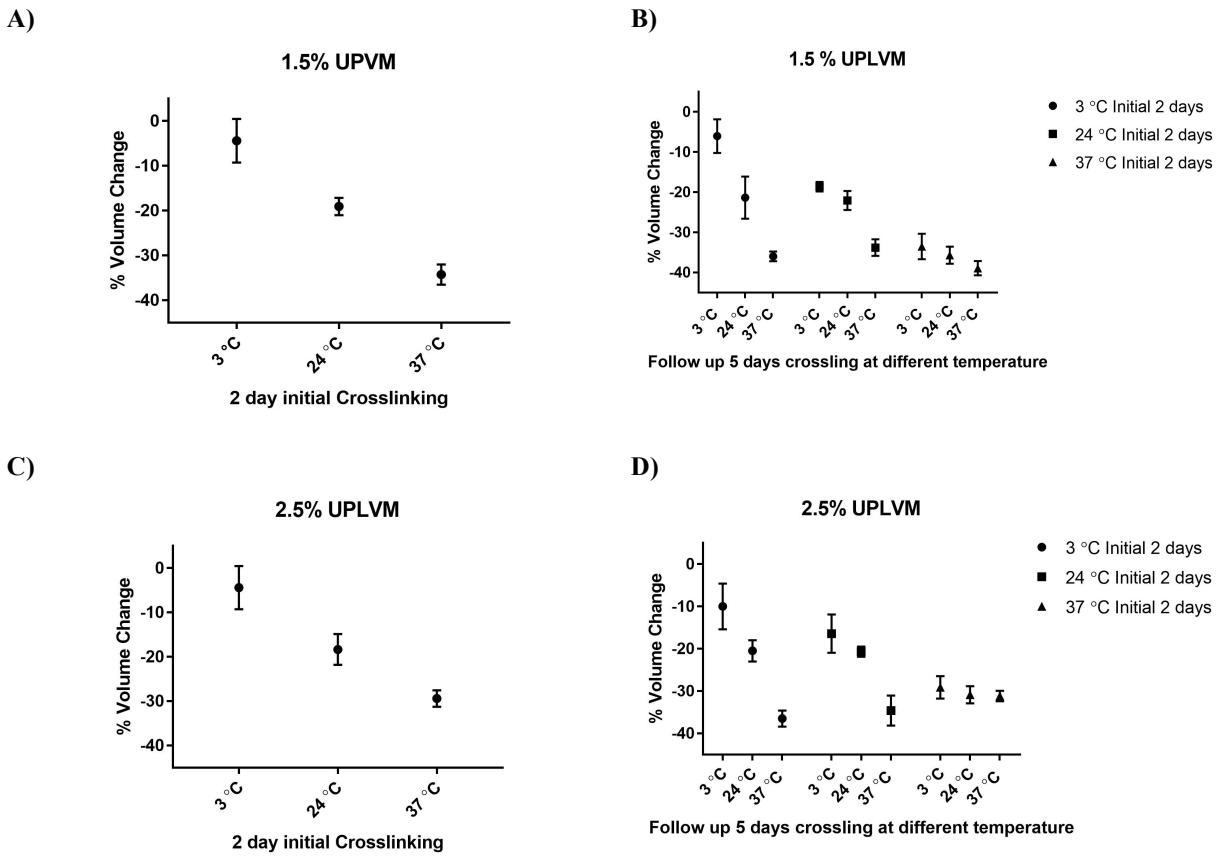

Figure 2.5: Change of volume in UPLVM alginate samples undergoing different temperature treatments. Samples were prepared by crosslinking at 24°C for 4 hours and they were then incubated in different starting temperatures (A and C) for 2 days, they were then placed in different temperature conditions and crosslinking continued for additional 5 days (B and D)

In practice, alginate microcapsules are eventually implanted into a tissue with physiological concentrations of Ca^{2+} which is around 1/40X that of the crosslinking solution, and also containing a host of ions not present in the $CaCl_2$ crosslinking solution. To study the volume changes *in vivo* alginate capsules of 1.5% and 2.5% UPLVM were implanted in subcutaneous and intraperitoneal space of CD1 nude mice for a duration of a week. Upon explantation and image analysis it was found that this implantation results in an increase in volume of the microcapsules (Fig. 2.6).

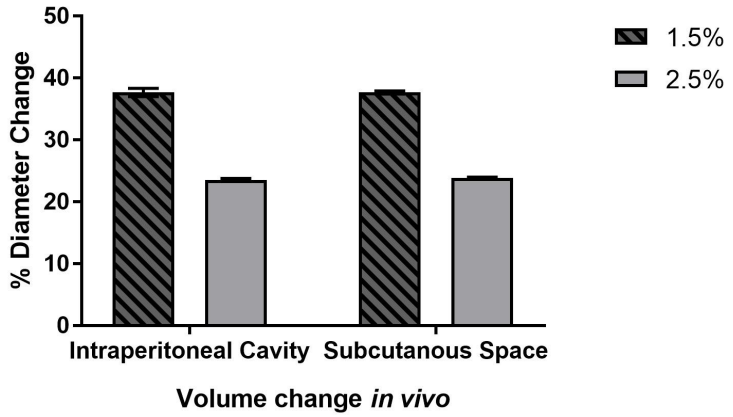

Figure 2.6: Changes in microcapsule diameter after seven days of implantation in the intraperitoneal cavity and subcutaneous space of immunocompetent CD1 mice.

2.3.2 Diffusion and permeability

Lower volume changes for higher concentration of alginate (2.5%) shown in both *in vivo* and i*n vitro* experiments seem to indicate a higher structural stability which can be beneficial in cellular therapy. To further investigate the characteristics of such alginate capsules a custom built hydrogel microencapsulator was built. Microcapsules were made from using 2.5% UPLVM alginate and were then divided into three groups and kept in crosslinking solution at 24℃ and 37℃ as well as the developed physiological media at 37℃. Microcapsules were then transferred to a glass-bottom well containing a solution of spectrally distinct fluorescently labeled dextrans having MW 10, 150, 500 kD. Figure 2.7 shows a three-channel fluorescence confocal image acquired ten minutes after transfer of microcapsules into the microwell.

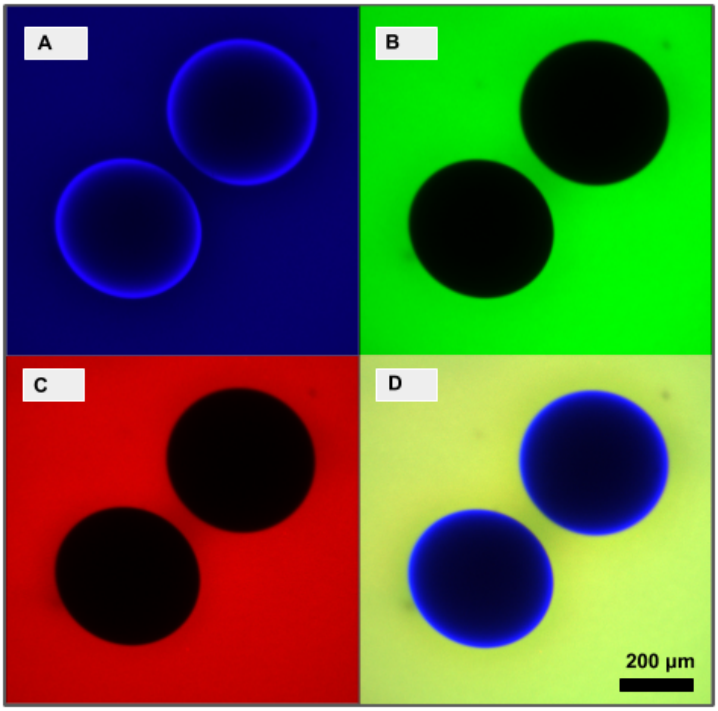

Figure 2.7: Confocal fluorescent images of capsules after 10 minutes incubation in the labeled dextran solution (A) blue channel (10 kD dextran), (B) green channel (150 kD dextran), and (C) red channel (500 kD dextran), (D) merged color image.

The confocal microscope simultaneously images the blue, green and red channels whose fluorescence originates from the 10, 150 and 500 kD labeled dextrans respectively. Note that while the 10 kD dextran (blue channel) can be seen penetrating the microcapsule, the 150 (green channel) and 500 kD (red channel) dextrans were not detected within the microcapsule. Analyzed fluorescent ratio dynamics (I/I_0) over time is plotted in Figure 2.8 for the three incubation conditions at the 7 days timepoint. In the first two conditions microcapsules are incubated in the crosslinking solution of 120 mM $CaCl_2$ in 24℃ and 37℃ and in the third condition they incubate in the physiological media at 37℃. As expected, the 10 kD dextran diffused faster than the larger dextrans in all three incubation conditions, a results consistent with the size selectivity of polymerized alginate [59].

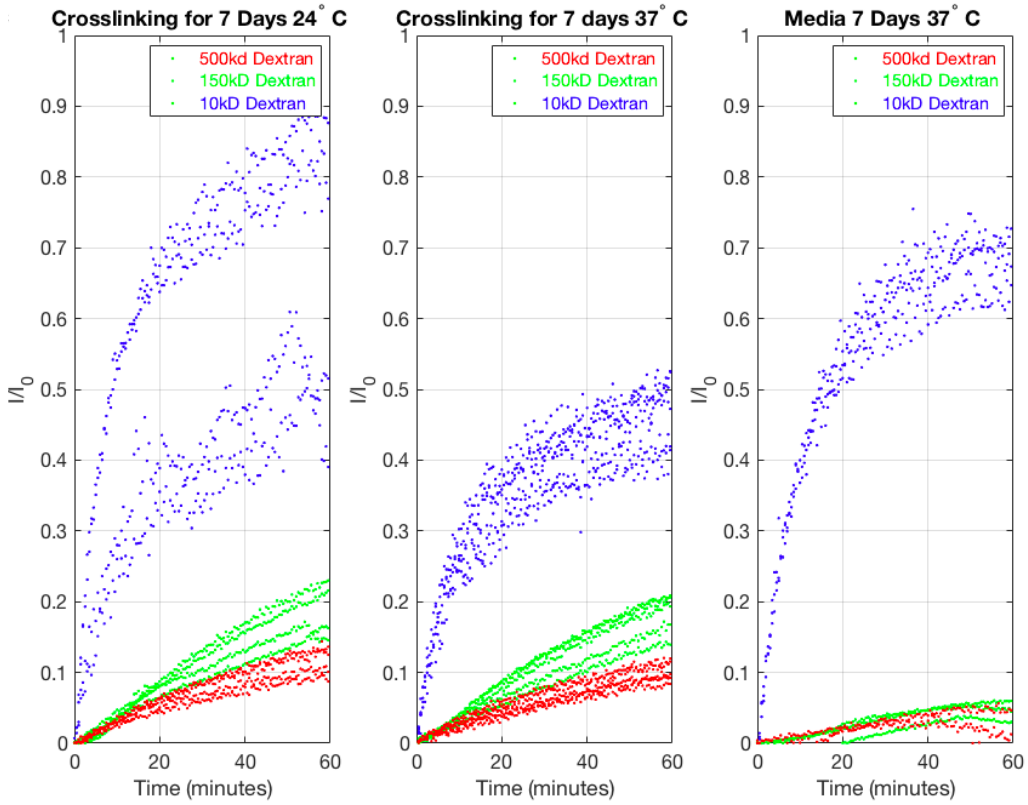

Figure 2.8: Changes of fluorescent ratio dynamics (I/I_0) after incubation at three different conditions is plotted over time. Each microcapsule undergoes an inward diffusion of 10 kD dextran (blue) 150 kD dextran (green) and 500 kD dextran (red) . The fluorescent ratio dynamics (I/I_0) of 10 kD dextran is shown to increase to higher values (above 0.3 in all cases)

As is previously shown in the literature, incubation in different conditions can result in structural changes of alginate microcapsules and lead to changes in their final volume [24, 60]. These changes may in turn affect the diffusivity of small molecules through the capsules. In order to observe any changes to the diffusivity the mathematical solution of non steady state diffusion (*2.2.4*) at the center of capsule was fit to image data over time. This method estimates the diffusion coefficients independent to microcapsule diameter. As shown in Figure 2.9 no statistical differences between diffusion coefficients of each fluorescent dextran dye after they are incubated in crosslinking solution either at 24℃ or 37℃ was found. However, incubation in media as compared to incubation at both crosslinking conditions (24℃ and 37℃) results in

significantly higher diffusion coefficients ($P<0.01$) for each molecular weight fluorescent dextran (10, 150 and 500 kD). Moreover, within each incubating condition, diffusion coefficient of the smallest molecular weight dextran (10 kD) is larger than that of higher molecular weight dextrans ($P<0.01$).

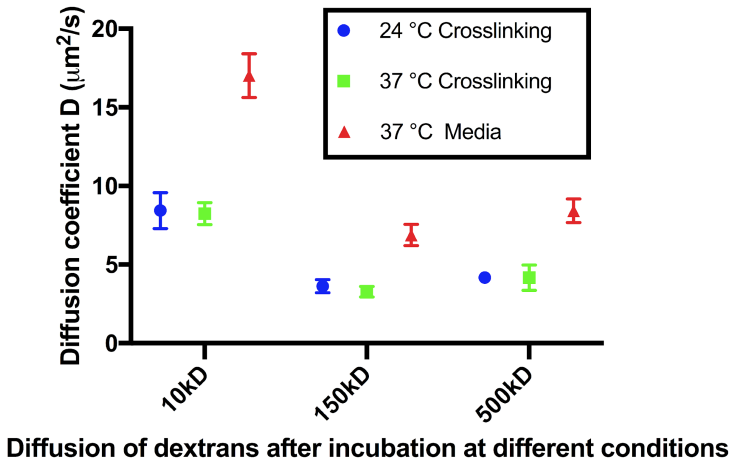

Figure 2.9: Estimated diffusion coefficients for fluorescent molecules of different molecular weights. Tested conditions are: (1) incubation at 120 mM $CaCl_2$ in (1) 24℃ and (2) 37℃ and in (3) developed physiological media at 37℃.

2.4 Discussion

This chapter studies the effects of crosslinking and physiological condition on volume and permeability of alginate hydrogels. The results indicate that alginate hydrogels undergo a volume decrease during crosslinking. This contraction can be due to newly formed bonds between Ca++ ions and alginate chains. This hypothesis is further tested by investigating the effects of temperature change on crosslinking and final volume of the gels. The results indicate that an increase in the temperature causes a higher level of contraction. This finding is consistent with the kinetic model where ON rates are greater than OFF rates, and both are temperature dependent. The increased alginate contraction at higher temperatures may be because of an

accelerated motion of calcium ions and faster crosslinking along with rotation of polysaccharide chains, as is previously discussed by Serp et al. [61]. Additionally *in vivo* implantation shows an increase in the volume of microcapsules. Such expansion is possibly due to the fact that high content of sodium in the media replaces the calcium inside the alginate structure [60], thus a lower inward electrostatic force is excreted on the matrix and consequently the gel expands. Importantly such an increase in volume can affect the pore size of the hydrogel and its selective permeability, possibly even compromising the diffusional and immunoisolation properties of the hydrogel.

To further understand the structural changes during crosslinking and exposure to physiological conditions, diffusion of dextran molecules of different molecular weights into alginate microcapsules after incubation in different conditions was investigated. The results show higher diffusion coefficients for smaller molecular weight dextrans diffusing into alginate microcapsules, consistent for all incubating conditions. Additionally, it was observed that all dextran dyes show a higher diffusion coefficient after microcapsules are kept in physiological media. The developed physiological solution mimics in vivo conditions in which implanted alginate microcapsules are exposed to physiological concentrations of Ca++ (2-3 mM), Na+ (145 mM) [62], and a host of ions not present in the $CaCl_2$ crosslinking solution. Importantly, it has been shown that incubation of alginate in such physiological environment can cause swelling and softening due to ionic exchange [60]. The observed increased diffusivity may therefore be a result of hydrogel swelling, which can increase pore size. The increase in pore size could compromise immunoisolation properties and increase controlled diffusion kinetics in vivo. This hypothesis is further supported by the fact that microcapsules kept in physiological condition

show a diameter (602.5± 19.2 μm) roughly 1.45 times higher than those incubated in crosslinking solution (24℃: 415.6 ± 7.47 μm , 37℃: 415.6 ± 20.6 μm) ($P<0.01$).

This study shows that volume changes can affect the structure of alginate hydrogels and alter the diffusional characteristics. It was shown that by using spherical geometries and estimating the diffusion coefficient through mathematical modeling of diffusion into microcapsules, this structural changes can be estimated. This strategy can possibly be implemented to better understand and tailor the hydrogels to provide selective passage, as well as controlled diffusion kinetics in vivo. These characteristics are important for providing immunoisolation in cellular therapy and better controlled release kinetics in drug delivery applications.

CHAPTER 3: Non-invasive optical monitoring of oxygen tension in subcutaneous medical devices

3.1 Introduction

Tissue engineering approaches to create bioartificial organs have been emerging in the past few decades [18]. In the case of the pancreas, evidence suggests that it is unnecessary to replace the whole organ. It is shown that transplantation of the islets of Langerhans that contain the endocrine cells also result in restoration of the endocrine function [4]. For example, transplantation of isolated pancreatic islets is used to treat Type 1 diabetes (T1D). T1D is caused by autoimmune destruction of pancreatic Beta cells [4, 5]. These cells normally synthesize and secrete insulin, which is an important hormone involved in physiological regulation of blood glucose. Self-monitoring of blood glucose (by finger stick glucose meters) in conjunction with multi-daily injections of insulin is the standard of care. However, the resulting glycemic control is imperfect and can cause harmful secondary complications such as cardiovascular diseases, retinopathy, and nephropathy [6–8]. A promising alternative to daily insulin injections is transplantation of pancreatic islet cells. This transplantation can provide autonomous regulation of blood glucose concentration and therefore result in stable glycemic control, thus preventing secondary complications [63]. Islet transplantation into the portal vein has shown 100% insulin independency in the first year, however the insulin independency was shown to decrease to less than 50% after five years [64, 65]. These finding support the potential for pancreatic islets to treat T1D, however in consideration of the five year half life, and inaccessibility for islet retrieval, and risk to the liver, better approaches are needed.

Polymer devices for islet housing are being developed to improve the outcomes of islet transplantation. A variety of polymers systems as well as implantation sites have been tested [20, 21, 66]. Literature suggests that the subcutaneous space can be advantageous for cellular transplantation because of ease of access and less invasive surgical procedures, but due to low oxygen tension and vascularization under the skin, hypoxia can occur [26, 27]. Hypoxia can induce apoptosis and necrosis and ultimately compromise the functionality of transplanted cells [67,68]. Several groups have shown that islet transplantation under the skin can be successful after modulation of the site with a polymer device [69, 70]. To accomplish this, vascularization of the polymer device is extremely important. Vascularization of these devices can be stimulated by using microporous structures [29, 70], inclusion of angiogenic factors [29, 30, 70], co-transplantation of vascular inductive cell types, or devices that can be implanted for prevascularization prior to transplantation of the cells [31].

In this study, an oxygen monitoring technology to study the vascularization and oxygen partial pressure inside subcutaneously implanted medical devices is developed. Oxygen measurements are performed using a developed optical monitor as well as oxygen sensitive implants that are inserted into the medical devices prior to implantation. This technology uses oxygen sensitive porphyrin dyes coated on the inner surface of transparent oxygen sensitive tubes (OST) made from silicone. The phosphorescence characteristics of such dyes change at different levels of oxygen. he developed system excites the embedded dye through using flashing LEDs and records the emitted light. The lifetime decay of the emission corresponds to oxygen partial pressure. Additionally, a developed protocol named Dynamic Inhalation Gas Test (DIGT) is used to indicate the rate of vascularization over time. In this protocol animals undergoes a step change in inhaled gas oxygen content. Such change of inhaled oxygen is

reflected in tissue oxygenation as well as within the geometry of the devices, which is then detected and calculated using the developed technology. It is hypothesized that faster changes of oxygen partial pressure within the device can indicate lower diffusional distance to the newly formed vasculature. Monitoring these changes over time can potentially show the rate of vascularization in implanted cellular therapy device.

In this work oxygenation and vascularization of medical devices designed for two stage implantation method, is studied. The strategy includes first, implantation of the devices to promote vascularization and then insertion of the transplant cells. This approach aims to result in a more vascularized device with reduced diffusional distances between the newly formed vasculature and the freshly transplanted cells. This methodology can potentially compensate for loss of interpenetrating islet capillary network after isolation, by providing faster transport of oxygen and nutrients and preventing the loss of cells through hypoxia and potentially resulting in a faster return to normoglycemia in T1D.

First, the oxygen partial pressure is monitored and vascularization inside devices made from biocompatible Polydimethylsiloxane (PDMS), implanted in subcutaneous space of athymic nude mice is studied. The developed PDMS devices provide mechanical support and protection to the pancreatic islets. Importantly they house the cells in single files inside microfluidic channels, increasing the availability of nutrients and oxygen to each islet cell. Additionally, the microfluidic channels that house the cells have openings on their sides which can allow the transfer of oxygen, nutrients and secreted hormones between the transplanted cells and newly formed vasculature, aiming to achieve better functionally and longer survival of the implant. Second, administration of hydrogen sulfide (H_2S) as a potential agent to improve the vascularization in the porous poly(D,L-lactide-co-ε-caprolactone) (PDLLCL) devices is studied.

The PDLLCL devices have already shown successful results in promoting islet-cell survival and achieving normoglycemia under the skin of athymic nude mice for the duration of the 70 day study [71]. H_2S used in this study is a gaseous signaling molecule, like nitric oxide and carbon monoxide, normally produced by the body. It was first described as a neuromodulator [72], but was later recognized for its effects on vascular cells [73]. Endogenous H_2S is enzymatically generated in vascular cells, where it exhibits vasoactive, anti-oxidant, anti-inflammatory, and anti-apoptotic properties [73]. The effects of H_2S are well described, but the molecular pathways of its action are poorly understood. Cai and coworkers were the first to show that intraperitoneal injections of the exogenous H_2S donor NaHS stimulate angiogenesis in subcutaneous Matrigel plugs in mice [74]. Increased angiogenesis was shown by higher hemoglobin levels and the presence of more capillaries at NaHS administration with concentrations of 10 and 50 μmol/(kg*d) as compared to untreated group. This work investigates whether H_2S will have similar effect on vascularization of PDLLCL devices implanted into the subcutaneous compartment. This is assessed by histology, CD31 expression, and an optical assessment of oxygen transport between vasculature and the device. The strategy to monitor the partial pressure of oxygen within the implant and measure the dynamic of oxygen changes prior to cell transplantation can potentially help with determination of the readiness of subcutaneously implanted medical devices for hosting cellular tissue. Such assessment can lead to eliminating hypoxia post transplantation and increase of cellular transplantation functionality.

3.2 Materials and methods

3.2.1 PDLLCL device fabrication

Devices were obtained from Polyganics B.V. (Groningen, The Netherlands). A 4% (w/v) PDLLCL solution was prepared in chloroform (Sigma-Aldrich, Zwijndrecht, The Netherlands). The PDLLCL solution was thoroughly mixed with natrium chloride particles (Sigma-Aldrich) of 250–425 μm (10:1 w/w) in order to create a porous structure. This solution was transferred into sterile glass petri dishes to allow the solvent to evaporate. To remove the salt particles, the polymer sheet (5 mm thick) was extensively washed with sterile H_2O. The polymer sheet was casted and resized, resulting in a 10 mm by 15 mm device. During the casting process three channels were created by introducing 400 μm iron rods. These channels were created to accommodate cells and in the current study they were used for insertion of the oxygen sensitive tubes (OSTs) to non-invasively monitor the oxygen tension *in vivo* (Fig. 3.1A). The scaffolds were stored in 70% ethanol for several days to sterilize the scaffolds before implantation.

3.2.2 PDMS device fabrication

PDMS devices (Sylgard® 184 Silicone Elastomer Kit, Dow Corning Corp., Midland, MI, USA), each containing a parallel array of four slits and three channels, were fabricated within a custom 3D printed mold similar to those previously described [75]. The devices had approximate overall dimensions of 10 mm x 13 mm x 1.2 mm. All slits within each sheet were 500 μm in width, the channels had the inner diameter of 700 μm, and windows connecting the channels and slits were 100 μm in height and 750 μm in width. Walls between channels and slits were 600 μm wide. Molds were designed in SolidWorks (Dassault Systemes Solidworks Corp., USA), exported to

an STL file, and printed by a high resolution stereolithography 3D printer (Pico Plus 27, Asiga, USA). The mold was made of a hard 405-nm light curable resin (PlasGRAY, Asiga) fabricated layer-by-layer in 25-μm-thick slices. After the build was finished, molds were washed three times in isopropanol and sonicated for 10 min in isopropanol to remove any uncured resin. Molds were air dried for 15 min, then further cured by 10 min exposure to an 8W 302 nm UV light source (Dual UV Transilluminator, VWR International, Radnor, USA), and subsequently baked in an oven overnight at 80°C. Finally, liquid PDMS (1:10 ratio of crosslinker to monomer base) was poured into the molds and baked at 80°C for 2 h. The polymerized devices were removed from the molds and bonded to a flat PDMS sheet after plasma treatment (Harrick Plasma, USA). Slits in the bottom sheet were cut out using the slits from the bonded piece as a guide.

3.2.3 Oxygen sensitive tube (OST) fabrication

OSTs comprise an oxygen permeable tube and filled with oxygen-sensitive dye. The selected oxygen sensitive dye is platinum(II)-meso-Tetra(4-fluorophenyl) Tetrabenzoporphyrin (PtTPTBPF), which has peak absorptions at 430 and 614 nm and emission peak at 773 nm (Frontier Scientific, Logan). This dye was mixed with polystyrene (MW 2500 ,Sigma, USA) and dissolved into a solution using chloroform (Sigma, USA) to form a dye solution. The solution contains 4 mg PtTPTBPF, 60 mg polystyrene and 900 μL chloroform. The dye solution was flushed through an oxygen permeable biocompatible silicone tubing with outer diameters of 0.64 mm and 0.94 mm for PDLLCL and PDMS devices (BTSIL-025 & BTSIL_047, Instech Laboratories, USA). The flushing process was repeated five times to form a homogenous inner coating of PtTPTBPF inside the silicone tubes. The tubes were stored in a well ventilated dark

environment at 24℃ for a duration of 24 hours to allow the remaining chloroform to evaporate. A stainless steel wire was then inserted into each tube in order to provide mechanical stability (Fig. 3.1B). Afterwards the tubes containing a wire were cut to a length matching the devices (12-15 mm) and the ends were sealed using medical grade silicone adhesive (MED-1000 Nusil, USA). The sealed tubes were kept at room air in a dark environment for two days to fully cure. OSTs were placed into device channels. Fully assembled devices were sterilized by immersion in 70% ethanol for 12 hours.

3.2.4 The oxygen monitor

An oxygen monitor was fabricated a previously described [56] that sits on the surface of skin, emits light through the skin and onto the implanted OSTs, and receives luminescence to record luminesce waveforms. This monitor comprises a printed circuit board that houses a silicon photodetector bracketed by two light emitting diodes (LEDs) having central emission wavelength of 617 nm (Fig. 3.1C). An optical bandpass filter is mounted onto the detector to reject the LED wavelengths while passing the dye emission. For each oxygen measurement both LEDs flash simultaneously 25 times at 1% duty cycle (100 μs on, 10200 μs off) to excite the oxygen sensitive porphyrin dye. The emission of the dye after each flash is passed through an optical filter and onto the photodiode. Photodiode electrical current is converted to voltage by an operational amplifier and sampled over a period of 200 microseconds at a sampling frequency of 500 kHz using a myRIO data acquisition module (National Instruments, Austin). LED and data acquisition timing is controlled by LABVIEW 2015 (National Instruments, Austin). The dye continues to emit light after the end of each LED emission period with a decay that can be modeled as exponential [76]. See equation 3.1.

$$V = V_0 e^{(\frac{-t}{\tau})} \qquad (3.1)$$

where V is the detector voltage, V_0 is the voltage at the start of the decay, t is the time in seconds after the end of LED emission, τ is the lifetime parameter reported in seconds. Lifetime values were computed from emission waveforms using the fit function in MATLAB (National Instruments, Austin) configured for nonlinear least squares regression. The average for all 25 cycles is hereafter reported as lifetime (τ). The porphyrin dye emission is quenched by oxygen and consequently lifetime values (τ) decrease with increasing PO_2. The mechanism in which the oxygen quenches the dye is not yet completely clear, however independent of the predominant mechanism the kinetics of quenching is very well described by Stern-Volmer equation [76]. See equation 3.2.

$$\frac{I_0}{I} = \frac{\tau_0}{\tau} = 1 + k_q \tau_0 pO_2 = 1 + k_{sv} pO_2 \qquad (3.2)$$

Where I and I_0 are the luminescence intensities in the presence and absence of the quencher, τ and τ_0 are the lifetime of the dye in the presence and absence of the quencher, k_q is the bimolecular quenching constant and k_{sv} is the Stern-Volmer quenching constant. Dye emission is quenched by the oxygen and consequently, τ decreases with increasing PO_2.

3.2.5 OST Calibration

A custom-built glass chamber with an inlet and outlet port was placed above the oxygen monitor. OST were individually placed inside the chamber and exposed to different gases. These gas including, room air (160 mmHg), 76, 38, 15.2 and 0 mmHg oxygen. τ was measured at different oxygen partial pressures to generate a calibration curve (Fig. 3.2A). This process is repeated for each oxygen sensitive tube individually. OSTs were matched for calibration in groups of 3 and

inserted into devices. The lifetime to oxygen conversion are performed using a custom written MATLAB (MathWorks, USA).

3.2.6 Animals for PDLLCL device H_2S administration study

The University of California Institutional Animal Care and Use Committee at the University of Irvine approved all described animal procedures (IACUC # 2008-2850). Animals were housed at the University of California Irvine animal facility and maintained under 12-hour light/dark cycles with ad libitum access to water and standard chow. Devices were implanted in male athymic nude mice ($Foxn1^{nu}$, Charles River, Wilmington, USA) of eight weeks old. Briefly, under anesthesia a small incision was made in the skin to create a subcutaneous pocket on the back of the mice. PDLLCL devices containing the calibrated OSTs and fibrin were placed into this pocket and the skin was closed using skin staples (Cellpoint Scientific, Gaithersburg, USA). All mice received ibuprofen water (Banner Pharmacaps, High Point, USA; 0.2 mg/mL) as analgesic post-surgery for two days. Since H_2S is a gas, we used a sodium hydrosulfide (NaHS) solution as a H_2S donor. NaHS is unstable in solution and therefore a new solution was prepared just prior to each injection. From the day of implantation, mice received twice daily an intraperitoneal injection of NaHS until 28 days after implantation. One group of mice (n=6) received a low dose of NaHS (25 μmol/kg), the other group (n=6) received a high dose of NaHS (50 μmol/kg), and mice receiving saline injections served as a control group (n=6).

3.2.7 Animals for PDMS device study

The University of California Institutional Animal Care and Use Committee at the University of Irvine approved all described animal procedures (IACUC # 2008-2850). Devices were implanted

in male athymic nude mice (n=5) of eight weeks old. Animals were housed at the University of California Irvine animal facility and maintained under 12-hour light/dark cycles with ad libitum access to water and standard chow. Animals were monitored daily, and at day 56 the devices were removed and they were sacrificed.

3.2.8 Dynamic Inhaled Gas Test (DIGT)

To closely follow the vascularization process *in vivo* DIGT measurements were performed. These measurement were done on mice with implanted PDMS at days 3, 7, 14, 21, 28, 35, 42, 49 and 56 post implantation (n=5 each group). For the H_2S administration study on PDLLCL devices, the tests were performed on days 3, 7, 21, 35, 49 and 63 after implantation on each animal (n=6 per group). For the DIGT measurements each mouse was anesthetized by 2-3% of isoflurane (Piramel Healthcare, Morpeth, United Kingdom) while breathing 760 mmHg oxygen. When the animals were under full anesthesia the gas was changed to 152 mmHg oxygen level and isoflurane level was reduced to 1.5%. The optical monitor was then placed on the skin directly above the implanted device. After 100 lifetime measurements (spaced by 4.25 s for a total of 425 s) the inhaled gas is switched back to 760 mmHg oxygen. It is expected that the tissue PO_2 will rise and fall as the inhaled PO_2 is increased and decreased respectively. Accordingly, once the inhaled gas is returned to 760 mmHg, lifetime values should reach a new plateau, where the time to plateau is an indication of the oxygen transport between the blood, tissue and OSTs within devices. Once the plateau is reached, animals were taken off of anesthesia and returned to their cages. The time to plateau is calculated using custom MATLAB code and reported here as *Falltime* (in minutes).

3.2.9 PDLLCL devices, vessel morphology and quantification

The PDLLCL devices were removed on day 63 days after implantation. OSTs were removed from the devices and devices were cut into two pieces, one half of the scaffold was processed for the histological analysis whereas the other half was used for the quantification of vessels by PCR (described below). For histology, the scaffolds were fixated in 2% paraformaldehyde and processed for paraffin embedding. Sections were stained with an overnight incubation of CD31 (1:200; R&D Systems, Abingdon, UK) after 15 minutes incubation at 100 °C for antigen retrieval (10 mM citrate buffer, pH 6.0) and a subsequent blocking step with 5% donkey serum (Sigma-Aldrich). The secondary donkey anti-goat alkaline phosphatase conjugated antibody (1:100; Abcam) was applied for 45 minutes. Alkaline phosphatase activity was demonstrated by incubating for ten minutes with SIGMAFAST^{TM} Fast Red (Sigma-Aldrich). A short incubation with hematoxylin was used as counterstain. All stained sections were scanned with the microscope scanner Hamamatsu Nanozoomer (Hamamatsu, Almere, The Netherlands). Scans were analyzed using Aperio ImageScope (Leica Microsystems B.V., Rijswijk, The Netherlands). To quantify the amount of vessels in the scaffolds, half of the scaffold at day 63 was processed for Real Time reverse transcription polymerase chain reaction (RT-PCR) for the vascularization marker CD31. RNA was isolated using Trizol according to manufacturer's protocol (Invitrogen, Fisher Scientific, Landsmeer, The Netherlands). The RNA concentration was determined using a NanoDrop 1000 spectrophotometer (NanoDrop products, Wilmington, USA). cDNA was reverse transcribed using a SuperScript® III Reverse Transcriptase kit according to the instructions of the manufacturer (Life technologies). Real Time RT-PCR was conducted using ViiA^{TM} Real Time PCR system (Life technologies) with a primer and probe set (TaqMan Gene Expression Assays) for CD31 (Mm01242576_m1; Thermo Scientific) and qPCR Mastermix Plus

(Eurogentec, Seraing, Belgium). Reactions were performed at 50 °C for 2 minutes, 95 °C for 10 minutes, 95 °C for 15 seconds and 60 °C for 60 seconds repeating in these last two steps for 40 cycles. Delta Ct values were calculated and normalized against the expression of the housekeeping gene GAPDH (Mm99999915_g1; Thermo Scientific). Delta Ct values were used to calculate the fold change compared to gene expression of the control mice.

3.2.10 PDMS devices, histological analysis and immunofluorescence staining

PDMS devices were removed on day 56 by cutting through the full thickness of surrounding skin while leaving the tissue above and below the sheet intact. The excised tissue was immediately fixed by submersion in a 4% solution of phosphate-buffered formalin for 24h. Samples were processed, embedded in paraffin, sectioned, and stained with hematoxylin and eosin (H&E) (JIT Labs, Irvine, CA, USA). For immunohistochemistry, sections were deparaffinized followed by antigen retrieval via overnight incubation in 0.1 M Tris/HCl buffer, pH = 9.0 at 80°C. Sections were then washed with phosphate-buffered saline (PBS), permeabilized with 0.5% Triton X-100, and blocked with 5% Donkey serum (Jackson ImmunoResearch, Inc., West Grove, PA, USA) for 30 min at room temperature. After serum blocking, slides were incubated with 1:200 monoclonal rabbit anti-alpha smooth muscle actin (αSMA) (Abcam, Cambridge, MA, USA) and 1:200 polyclonal goat anti-CD31/PECAM-1 (sc-1506, Santa Cruz Biotechnology, Santa Cruz, CA, USA) in 1× PBS supplemented with 5% Donkey serum and 0.5% Triton X-100 at 4°C overnight. Slides were then washed with PBS and incubated with 1:500 AlexaFluor® 488 donkey anti-rabbit (Life Technologies, Carlsbad, CA, USA) and 1:400 AlexaFluor® 594 donkey anti-goat (Jackson ImmunoResearch, Inc. West Grove, PA, USA). Images were taken on an Olympus IX83 microscope at 20× with an Orca R2 camera (Hamamatsu Photonics K.K., Hamamatsu City,

Japan) through Micro- Manager and stitched together using FIJI.

3.2.11 Statistics

Statistical analysis was carried out in GraphPad Prism (version 7.0d; GraphPad Software, Inc., La Jolla, USA). A Shapiro-Wilk normality test was performed to test the data for normality. A Kruskal-Wallis test with Dunn's multiple comparison was performed to study the statistical significant differences for nonparametric distributions. One-way ANOVA with a Tukey post-hoc was performed for parametrically distributed data. p-values < 0.05 were considered significant. The data is presented in mean ± standard deviation in case of parametric distribution and median ± interquartile range in case of nonparametric distribution.

3.3 Results

3.3.1 PDLLCL devices and H_2S administration study

3.3.1.1 OST calibration and DIGT

Prior to implantation, each OST (Fig. 3.1B) undergoes a gas calibration inside a glass chamber. In this calibration gases with 160, 76, 38, and 0 mmHg oxygen levels are inserted into the chamber in order.

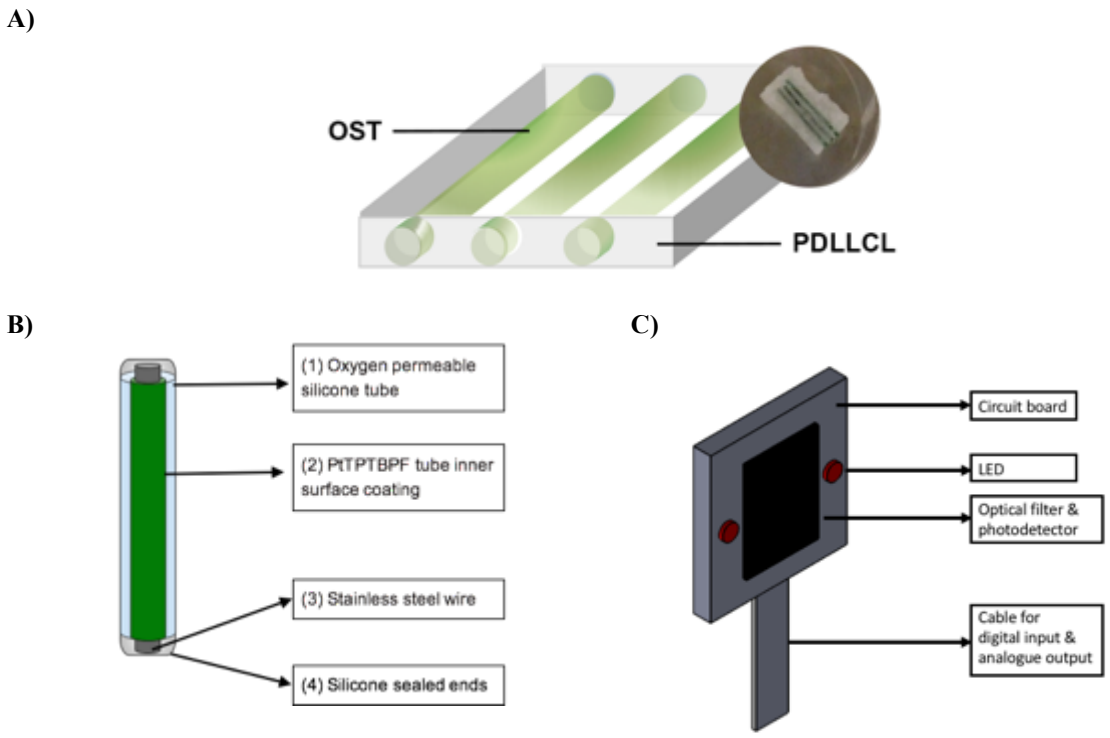

Figure 3.1: (A) Oxygen sensitive tubes inserted into channels of PDLLCL device. (B) Oxygen sensitive tube (OST) made of permeable silicone tubing coated on the inner surface with a layer of PtTPTBPF and reinforced with stainless steel wire. Both ends are sealed using medical grade silicone adhesive. (C) Oxygen monitor comprising a printed circuit board that houses two LEDs, photodetector and optical filter

Fig. 3.2A shows a calibration process during which the gas mixtures were cycled through three times. With each gas exchange, the corresponding τ is recorded as the mean value of the subsequent plateau. Lifetime values at each oxygen concentration across all three cycles show low variation (standard deviation < 0.08 μs). This result demonstrates the repeatability and reliability of oxygen measurements using OST. Following the calibrations, OSTs were inserted into devices, which were implanted as described above. Fig. 3.2B shows an example of the calculated lifetime values during a DIGT test (refer to *3.2.8* for description of DIGT). Note that lifetime falls with increasing PO_2, so that the curve in Fig. 3.2B indicates increasing PO_2 values as reported by the OSTs.

A)

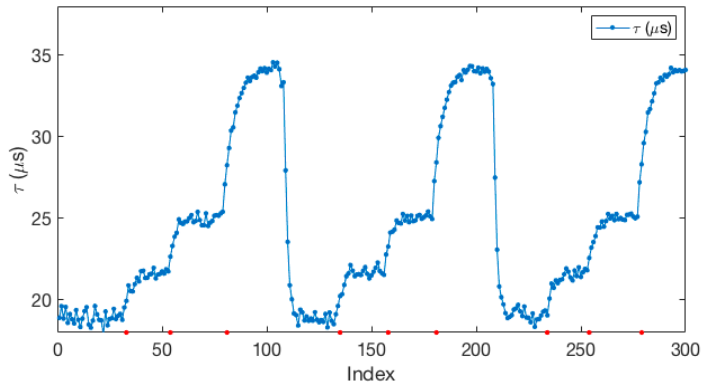

B)

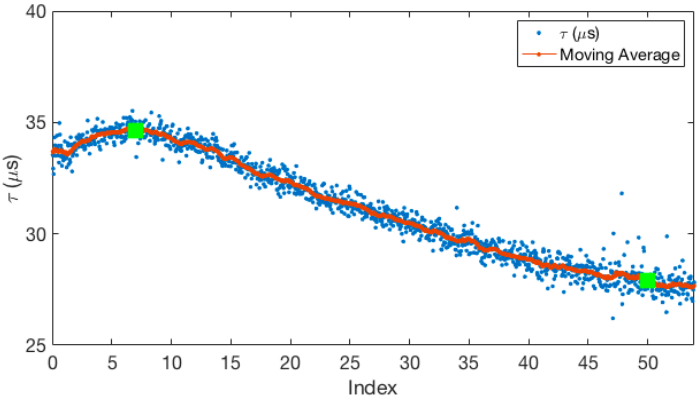

Figure 3.2: (A) Three calibration cycles of a single oxygen sensitive tube (PO_2: 160, 76, 38, and 0 mmHg in order). The average lifetimes for each plateau across the three cycles are 19.0 ± 0.07, 21.6 ± 0.08, 24.9 ± 0.04 and 34.1 ± 0.06 µs for PO_2 values in the same order (B) DIGT performed on an animal three days after device implantation. *Falltime* is defined as elapsed time between exchanging inhaled gas from 152 to 760 mmHg (left green square) and steady state (right green square)

3.3.1.2 Animal study and H_2S administrations

Animals received injections of NaHS (low and high dosage groups of 25µmol/kg and 50µmol/kg) and saline (control group) as described above. Injections occurred twice daily for the first four weeks (day 28) followed by another five weeks of no injections (up to day 63). The follow up period of five weeks with no injections (day 28 to day 63) aims to provide necessary time for device vascularization to complete. The DIGT was performed on all animals (n=6 per group) on days 3, 7, 21, 35, 49, and 63. Fig. 3.3 (A-C) shows the *Falltime* values calculated from

the DIGT measurements on all animals. Statistical differences in lifetimes values were not observed either for each treatment condition across all days, or between treatment conditions on each day. This observation indicates vascularization of implants may be occurring independent of administration of the proangiogenic H_2S. Histological and gene expression evaluations were performed on the explanted devices (explanation on day 63). Surprisingly, statistically different values were observed for the expression of the endothelial cell marker CD31 between treatment groups (Fig. 3.3D). The treatment with a low dose of H_2S seems to significantly downregulate the gene expression of CD31 (fold change of 0.57 ± 0.02) compared to the control group and the high dose group.

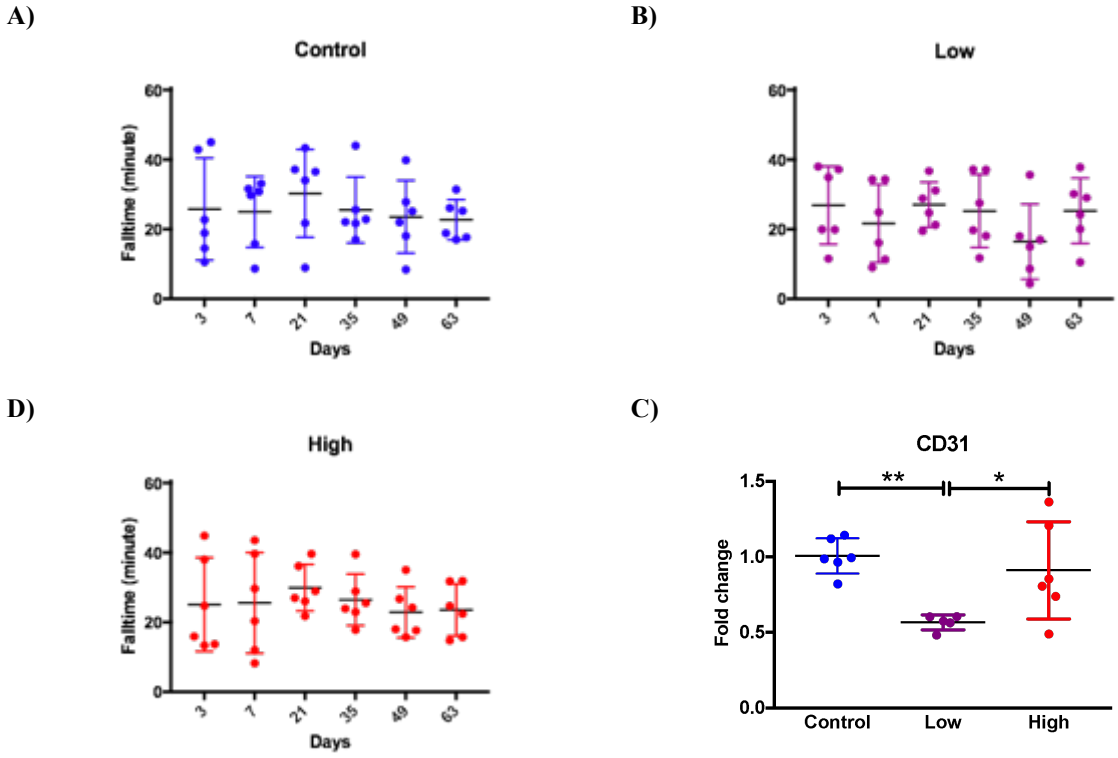

Figure 3.3: (A-C) DIGT *Falltime* measured for three groups: control (saline), low (25 µmol/kg body weight) and high (50 µmol/kg body weight) NaHS dosages (n=6 per group). All groups undergo twice daily injections for the first 28 days followed by 35 days without injections (day 28 to 63). No statistical differences in *Falltime* were detected between groups. (D) Gene expression of the endothelial cell marker CD31 after 63 days of implantation. Data is plotted as mean with the standard error of mean; one-way ANOVA with a Tukey post-hoc test was used to test statistical differences, $p<0.05$(*)

Histological analysis of CD31 expression shows a similar trend at the protein level (Fig. 3.4). Here, CD31-positive vessels were counted in each sample. While the control mice had a mean vessel area density of 40.5 ± 7.5 blood vessels per mm^2 of scaffold, both the low and high treatment groups showed significantly decreased values of 15.0 ± 2 and 18.7 ± 8.3 blood vessels per mm^2 of scaffold, respectively. These results indicate that the vascularization inside the devices is negatively affected by the H_2S administrations.

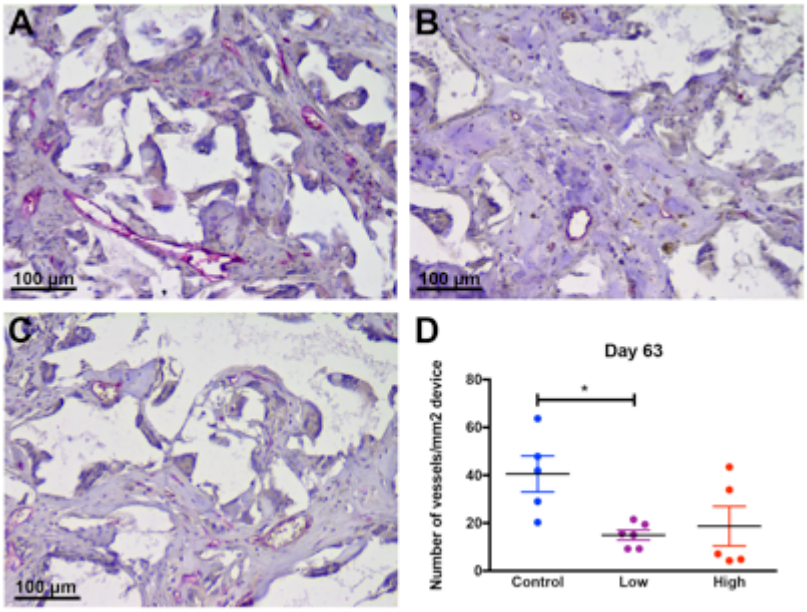

Figure 3.4: Histological analysis of blood vessels after 63 days of implantation. Blood vessels in the control (A), low H_2S dosage (B), and high H_2S dosage (C) treated groups were stained by using the endothelial cell marker CD31 (pink color). (D) The number of vessels per area (mm^2) in each device was calculated and mean with standard error of mean are plotted. A statistical analysis was carried out using a one-way ANOVA with a Tukey post-hoc test, $p < 0.05$ (*)

3.3.2 PDMS devices vascularization over eight weeks

OSTs were calibrated individually at different oxygen levels of 160, 76, 38, and 0 mmHg. They were matched in groups of three based on their lifetime values and inserted into the PDMS devices (Fig 3.5A). Each device, containing three OSTs is then calibrated at similar oxygen

levels prior to implantation. Figure 3.5B shows a step change in lifetime values with changing the inserted gas oxygen concentration. A custom written MATLAB code calculates the average lifetime values (τ) at each oxygen concentrations (PO_2) and the mathematical relationship between τ and PO_2.

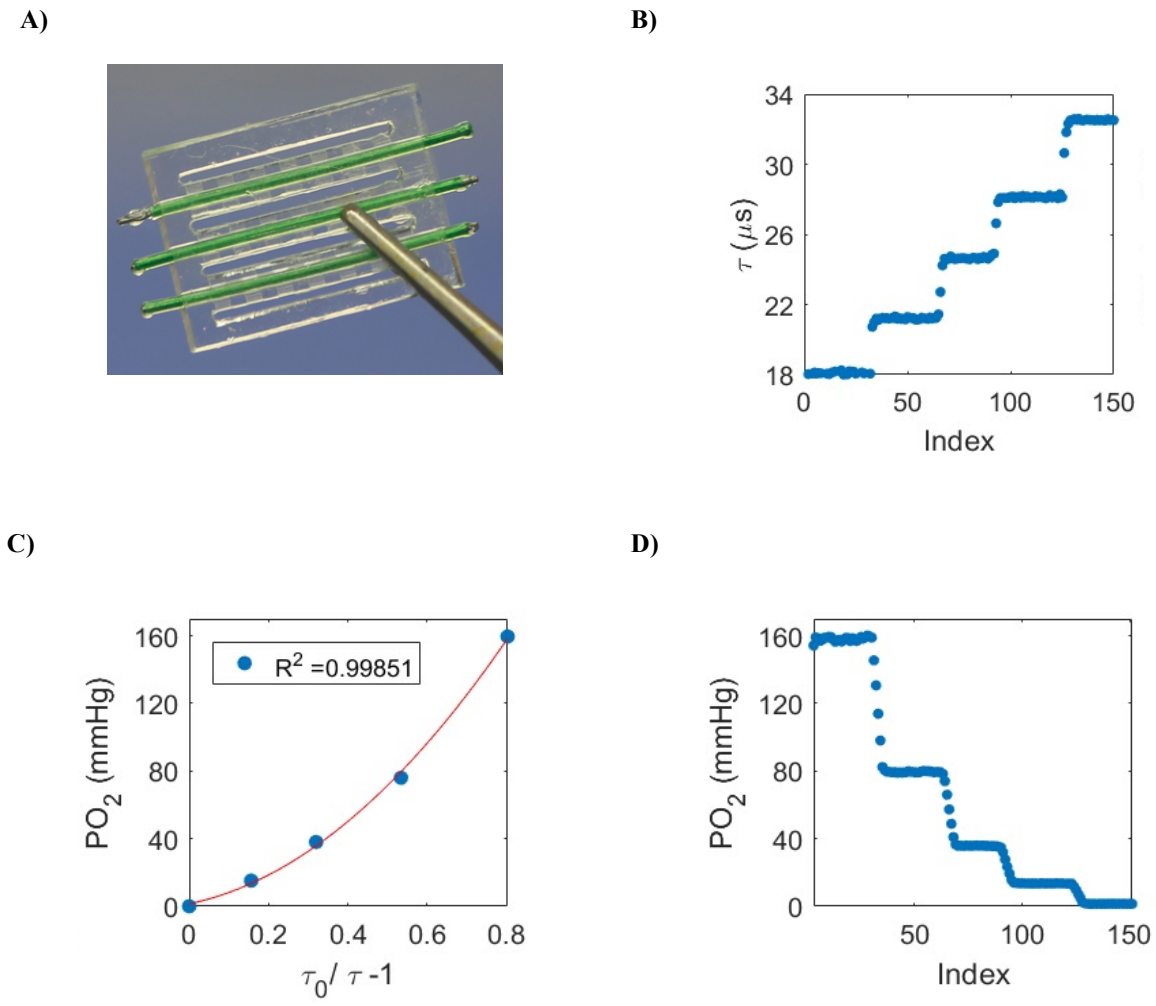

Figure 3.5: OST calibration of device prior to implantation. (A) three oxygen sensitive tubes with matching lifetime values are inserted inside PDMS devices. (B) the PDMS devices are calibrated at 160, 76, 38, 15.2 and 0 mmHg in order. C) Custom written MATLAB code finds the average lifetime values at each oxygen plateau and finds a mathematical fit between τ and PO_2. The converted oxygen values from lifetime based on the mathematical fit matches the inserted oxygen level, validating the conversion technique.

Prior to implantation, the advantages of using phosphorescence emission decay over fluorescence intensity of oxygen sensitive dyes is studied. Both such characteristics of porphyrin

dyes have been used in oxygen sensing [76]. Using phosphorescence characteristics aims to make the non-invasive monitoring independent of the signal amplitude changes. Therefore, scattering of light and reduction of its intensity due to passing through the medical device and its surrounding tissue, and possible misalignment of the oxygen probe over the skin of animal, would not change the signal analysis and oxygen measurements. For this study, an experiment is designed in which a PDMS device inserted with three OSTs is placed inside a glass chamber directly above the oxygen monitor. The probe is then moved in the x direction (parallel to length of OST). The emission decay is recorded at 2 mm increments and the average fluorescence emission intensity and calculated lifetime (τ) values of ten measurements is reported. Figure 3.6 shows that increasing distance results in reduced signal intensity, however the calculated average lifetime value remains relatively constant for up to 10 mm misalignment, which is close to the length of OSTs.

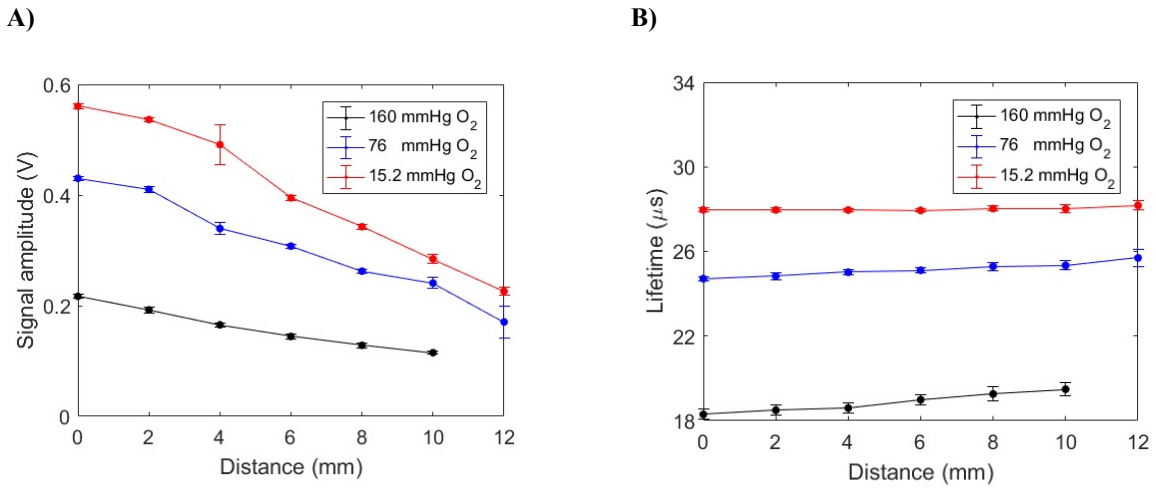

Figure 3.6: Movement of the probe shows that (A) misalignment reduces the emission intensity in all three oxygen levels of 160, 76 and 15.2 mmHg, however, the calculated average lifetime (B) values remain relatively constant. This experiment validates the advantage of using emission decay lifetime values for *in vivo* monitoring oxygen partial pressure.

After implantation DIGT measurements were performed on days 3, 7, 14, 21, 28, 35, 42, 49 and 56 (refer to *3.2.8* for description of DIGT). A DIGT graph converted to PO_2 values using the custom written MATLAB code and calibration is shown in Figure 3.7A. The time period in which the animal is breathing 760 mmHg PO_2 is used as metric for quantifying the oxygen dynamics. This period corresponds to a drop in calculated lifetime values (with increasing PO_2) and is named *Falltime.* Figure 3.7B shows the all the calculated *Falltime* values for every animal and timepoint.

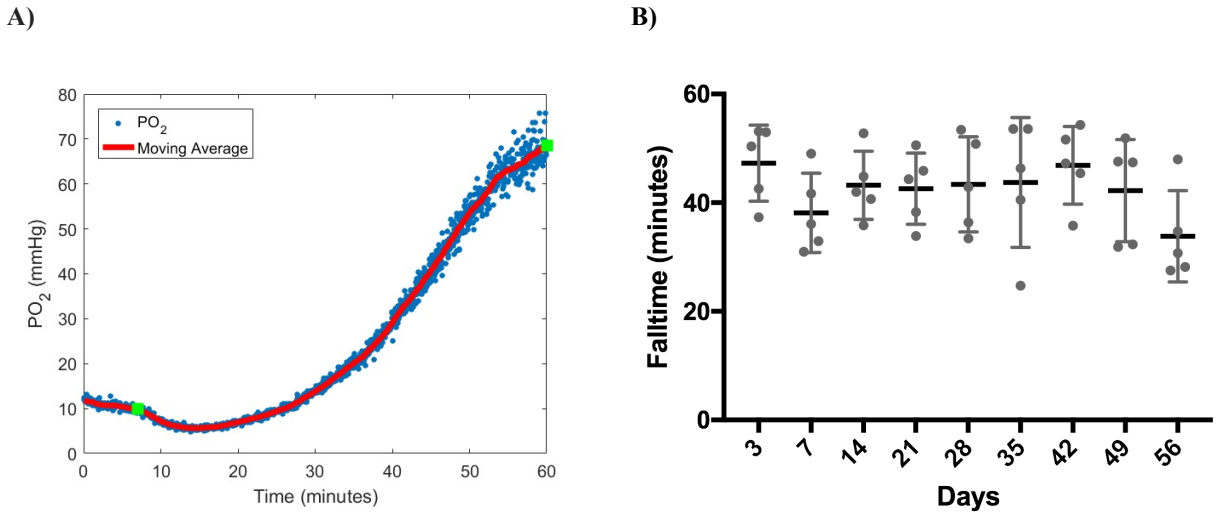

Figure 3.7: (A) DIGT test after conversion of lifetime values to PO_2 shows an increase in device oxygenation. The green boxes indicate the period in which the animal is breathing 760 mmHg, the elapsed time in this period is defined as *Falltime.* (B) *Falltime* values calculated after DIGT test on all five animals, each data point representing a single DIGT test. No statistical differences in *Falltime* values were detected between different timepoitns.

The devices are explanted on day 58. Immunostaining for CD31 and αSMACD31 and αSMA confirms the presence of new vasculature inside the devices. Histological analysis performed on vertical slices of the PDMS devices confirms the presence of blood vessels inside the openings of the connecting microchannels (Fig. 3.8).

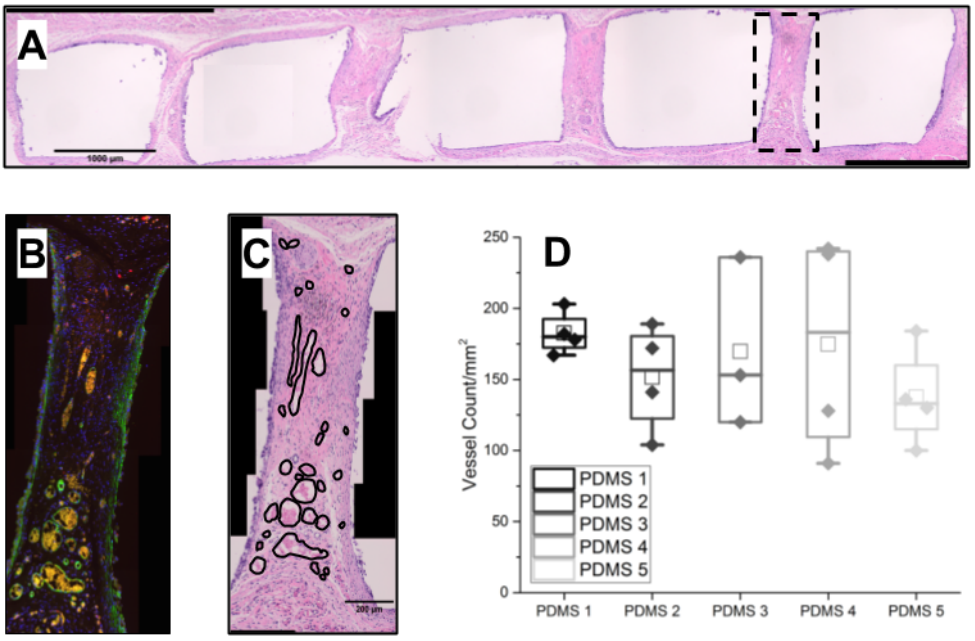

Figure 3.8: Histology results of slit tissue within PDMS devices after 8 weeks of implantation. (A) H&E staining of a vertical view of the opening tissue surrounding the device. (B) A zoomed in view of immunostaining of the same opening tissue for αSMA (green) and CD31 (red) shows a vascularized area (C) Black outlines were hand drawn on H&E images to get vessel counts per slit area. (D) Quantification of vessel count within the openings tissue of PDMS devices. The vessel count for all 5 devices showed similar values that were not significantly different from each other (p=0.7).

3.4 Discussion

The success of subcutaneously implanted cellular therapy devices depends on the ability to transfer nutrients and oxygen to implanted cells. It is shown that implantation of such devices can trigger a series of host reactions at the implantation site, such as chronic inflammatory response, granulation tissue development, foreign body reaction, and fibrosis and fibrous capsule development [77-82]. Invariably, this foreign body reaction can cause formation of diffusional barriers that can result in lower availability of nutrients and importantly oxygen within the implanted devices. This low availability can then result in reduced functionality of the cells and formation of hypoxic conditions which ultimately can lead to cell death and device failure [83]. It is therefore necessary to ensure the availability of oxygen and nutrients through engineering

subcutaneous devices capable of vascularization. For such vascularization purposes, porous biomaterials as well as three dimensionally designed implants that simulate vascularization have been used as subcutaneous medical devices in the field of tissue engineering [29, 69, 71, 84]. The structure of implants allows blood vessel infiltration and thereby reduction of diffusional distances between the neovasculature and the cells. Although several techniques such as ex vivo culturing with endothelial cells and addition of angiogenic growth factors have shown to increase the vascularization in such medical devices, the effectiveness of angiogenesis in these approaches is limited without having an appropriate structure [85-87].

In this study, the rate of vascularization and oxygen availability inside porous PDLLCL devices implanted in animals that undergo H_2S administration are investigated. The PDLLCL devices used in this study have already shown success in preserving functionality of pancreatic islet cells after subcutaneous implantation, which resulted in achieving normoglycemia in type 1 diabetic animals [71, 88]. Here the effects of the proangiogenic factor H_2S on the rate of vascularization of the PDLLCL devices is investigated. H_2S has previously shown to stimulate endothelial proliferation and migration as well as the development of a new vasculature within Matrigel constructs implanted subcutaneously [74]. The results from the non-invasive optical measurements to assess the level of vascularization *in vivo*, showed no significant differences between the control and H_2S administered groups over the 63 days period of the study. Interestingly, histological and gene expression analysis indicate that H_2S administration may have resulted in lowered formation of neovasculature, an observation not reflected in oxygen dynamics between treatments groups and across days. This suggests that any differences in the extent of vascularization may not be large enough to elicit observable changes in oxygen transport dynamics. The findings indicate that the potentiation of vasculature growth by

administration of H_2S in Matrigel [74], is not observed for the PDLLCL devices. A previous study by Cai et al. (2007) showed improved angiogenesis in a Matrigel plug after 7 days of intraperitoneal injections of NaHS [74]. The mice in the current work were treated mice for 28 days with NaHS, indicating that long-term treatment with H_2S may not significantly affect the vascularization. Further, Dufton et al. [89] suggest that the administration of hydrogen sulfide using NaHS can result in an increased inflammatory response and triggering of TNF-α formation. Such inflammatory response caused by the injections during the first four weeks of implantation, which is also accompanied by foreign body response, may then result in hampering the proangiogenic characteristics of the H_2S.

In the second study, vascularization inside developed PDMS devices was investigates. The histological analysis and immunostaining, confirm the presence of newly grown blood vessels. However, the oxygen measurement do not show significant changes in the oxygen dynamics within the implanted PDMS devices over the 58 days period of the study. This observation may be due to different induced foreign body responses in each animal. The results indicate that including histological analysis at different timepoints can provide a quantitative understanding of the vascularization rate, which can potentially be help with better understanding the changes in oxygen transport dynamics measured by the developed non-invasive technology.

In summary, this chapter shows that the subcutaneously implanted PDMS devices become vascularized, however the oxygen dynamics show no significant changes over time. This may be due to differences in foreign body responses. Explantation at different timepoints as well as repeating the experiments on diabetic animals with an added step in which the OSTs are removed after a period of time and then the devices are inserted with pancreatic islets, can shed

light on the relationship between the monitored oxygen dynamics and vessel growth. Furthermore, the described investigations show that PDLLCL devices become vascularized independent of H_2S treatments. This may indicate that material properties of the PDLLCL, device geometry, and pore characteristics play roles in governing vascularization, a hypothesis supported by previous work and consistent with current thinking in area of biomaterials.

CHAPTER 4: Composite matrix for photonic analyte biosensors

4.1 Introduction

Biosensor technology has advanced rapidly in the past few decades and can soon play a key role in providing powerful analytical tool with major applications in medicine. A biosensor can be defined as a compact analytical device or unit incorporating a biological or biologically derived sensitive recognition element integrated or associated with a physio-chemical transducer [90]. There are three main parts in a biosensor: (1) the biological recognition elements that differentiate the target molecules in the presence of various chemicals, (2) a transducer that converts the biorecognition event into a measurable signal, and (3) a signal processing system that converts the signal into a readable form [91, 92]. The molecular recognition elements include receptors, enzymes, antibodies, nucleic acids, microorganisms and lectins [93, 94] Today's biosensing market is mostly dominated by glucose biosensors also known as CGMs (continuous glucose monitor). CGM has shown to provide an improved glycemic control in diabetic patients [95]. This biosensor eliminates the need for multiple daily blood measurements and importantly provides a continuous reading throughout the period of use, resulting in better understanding and more collected information regarding the changes of glucose levels in an individual patient. Information collected by this technology can then used by the diabetic patient to better administer insulin and therefore achieve a tighter glycemic control. Another technology that is currently aiming to join the CGM is automatic insulin pumps. The combination of both technologies is named Artificial Pancreas (AP) [95, 96]. In an AP, continuous glucose monitor (CGM) provides a steady stream of information that reflects the patient's blood glucose level using a sensor subcutaneously implanted under the skin. A small transmitter sends the

information to a receiver. CGM is providing an estimate of the blood glucose level, its direction and rate of changes. After the information is received by a receiver it then analyzed through a series of mathematical calculations, based on which a dosing signal is then sent to the automatic insulin pump. This algorithm can run by a laptop, smartphone or even the insulin pump itself. Based on the information provided, the pump then injects the insulin to the tissue under the skin. The goal of this technology merge (CGM and insulin pump) is to provide hands free continuous administration of insulin without the possible risks of individual's decision making error. An advanced AP aims to process and analyze multiple complex parameters including food intake, physical activity, insulin dosing, insulin sensitivity and previous observations on glucose level responses to achieve a perfect glycemic control in type 1 diabetes (T1D) patients, importantly for those who find the process of manual glucose measurement and insulin injection more challenging, for example diabetic children.

The current state of AP technology however is somewhat limited in providing ample information for accurate glycemic predictions that are needed for perfect insulin administrations. For instance, exercise in individuals with T1D can affect the blood glucose level, leading to either hypoglycemia or hyperglycemia based on its type and intensity [97, 98]. Moderate physical activity has shown to result in an increase in the body glucose uptake (glucose disposal rate) , therefore reducing the blood glucose level [99]. In healthy individuals this decrease is balanced by a decrease in endogenous insulin secretion to maintain euglycemia, however in T1D patients no such change in endogenous insulin occurs, causing a drop in glucose level and therefore hypoglycemia [100-102]. Another type of glycemic change induced by physical activity is after the individual passes their anaerobic threshold. Anaerobic threshold is reached, when high intensity of the exercise requires quickly available energy, and production of aerobic

ATP is no longer sufficient [101]. During such intense activity the body depletes its stored energy, resulting in an increase in blood glucose level that can exceed the rate of its uptake (glucose disposal rate) [103]. Similarly, in healthy individuals this glucose increase can be balanced by endogenous insulin secretion, however in T1D patients it may lead to hyperglycemia [101, 104]. The possibility of experiencing fast changes of glucose level in opposing directions can make regular exercise difficult for diabetic patients, discouraging them from performing physical activities [105]. This can be detrimental in their overall health, as it has been shown that regular exercise can improve metabolic control, body weight, blood pressure, insulin sensitivity and reduce the risk of vascular diseases [106, 107].

A promising technique to create a more predictive algorithm for insulin administration for AP is including additional metrics that can indicate occurrence, length and intensity of physical activities. Currently, blood pressure and heart rate have been used for quantifying the exercise, however these inputs are not particularly reliable as non exercise factors can significantly affect them [108, 109]. This work explores continuous measurements of lactate as a new promising metric for advancing the artificial pancreas in prediction of glucose level, after and during exercise. Blood and plasma lactate have been used for decades as standard measure of exercise because they strongly correlate to exercise intensity and duration [37, 110, 111]. This correlation exists because glycolysis, which happens during exercise, results in production of lactate in the process of carbohydrate metabolism in the absence of oxidative phosphorylation [112]. As the exercise intensity increases the lactate clearance cannot match its production and therefore the lactate level increases. While a lactate build up is primarily indicating an intense activity, it has shown to correlate with the intensity in ramped efforts tests [113]. Lactate measurements can also provide information regarding whether the individual has reached the

anaerobic threshold, and if instead of hypoglycemia a hyperglycemic period will be likely to occur.

The primary focus of this chapter, is development of long lasting, biocompatible and sensitive glucose and lactate sensors that can be used in an Artificial Pancreas. However, it is worth noting that developed lactate sensors can have applications beyond the scope of diabetes. For example, it is known that lactate levels rise during critical illness conditions due to increased reliance on anaerobic metabolism for survival. Such rise can indicate conditions such as hemorrhage, sepsis, cardiogenic shock, and trauma [114-116]. Medical research has provided evidence that an upcoming shock can be predicted by changes in body lactate levels. Additionally, literature suggests that a lactate guided medical therapy can reduce the chances of mortality [117]. Continuous lactate monitor (CLM) can therefore be used in treatment of critically ill patients in intensive care unit (ICU).

The developed biosensors in this chapter function based on enzymatic reactions with glucose and lactate analytes, during which oxidase based enzymes catalyze a reaction that consumes both oxygen and the analyte, resulting in decreased oxygen levels. The enzymes used in the sensors are glucose oxidase (GOX) and lactate oxidase (LOX) and their biochemical reactions are as follows [118, 119]:

- *Glucose Oxidase (GOX): glucose* + $O_2 \rightarrow$ *gluconic acid(GA)* + H_2O_2
- *Lactate Oxidase (LOX): L-Lactate* + $O_2 \rightarrow$ *pyruvate* + H_2O_2

The oxygen level change, can be measured and monitored by technology developed and described previously (*3.2*). A comparison between the recorded oxygen change in the enzyme

vicinity and the surrounding environment can be used to measure the rate of oxygen consumption and calculate the analyte concentration.

The main focus of this study is finding a new method to immobilize the enzymes to achieve long lasting, active glucose and lactate sensors that operate based on monitoring the luminescence of metal porphyrin dyes. In this developed technology the sensor reagents and dye particles are attached to a light source that can provide excitation to the dye. In the current technique, the light source is light emitting diodes (LEDs) soldered onto a small narrow flexible circuit that can be inserted subcutaneously and can flash and excite the embedded luminescence dye. The emission of the dye is then recorded using a detector circuit placed above the skin and within the path of the emission light. As was previously described (*3.2*) the phosphorescence characteristics of such oxygen sensitive dyes change with different levels of oxygen, exhibiting longer decay times in lower surrounding oxygen levels [76]. The oxygen sensitive dyes selected for this study have absorption and emission in the red and near infrared range of the spectrum, which has shown to have better penetration through the tissue [76]. As mentioned, this technology relies on detection of oxygen changes within the reagents of the sensors, requiring that the enzymes and the dye particles are in proximity of each other.

This chapter describes invention of a composite material for embedding the enzyme molecules into a dye coated porous structure, utilizing physical entrapment within pores of an infused photocurable hydrogel. This technique aims to maintain enzyme activity with avoiding formation of covalent bonds between the enzyme molecules and their surrounding matrix. The invention also aims to provide a close proximity between enzyme molecules and the luminescence oxygen sensitive dye particles, and therefore result in a higher sensitivity to changes in analyte levels. To finalize the formulation of the invented composite material,

multiple iterations were fabricated using, porous reinforcement constituent of different thicknesses, oxygen sensitive dyes of different emission decay ranges, photocurable hydrogels of different molecular weights, different enzyme to hydrogel ratios, and also additions of different levels of Catalase enzyme. To accelerate the time for characterizing all the different formulations, a system capable of performing 16 simultaneous calibrations was developed.

After narrowing down the formulation, the developed composite material successfully addressed and solved the key following challenges in the current state of biosensor technology, (1) reduction of active enzyme-dye media thickness to reduce the size of an insertion needle, thus reducing the pain of insertion, (2) maintaining high activity and stability of the enzymes overtime, both during operation and storage, (3) showing sensitivity within physiological ranges of analytes and oxygen tissue concentrations, (4) demonstrating fast response times of less than five minutes to changes in analyte concentration (5) improving the mechanical and adhesion stability of the luminescence dye/enzyme component, (6) enhancing the luminescence dye-enzyme component attachment to a surface, (7) exhibiting repeatable results in sensors made from the same composite material and (8) improving the fabrication process for large scale manufacturability.

4.2 Materials and methods

4.2.1 Composite film fabrication

Enzyme molecules, Glucose Oxidase (Sigma aldrich, USA) with 135.2 unit/mg activity and Lactate Oxidase (Toyobo, Japan) with 106 unit/mg activity were used in this study. Different weights of the enzyme molecules are mixed into different types photocurable Polyethylene glycols (PEG). Different PEGs used in this study include, Polyethylene glycol dimethacrylate

with molecular weights of 200 and 400 (Polysciences, USA), and Polyethylene glycol monomethacrylate with molecular weights of 200 and 400 (Polysciences, USA) as well as trimethylolpropane ethoxylate with molecular weight of 428 (Sigma Aldrich, USA). In some mixture formulations Catalase (MP Biomedicals, USA) is also added to the mixture. The mixture is stirred overnight at room temperature in a dark environment to achieve homogeneous distribution of enzyme particles. Photoinitiator agent 2,2 Dimethoxy-2-phenyacetophenone (Sigma Aldrich, USA) is then added with the ratio of 20 mg/ml and the mixture is stirred for another hour. A typical relative ratio of mixture is : 1 ml PEG, 200 mg enzyme, 20 mg photoinitiator and 10 mg Catalase. During this study to achieve the best formulation different variations have been tested, as explained in section *4.3.3*.

In parallel a luminescence oxygen sensitive dye is used to coat a porous Teflon (PTFE) membrane. The porosity in the PTFE membranes were introduced by the supplier's expansion, or electrospinning of PTFE fibers. Different types of PTFE sheets including, electrospun PTFE membranes with thicknesses 10 , 25 and 60 μm (Zeus, USA) as well as expanded 50 μm PTFE (Sterlitech, USA) were used in this study. The oxygen sensitive dye used are platinum (II) meso-Tetraphenyl Tetrabenzoporphine (PtTPTBP) (Frontier Scientific, USA) and Pd (II) meso-Tetraphenyl Tetrabenzoporphine (PdTPTBP) (Frontier Scientific, USA) with high absorptions at 614 and 628 nm and maximum emissions at 770 and 800 nm respectively. The photosensitive dye is mixed with polystyrene with molecular weight of 2500 (Sigma, USA) and the mixture is then dissolved in chloroform (Sigma, St. Louis, USA). The ratio for the dye mixture is: 1 mg dye, 15 mg polystyrene and 225 μl chloroform. The PTFE sheet is then coated on both sides with the dye-containing solution, this coating can be done through different processes including but not limited to knife coating, spraying, convection and etc. The dye coated sheets are then placed

in a dark environment overnight to fully evaporate out the chloroform. The polystyrene-dye-PTFE sheet is then plasma treated on both sides, each for a duration of approximately 5 minutes or less to increase the surface hydrophilicity. The PEG-enzyme mixture is then knife-coated onto both sides of the sheet. The coated porous sheet with the impregnated enzyme-PEG mixture is then placed in between two glass substrate and pressure is applied to fully force the mixture to penetrate the coated sheet as well as limit the final thickness of the composite. The glass substrates are then placed under UV lamp for duration of 5 minutes on each side facing the UV light. The polymerization time can change based on the type of photoinitiator or hydrogel used, the thickness of the film, the power and wavelength of the UV lamp and so on. The glass substrates are then removed and separated from the composite sheet. Oxygen reference sheets without enzyme or hydrogel is also fabricated by only coating the porous PTFE sheet with a porphyrin dye.

4.2.2 Flexible circuit sensor calibrations

The Botvinick lab sensor technology comprises a custom made flexible circuit with light sources placed on it. In some variations small LEDs are soldered onto the circuit, in other variations the LEDs are positioned on the circuit by the manufacturer. The emission wavelength of the LEDs are within 620 to 630 nm to match the absorption emission of the dyes. The current flexible circuits are equipped with two LEDs for the attachment of one analyte sensor sheet and one oxygen reference sensor sheet. The fabricated sheets (explained in *4.2.1*) are cut into small pieces and attached to LEDs using biocompatible adhesives Loctite 4541, or Loctite 4981 (Henkel, USA). The LED surfaces were knife coated with the adhesive and the cut sheets were pressed to adhere. The flex circuit was kept in a dark environment for 24 hours prior to first use

to allow the adhesives to fully cure. After the curing process is complete the prepared flex circuits were connected to a developed sensor. The developed sensor was designed and made previously at Professor Botvinick lab [120] and it comprises the explained flexible circuits as well as a receiver. The receiver contains an off the shelf amplified photodiode and an optical filter to only pass the near infrared emitted light from the dye. The sensor system is operated by myRIO and LabVIEW (National Instruments, Austin) software. During the operation LEDs are turned on to excite the dye and quickly turned off. The LEDs for each sheet turn on in sequence so that the detector records light only from one sheet at a time. Immediately following the LED turning off, the emission decay from the oxygen sensitive dye was recorded by the photodiode for 200 μs for sensors made of PtTPTBP and 500 μs for sensors made of PdTPTBP. The sampling rate is set to 500 kHz. The data was analyzed in LabVIEW (National Instruments, Austin) in real time and later on by MATLAB (MathWorks, USA). For each timepoint, 25 rapidly acquired decay measurements were averaged. The averaged recorded emission decay data was used to calculate the decay lifetime values from both the enzyme-containing and the oxygen reference (no enzyme) sheets. The analyte reacts with oxygen, thus depleting oxygen relative to the reference. Analyte concentration was computed by relating these two oxygen levels. For *in vitro* calibrations, the tip of the flexible circuit is inserted inside a transparent cylindrical tube with a channel to change the containing solution and inlet/outlet for gas insertion. The calibrations are performed by inserting a series of solutions containing different analyte concentrations, for example ranging from pure 1xPBS to 1, 3, 4, 5, 10, 15, 16, 20 and 22 mM. The analytes solutions are made from the powdered D-(+)-Glucose (Sigma, USA) and L-(+)- Lactic Acid (Fisher bioreagents, USA). All calibrations are performed while a gas with certain level of oxygen is inserted into the cylindrical tube.

4.2.3 Multiple calibration system

The multiple calibration system was designed for simultaneous calibration of 16 samples of composite sheet adhered onto a developed chamber setting. The calibration system comprises a 4x4 array of LEDs (615 nm peak excitation) soldered onto custom designed PCB board. The PCB board was previously designed at Professor Botvinick lab. The setup is developed to hold a transparent chamber vertically in place between the LEDs on the PCB and a sliding photodetector receiver. The receiver circuit contains a lens to direct the light, optical filter to only pass the near infrared emission of the dye and an off the shelf amplified photodiode. The system is made using optomechanical hardware (Thorlabs, USA) to keep components well aligned. The developed chambers comprise 16 films adhered on the inside of the chamber, onto a transparent polycarbonate substrate with dimension of 25 mm x 75 mm. The sensor sheets are cut to match the dimensions of the LEDs on the PCB board. Importantly, prior to adhesion to substrate, the sensor sheets are perfectly spaced to match the distances in the 4x4 LED array. The sheets are then adhered to the polycarbonate substrate using Loctite 4981 (Henkel, USA). After adhesion, the polycarbonate-sensor is kept in dark environment for 24 hours for the adhesive to fully cure. Afterwards a rectangular rubber frame is adhered to the polycarbonate sheet with the 4x4 sensors sheets facing inside. The rubber frame has the dimensions of 25 mm x 75 mm on the outside and 15 mm x 65 mm inside. The thickness of the frame is 2 mm. The chamber is closed with a glass slide on the opposite side (25 mm x 75mm) and sealed closed. The attachments and sealing are performed using Loctite 4981 (Henkel, USA). Afterwards the chambers are kept for 48 hours in dark environment for the adhesives to fully cure. Each chamber is equipped with a channel for fluid exchange as well as gas inlet and outlet. This is accommodated using three needles inserted into chambers through the rubber frame. Two needles on top and one the

bottom, with the bottom one acting as the fluid exchange channel. The calibrations are performed after 48 hours of incubation at 1x PBS and 37℃. During the calibrations a series of solutions containing different analyte concentrations, for example ranging from pure 1x PBS to 1, 3, 4, 5, 10, 15, 16 , 20 and 22 mM are inserted into the chamber. All calibrations are done while a gas with certain level of oxygen is continuously inserted into the chamber. During calibrations LEDs flash in sequence and luminescence from each attached sheet is collected using a photodetector (similar to *4.2.2*). This process is controlled by myRIO and LABVIEW (National Instruments, Austin) and the collected information is analyzed by LABVIEW in real time and later on by MATLAB (MathWorks, USA).

4.2.4 Photodetector and lifetime measurements

The photodetector circuit comprises an optical bandpass filter mounted onto the detector to reject the LED wavelengths while passing the dye emission. For each oxygen measurement an LED flashes 25 times at 1% duty cycle (100 µs on, 10200 µs off) to excite the oxygen sensitive porphyrin dye. The emission of the dye after each flash is passed through an optical filter and onto the photodiode. Photodiode electrical current is converted to voltage by an operational amplifier and sampled for 200 µs for sensors made of PtTPTBP and 500 µs for sensors made of PdTPTBP. The sampling frequency is set to 500 kHz using a myRIO data acquisition module (National Instruments, Austin). LED and data acquisition timing is controlled by LABVIEW (National Instruments, Austin). The dye continues to emit light after the end of each LED emission period with a decay that can be modeled as exponential. See equation 4.1.

$$V = V_0 e^{(\frac{-t}{\tau})} \qquad (4.1)$$

where V is the detector voltage, V_0 is the voltage at the start of the decay, t is the time in seconds after the end of LED emission, τ is the lifetime parameter reported in seconds. Lifetime values were computed from emission waveforms using the fit function in MATLAB (MathWorks, USA) configured for nonlinear least squares regression. The average for all 25 cycles is hereafter reported as lifetime (τ). The porphyrin dye emission is quenched by oxygen and consequently lifetime values (τ) decrease with increasing PO_2. The mechanism in which the oxygen quenches the dye is not yet completely clear, however independent of the predominant mechanism the kinetics of quenching is very well described by Stern-Volmer equation. See equation 4.2.

$$\frac{I_0}{I} = \frac{\tau_0}{\tau} = 1 + k_q \tau_0 pO_2 = 1 + k_{sv} pO_2 \qquad (4.2)$$

Where I and I_0 are the luminescence intensities in the presence and absence of the quencher, τ and τ_0 are the lifetime of the dye in the presence and absence of the quencher, k_q is the bimolecular quenching constant and k_{sv} is the Stern-Volmer quenching constant. Dye emission is quenched by the oxygen and consequently, τ decreases with increasing pO_2 [76].

4.2.5 Pilot *In vivo* study

Animal procedures were reviewed and approved by the University of California Irvine (UCI) Institutional Animal Care and Use Committee (IACUC). A rabbit cyanide poisoning model developed by Dr Mathew Brenner's lab was used to test the functionality of the lactate sensors [121]. One pathogen-free New Zealand White rabbit (Western Oregon Rabbit Supply, Philomath, Oregon), weighing 3.9 kg was used in this study. Animal was anesthetized with an intramuscular injection of Ketamine HCl 50mg/kg (Ketaject, Phoenix Pharmaceutical Inc., St. Joseph, MI) and Xylazine 5mg/kg (Anased, Lloyed Laboratories, Shenandoah, IA) and intubated. After the initial injection, a catheter was placed in the animal's marginal ear vein to

administer continuous intravenous anesthesia with Ketamine/Xylazine. Animals were mechanically ventilated (dual phase control respirator, model 32A4BEPM-5R, Harvard Apparatus, Chicago, IL) at a rate of 20 respirations per min, a tidal volume of 50 cc, and inspired O2 concentration of 100%. A pulse oximeter (Biox 3700 Pulse Oximeter, Ohmeda, Boulder, CO) with a probe was placed on the tongue, to measure SpO2 and heart rate. Arterial and venous femoral lines were placed. A lactate sensor was made prior to implantation. The rabbit belly was shaved and an incision was made penetrating to the subcutaneous space. The tip of the flex circuit containing lactate sensing sheet and oxygen reference sheet was inserted subcutaneously under the skin the receiver was placed directly above the sensors tip and fixed in placed with Tegaderm (3M, USA). LEDs of the sensor flashed in sequence and the emitted light was recorded and lifetime values calculated as explained in *4.2.4*. 10 minutes after the data collection, 20 mg of sodium cyanide (Sigma-Aldrich, USA) dissolved in 60 ml of 0.9% NaCl was infused intravenously at 0.33 mg/min (1 cc/min). Cyanide was continuously infused for 30 minutes with 100% oxygen input from the ventilator. Timepoint measurements, which include arterial and venous blood gases, systemic pressures, heart rate, SpO_2, blood lactate concentration and pH were taken after each blood draw. The rabbit's blood pressure was monitored throughout the experiment and euthanasia was administered after 120 minutes of data collection. The animal was euthanized with an intravenous injection of 1.0-2.0cc Euthasol (Virbac, Ft. Worth, TX) through the marginal ear vein catheter and the lactate sensor was retrieved.

4.2.6 Scanning electron microscopy

The surface structure of sheets are studied using scanning electron microscopy (FEI Quanta 3D FEG Dual Beam SEM, Hilsboro,OR). Prior to scanning the sheets are sputter coated with Iridium to a thickness of 5nm. The images were taken with 5 keV.

4.2.7 Statistical analysis

Statistical analysis was carried out in GraphPad Prism (version 7.0d; GraphPad Software, Inc., La Jolla, USA).

4.3 Results

4.3.1 Composite film fabrication

The fabrication process of the composite sheet is demonstrated in Figure 4.1. First the reinforcement constituent which is a porous mesh, for example electrospun PTFE, is coated with an oxygen sensitive dye, for example PtTPTBP or PdTPTBP. The coated porous mesh is then plasma treated to increase surface hydrophilicity. Afterwards a well mixed photocurable enzyme-hydrogel mixture is added to both sides of the coated sheet (described in *4.2.1*). After the addition, the mesh and the enzyme-hydrogel mixture are pressed together using transparent glass substrates to infuse the gel into the mesh. The composite mesh is it then UV polymerized while pressed in between glass substrates to form a mechanically stable dye coated enzyme penetrated sheet.

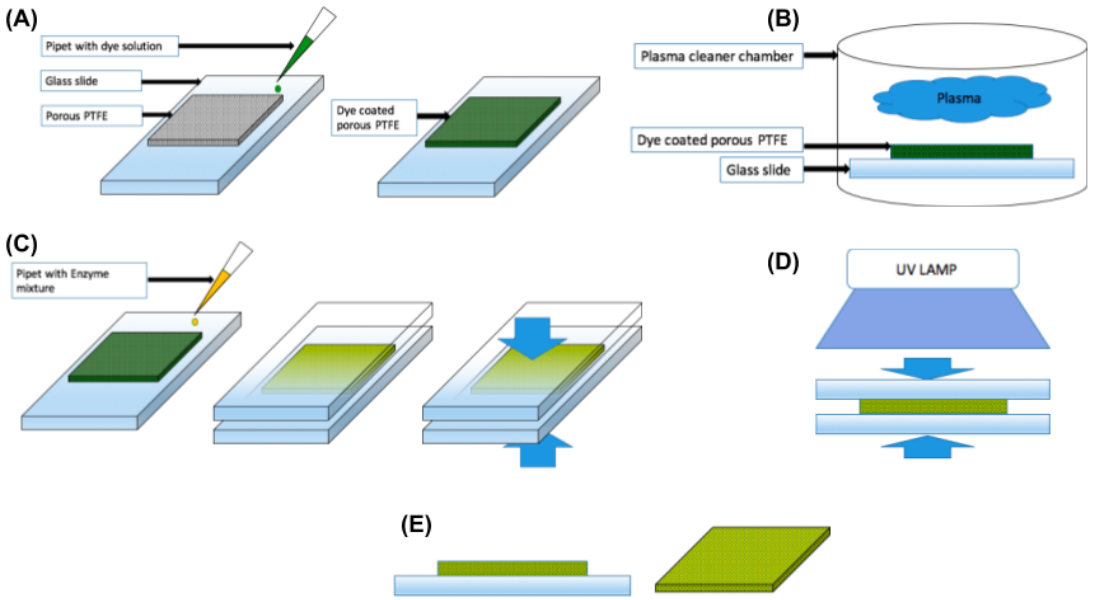

Figure 4.1: Schematics showing the fabrication process of the composite sheet. (A) oxygen sensitive dye solution containing, for example PtTPTBP or PdTPTBP is added to a porous PTFE mesh. (B) The dye coated mesh is plasma treated to increase surface hydrophilicity, (C) a well mixed enzyme-hydrogel mixture is then added to the coated mesh and then the components are pressed between transparent glass substrates. (D) The glass substrates are placed under the UV lamp to polymerize the hydrogel mixture. (E) A solid mechanically stable composite sheet is formed after UV polymerization.

Figure 4.2 depicts the structure of the invented composite, in which fibers of a porous mesh are coated with the oxygen dye and the enzyme mixture is dispersed throughout the structure (Fig. 4.2A). This setting is significantly different from the conventional method of making such sensors, in which dye substrate is placed adjacent to the enzyme mixture in a sandwich layer geometry (Fig. 4.2B). For example, in a porous composite setting there is higher surface area of the dye that is in close proximity with the enzyme, therefore the dye particles better represent the oxygen consuming bioreaction. Whereas, in the sandwich layer geometry some volume of the dye is typically insensitive to the reaction, however it emits light which can result in unwanted background signals.

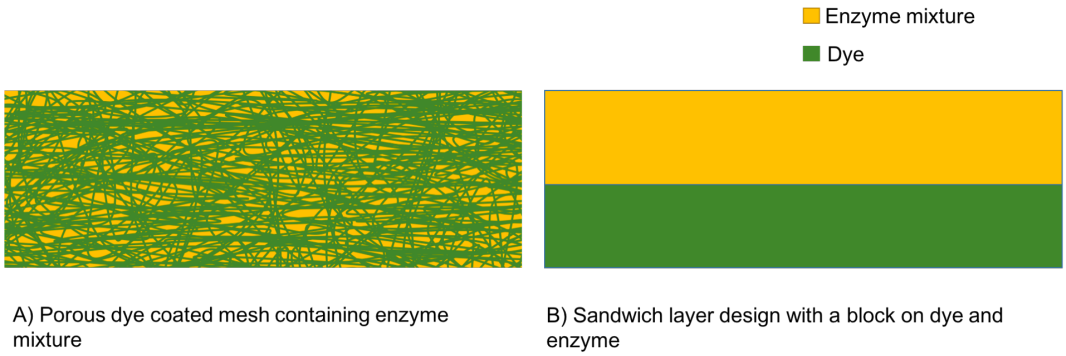

Figure 4.2: (A) The invented geometry showing dye coated fibers and pores that contain the enzyme mixture. (B) Conventional setting in which the dye and enzyme mixture are layered adjacent to each other.

Scanning electron microscopy (SEM) shows the dye particles are homogeneously coating the electrospun and expanded PTFE sheets (Fig. 4.3 A-B). After the addition of the enzyme mixture and polymerization, SEM images show a complete penetration gel mixture inside the porous mesh (Fig 3 C-D)

A)

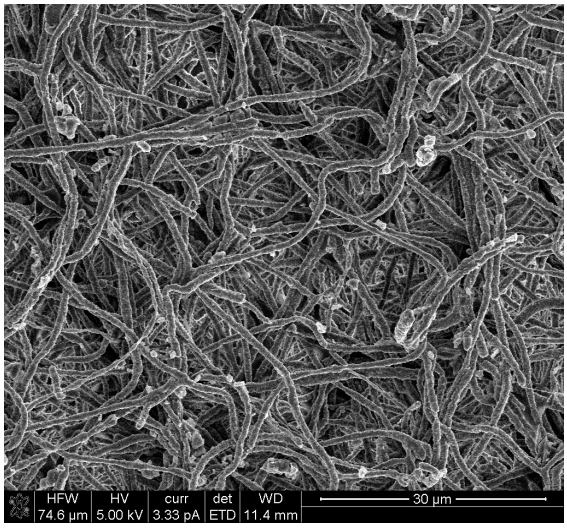

B)

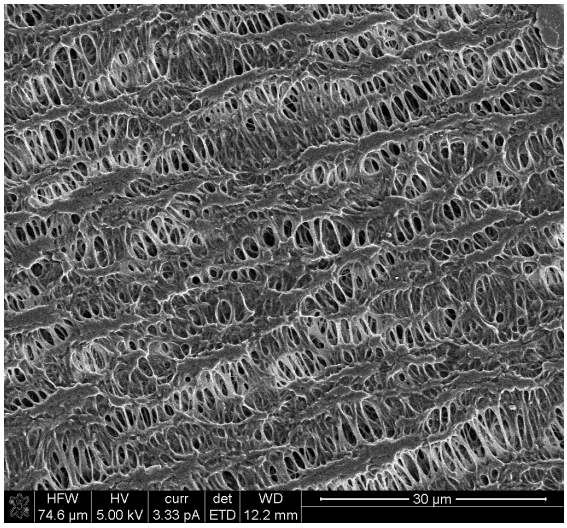

C)

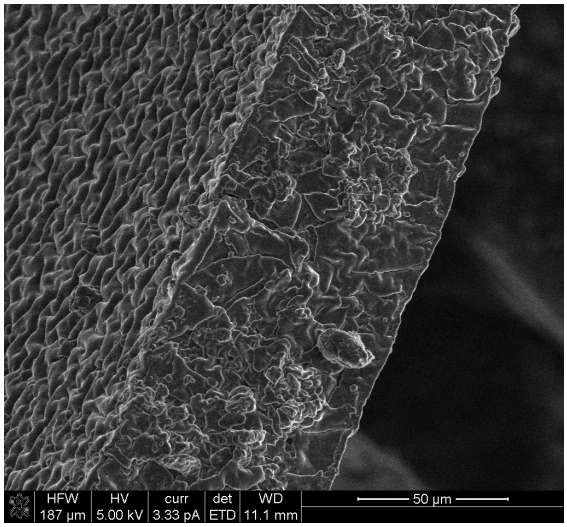

D)

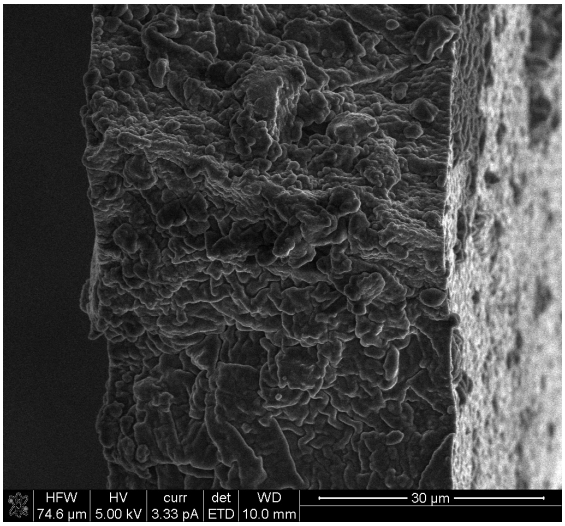

Figure 4.3: Scanning electron microscopy image shows (A) electrospun and (B) expanded PTFE sheets coated with platinum (II) meso-Tetraphenyl Tetrabenzoporphine (PtTPTBP) dye. Enzyme hydrogel mixture is pressed into the porous electrospun (C) and expanded (D) PTFE and photocured to form enzyme-hydrogel interpenetrating solid composite sheets.

4.3.2 Initial calibrations and proof of concept

The first iterations of the composite sheets showed activity in different analyte concentrations. Different types of composite sheets were made at this step and attached to the LEDs of the flexible circuits for calibration. Composite sheets were made using different types of photocurable Polyethylene glycols as well as different types of PTFE sheets (explained in *4.2.1*). The results indicated that composites formed with PEGDM400 (Polyethylene glycol Mn=400) hydrogel showed repeatable results and sensitivity in physiological range of analytes and tissue oxygen concentrations.

The composite sheets were stored dry and tested for their storage shelf life at different timepoints. The results showed that they maintained activity and sensitivity after long periods storage. Figure 4.4 shows a calibration of a lactate sensor made from 200 mg/ml LOX, PEGDM400, 60 µm electrospun PTFE and PtTPTBP Dye, after 5 months of dry storage at room

temperature. In this calibration, the tip of the sensor is placed inside a transparent cylindrical tube and solutions containing different levels of lactate are then injected inside (20, 15, 10, 4 and 1 mM lactate respectively). Throughout the experiment 160 mmHg O_2 is injected into the tube in order to mix the solution and avoid oxygen depletion at the lactate sensor sheet. It is observed that the oxygen reference sheet maintains its calculated lifetime values throughout the experiment, confirming the continued existence of 160 mmHg oxygen in the fluid chamber. The enzyme molecules in the lactate sensor sheet however undergo oxygen consumption after the injection of lactate solutions into the chamber. This oxygen consumption reduces the local oxygen levels and therefore increases the measured lifetime values. The measured lifetime values decrease with injection of solutions that contain lower levels of lactate. The difference between the lifetime values of the lactate sensor and the oxygen reference sheet ($\Delta\tau$) is then measured. In Fig. 4.4C, the average of $\Delta\tau$ at each lactate concentration is used for finding a calibration curve between lifetime values and analyte levels.

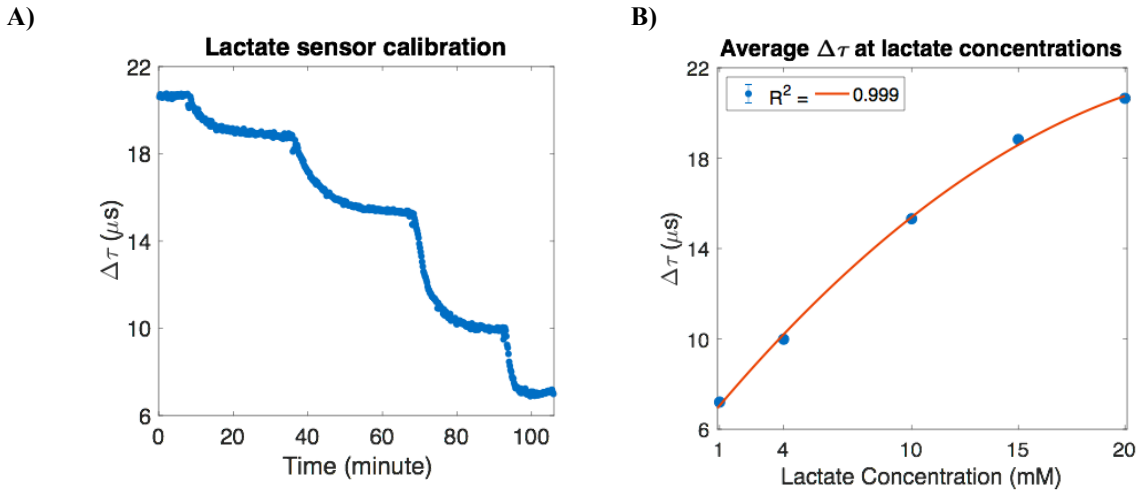

Figure 4.4: Lactate sensor calibration at 22,15,10,4 and 1 mM lactate solutions respectively. (A) The measured $\Delta\tau$ indicates the difference in the oxygen level at the lactate sensor sheet and the oxygen reference sheet. Each plateau indicates the $\Delta\tau$ at each different lactate concentration. (B) using a mathematical analysis the average $\Delta\tau$ at each plateau for different concentrations of lactate is calculated. The average values are then graphed against their corresponding analyte concentrations and fit into a polynomial level 2 model.

The preliminary results showed that composite sheets maintained sensitivity to analytes over a long period of dry storage. This observation indicates that embedding the enzymes into the composite can potentially advance the biosensing technology. The following step is to find the perfect composite formulation with sensitivity throughout the physiological concentrations of analytes as well as tissue oxygen concentrations. Importantly, it is imperative to show that each fabricated sheet has homogeneous characteristics. In other words, sensors created from different sections of each sheet show similar activity and sensitivity to analytes. This aim required the development of a multiple calibration system to accelerate the rate of data collection.

4.3.3 Multiple calibration system development

Multiple Calibration System was designed for simultaneous calibration of 16 composite sheets. This setup increases the rate of collecting information on enzyme activity and analyte sensitivity of the fabricated composites. Figure 4.5 shows the setup comprising a 4x4 array of LEDs soldered onto a custom designed PCB board. The LEDs are controlled through a developed LABVIEW interface in which they flash in sequence and excite the dye on their corresponding aligned sheets. The emission of the dye is then recorded using a photodetector circuit. The system includes optomechanical hardware to align an enclosed chamber to the array of LEDs (Fig. 4.5A). The developed chambers comprise 16 composite sheets adhered to the inside of the chamber. Each chamber includes a fluid exchange channel as well as gas inlet/outlet, to change the analyte solutions and maintain a physiological oxygen concentration throughout the calibration. (Fig. 4.5B).

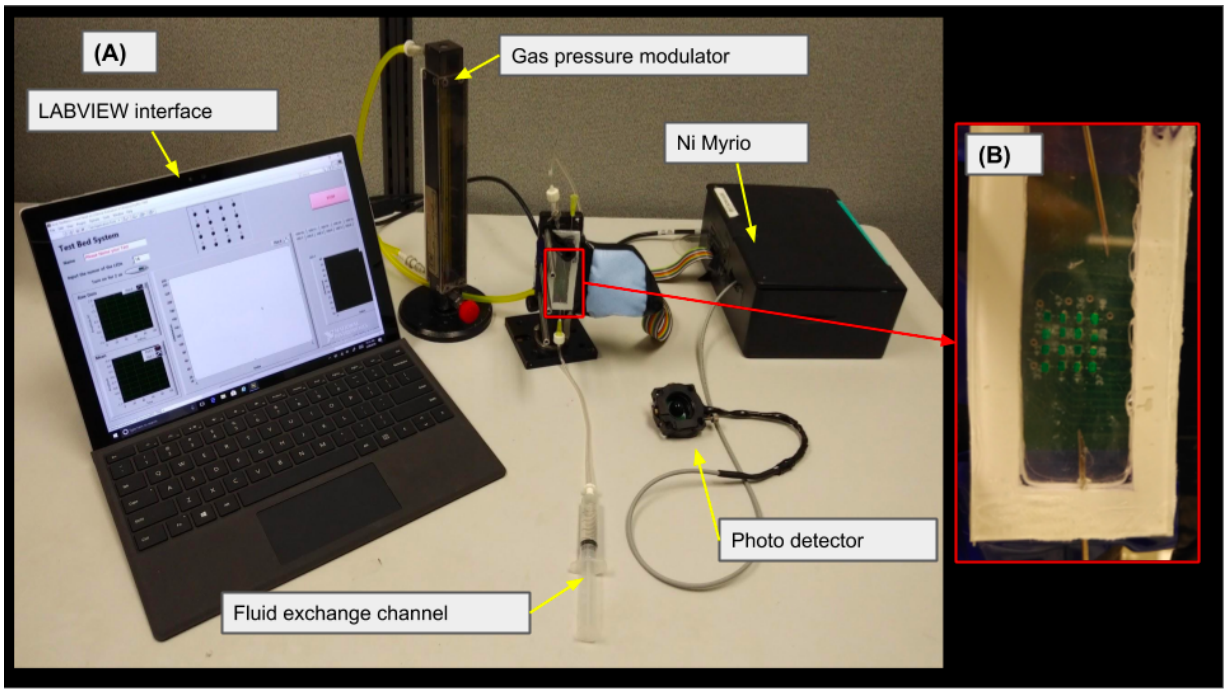

Figure 4.5: The developed multiple calibration system includes a 4x4 array of LEDs that are controlled by a LABVIEW interface. The LEDs flash in sequence and excite different sheets placed inside a vertically held chamber. The emission from each composite sheet within the chamber is then recorded by a photodetector circuit. (B) The chamber is fully sealed and contains an array of 4x4 composite sheets adhered on the inside. The chamber includes gas inlet/outlet and a fluid exchange channel to change the analyte levels while maintaining a certain oxygen concentration.

To assess the repeatability and reliability of the developed multiple calibration system, a chamber containing eight similar reference oxygen sensor sheets was made from PtTPTBP coated ,60 µm electrospun PTFE. The chamber was then calibrated at different oxygen levels. This test is performed dry and with no solution injection. During the calibration the enclosed chamber is injected with gases of 160 ,76, 38, 15.2 and 0 mmHg oxygen respectively. The changes in the luminescence lifetime values collected from each sheet is graphed (Fig. 4.6A). The average lifetime values at each oxygen level for all conditions is calculated (τ_{0av}), and using Stern_Volmer equation [76], the calibration curve for each individual sensor sheet at relevant physiological oxygen concentrations is derived (Fig. 4.6B). Importantly based on Stern_Volmer conversion of average lifetimes (explained in *4.2.4*), the derived general calibration curve shoes

that error in oxygen measurements using the composite sheets is less than 2.6 mmHg (Fig. 4.6C). This experiment confirm the repeatability of the measurements using the multiple calibration system. This developed system can further be used to determine the repeatability of analyte calibrations in sensor sheets made from composite material.

A)

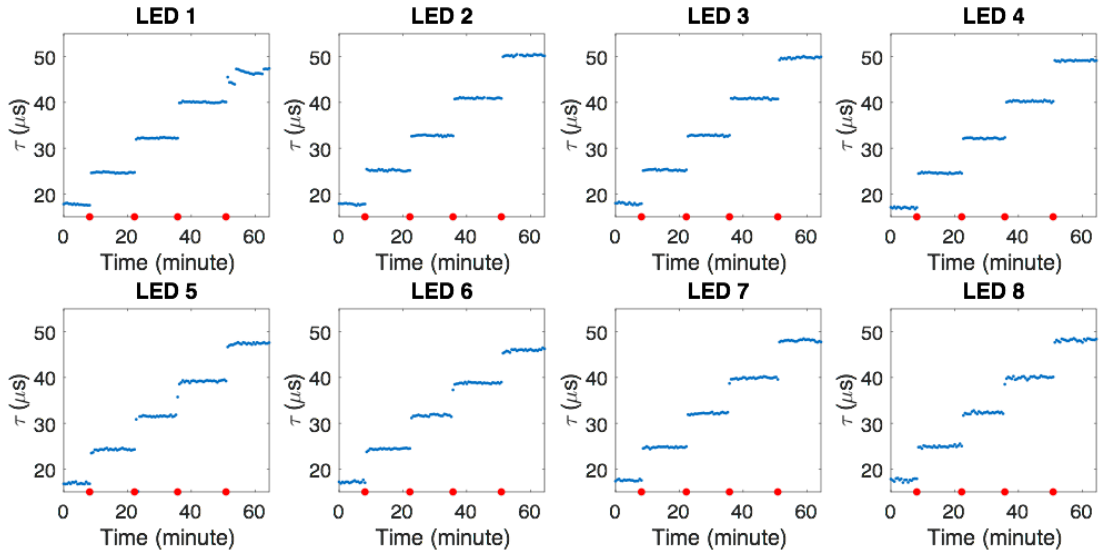

B)

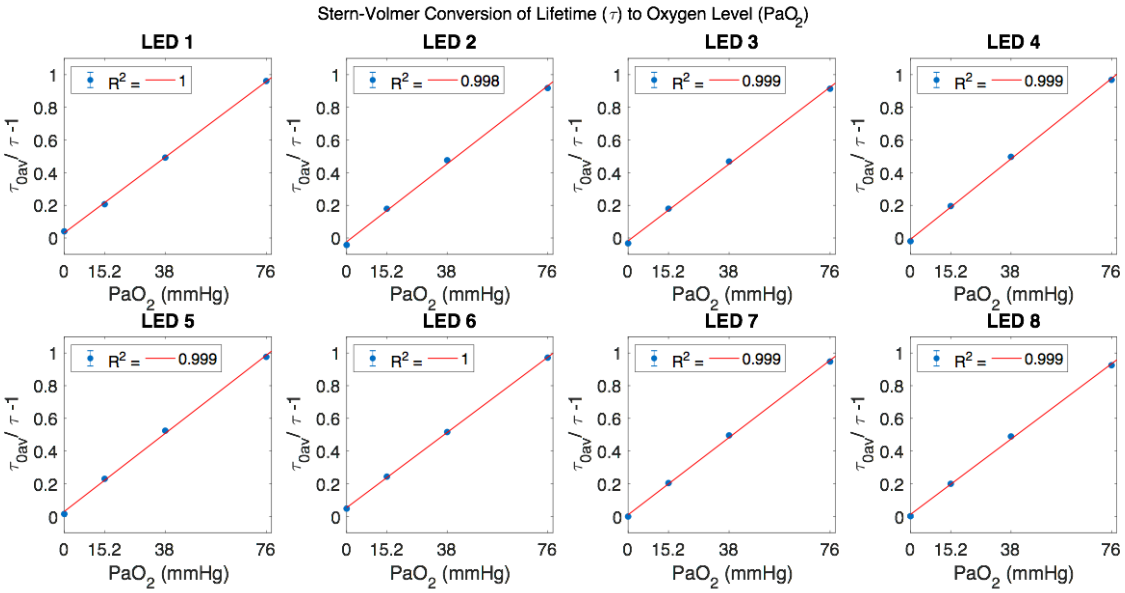

C)

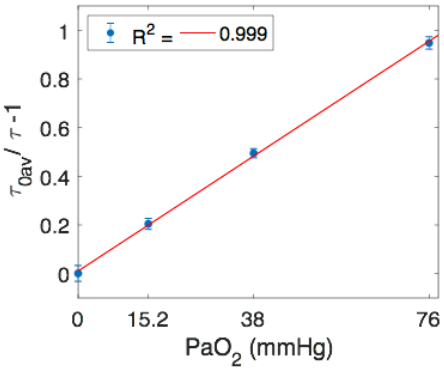

Figure 4.6: (A) Calibration of 8 oxygen reference sheets at 160 ,76, 38, 15.2 and 0 mmHg oxygen shows similar lifetime values of lifetime obtained from each sheet. (B) Individual calibration curves for reference sheets based on average lifetime values at each gas condition. τ_{0av} represents the average lifetime for all eight sensors at 0 mmHg PO_2. (C) General calibration curve at physiological oxygen levels for all reference films shows that the error of the calibration based on the standard deviation is less than 2.6 mmHg.

4.3.3 Finalizing composite formulation using multiple calibration system

Subsequent to the development of the multiple calibration system, different formulation and methods for making the composite sheet were investigated. Multiple factors were tested to narrow down the formulation of the sensors to achieve (1) sensitivity at physiological concentration ranges of glucose and lactate while at tissue oxygen level, (2) response times of less than five minutes, repeatability of sensors, and (3) high shelf life storage. As was described, the developed biosensors operate based on oxygen consumption during a biochemical reaction, the emission decay of the incorporated dye acts as a metric to measure the oxygen level in the reference and the sensor, correlation of which can determine the analyte concentration. Important to the technology, the developed sensors are required to have oxygen sensitivity and strong emission signals that can penetrate the tissue and be recorded by the receiver. Two different type of dyes have been tested for the formation of the composites. Pd (II) meso-Tetraphenyl Tetrabenzoporphine (PdTPTBP) with a longer ranges of lifetime values yet possessing lower emission intensity , and platinum (II) meso-Tetraphenyl Tetrabenzoporphine (PtTPTBP) with

lower ranges of lifetime values but a higher intensity of emission [76]. Another important factor investigated in the formation of the composite sheets is the thickness of the porous reinforcement constituent. A thin sheet can result in smaller final dimensions of the sensor and as a result an easier painless insertion of the sensors into the patients. However, using a thin porous structure provides lower surface area for dye coating as well as decreased space for embedding hydrogel enzyme mixture. Additionally, changes in Polyethylene glycol (PEG) hydrogel was also explored, since using different PEGs with different molecular weights can result in different pore sizes which can affect the diffusion characteristics of the composite. Lastly, changing the concentrations of the enzyme in the hydrogel mixture was tested. Such changes in enzyme-hydrogel ratio can affect the analyte sensitivity. For example, excessive amounts of enzyme can lead to a complete depletion of oxygen in the sensor and loss of sensitivity, while low concentration can result in limited number of biochemical reactions and therefore insufficient sensitivity of the sensor.

Table 4.1 shows the different formulations calibrated using the multiple calibration system. These formulations belong to 20 different types of fabricated composite sheets, made from, different types of dye, different porous PTFE sheets, different types of photocurable PEG and different concentrations of enzyme. In some variations Catalase is also added to the mixture to potentially increase the operational life of the sensors by catalyzing decomposition of a byproduct hydrogen peroxide (H_2O_2) into water and oxygen [122].

Table 4.1. Different composite sheets are made and tested using the developed multiple calibration system. Different variations are made from using enzymes Glucose Oxidase (GOX) for glucose sensors, Lactate Oxidase (LOX) for lactate sensors. Oxygen sensitive dyes used are PtTPTBP or PdTPTBP (Shown in table as Pt and Pd respectively). Different type of porous sheets used are expanded and electrospun PTFE. PEGDM stands for Polyehylene glycol Dimetharylate, TriP represents trimethylolpropane ethoxylate, EG represents ethylene glycol and MW represents molecular weight .

Sheet #	Enzyme	Dye	Hydrogel	MW	PTFE type	Thickness (μm)	Enzyme-Hydrogel Ratio (mg/ml)	Catalase-Hydrogel Ratio (mg/ml)	Date Made
(1)	GOX	Pt	PEGDM	400	expanded	50	200	0	9/20/2017
(2)	GOX	Pt	PEGDM	400	electrospun	60	200	0	9/20/2017
(3)	LOX	Pt	PEGDM	400	expanded	50	200	0	9/20/2017
(4)	LOX	Pt	PEGDM	400	electrospun	60	200	0	9/20/2017
(5)	GOX	Pt	PEGDM	400	electrospun	25	200	0	9/20/2017
(6)	GOX	Pd	PEGDM	400	electrospun	60	200	0	1/18/2018
(7)	LOX	Pd	PEGDM	400	electrospun	60	200	0	1/18/2018
(8)	LOX	Pt	PEGDM	400	electrospun	60	200	0	2/17/2018
(9)	GOX	Pt	PEGDM	400	electrospun	60	200	0	3/14/2018
(10)	GOX	Pt	PEGDM + EG	400	electrospun	60	200	0	3/14/2018
(11)	LOX	Pt	PEGDM	400	electrospun	60	200	0	4/10/2018
(12)	LOX	Pt	TriP	428	electrospun	25	200	0	4/20/18
(13)	LOX	Pt	(½)TriP+(½)Water	428	electrospun	25	200	0	4/26/18
(14)	LOX	Pt	PEGDM	400	electrospun	25	200	0	4/26/18
(15)	LOX	Pt	PEGDM	400	electrospun	25	200	15	4/26/2018
(16)	LOX	Pt	PEGDM	400	electrospun	25	100	100	4/26/2018
(17)	GOX	Pt	PEGDM	400	electrospun	25	200	20	6/28/2018
(18)	GOX	Pt	PEGDM	400	electrospun	25	100	10	8/23/2018
(19)	GOX	Pd	PEGDM	400	electrospun	25	140	10	8/31/2018
(20)	LOX	Pd	PEGDM	400	electrospun	25	200	10	9/04/2018

Chambers from different formulations were made and tested to find repeatable sensitivity and activity within *in vitro* simulated physiological condition. After multiple iterations and calibrations the desirable formulations were determined. Figure 4.7 shows the results of an analyte calibration performed on a chamber that contains 16 sensor sheets. The sensor sheets within the chamber are, four oxygen reference sheets made from 25 µm electrospun 25 µm PTFE and PtTPTBP dye placed in row 1, aligned with LEDs 1:4, four lactate sensor sheets made from composite sheet #14 (table 4.1) placed in row 2 and aligned with LEDs 5:8, four lactate sensor sheets made from composite sheet #15 (table 4.1) placed in row 3 aligned with LEDs 9:12, and four lactate sensor sheets made from composite sheet #16 (table 4.1) placed on row 4 aligned with LEDs 13:16. The chamber undergoes a series of solution changes during the calibration. These solutions used are 1x PBS, 20, 15, 10, 6, 4 and 1 mM lactate followed by 1x PBS respectively. The calibration is performed while 76 mmHg O_2 is injected into the chamber. The results indicate that the sensors are sensitive in the physiological ranges of lactate and tissue oxygen. Further repeats and more detailed fabrication of the sheets shows repeatability in the similar ranges of gel mixture.

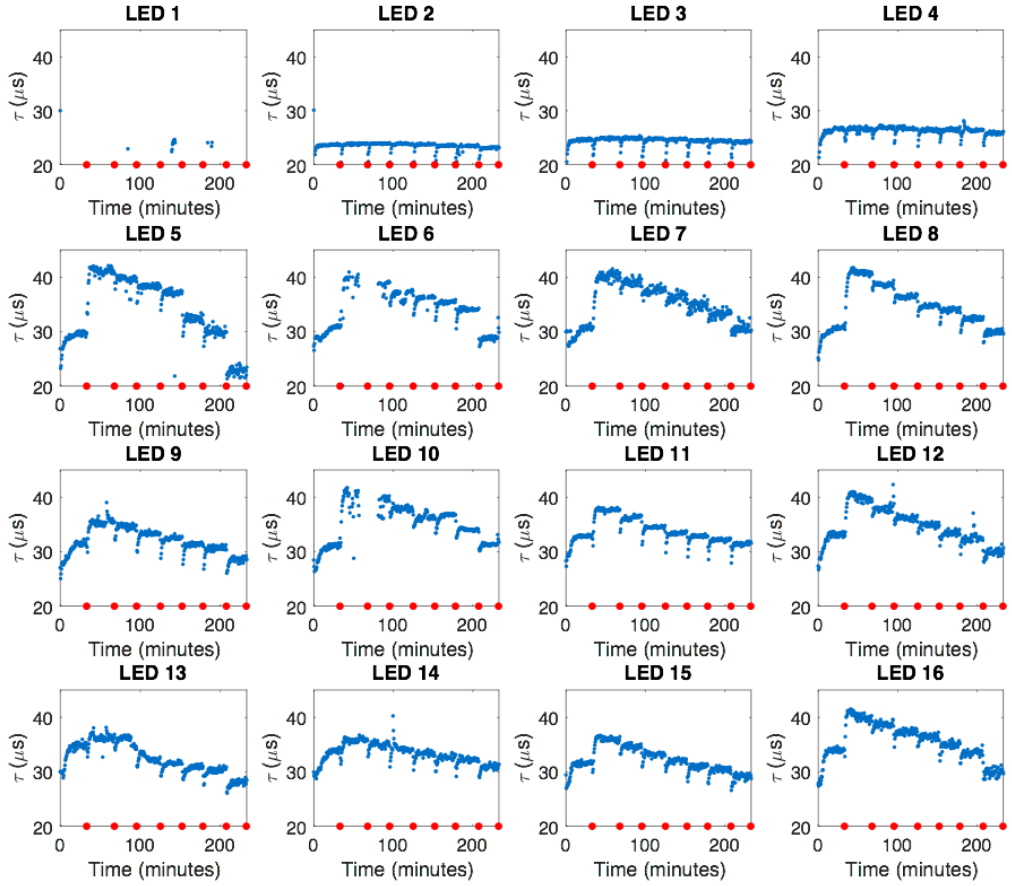

Figure 4.7: Lactate calibration of a chamber containing 16 sensors. Different solutions of 1x PBS, 20, 15, 10, 6, 4 and 1 mM lactate followed by 1x PBS are injected into the chamber while a 76 mmHg O_2 is injected into the chamber to maintain the physiological oxygen concentration. The chamber calibrated comprises 4 oxygen reference sheets made from 25 µm electrospun PTFE and PtTPTBP dye placed in row 1 aligned with LEDs 1:4, four lactate sensor sheets made from composite sheet #14 (table 4.1) placed in row 2 aligned with LEDs 5:8, four lactate sensor sheets made from composite sheet #15 (table 4.1) placed in row 3 aligned with LEDs 9:12, and four lactate sensors sheets made from composite sheet #16 (table 4.1) placed on row 4 aligned with LEDs 13:16. (LED 1 was not operating during the experiment).

Using the developed multiple calibration system as a powerful technique to collect data, determined that a glucose sensor that works in the physiological analyte and oxygen concentrations requires lower amounts of embedded enzyme as compared to the lactate sensors. This may be due to the higher activity of the powdered enzyme (GOX :135.2 U/mg, LOX:106 U/mg) or potentially it's better dispersion in the hydrogel mixture.

Importantly, to successfully narrow down the formulation it became necessary to minimize the fabrication errors. At this step the composite formation process was upgraded. In brief, enzyme powder is gently pressed down to break down larger compacted masses to a finer powder. For making each composite sheet small batches of the enzyme-gel with 100µl of total volume were made. This was done to reduce the total volume of the stirred solution therefore resulting in a more homogenous mixing. The enzyme powder was added to a stirring solution of Polyethylene glycol in three intervals of 8 hours, each time ⅓ of the targeted final enzyme weight is added. Every powder addition happened over a period of few minutes while the solution was being stirred. After 24 hours the stirring process was stopped. Afterwards, a controlled amount of enzyme-gel mixture was added to both sides of a plasma treated dye coated sheet (10µl on each side of a 12 mm x12 mm sheet). The sheet and enzyme mixture were then pressed together using glass substrates and photopolymerized. Lastly, the sheets were cut to pieces that have the maximum similarity in size (achieved by manual cutting). They were then attached to the polycarbonate substrate of the chambers using minimal amounts of adhesive.

Figure 4.8 shows an analyte calibration performed on a chamber made with the last current iteration of the composite glucose sensor sheet (composite sheet #19, table 4.1). After the chamber was made it was injected with 1x PBS solution and placed in incubator at 37℃ for a period of 48 hours. The sensors within the chamber were all made using PdTPTBP dye. This dye has possess a larger range of lifetime values in physiological oxygen levels [76] and it may provide higher accuracy if the signal strength is maintained. The chamber tested contains; four oxygen reference sheets made from 25 µm electrospun PTFE coated with PdTPTBP dye placed in row 1 aligned with LEDs 1:4. The rows 2, 3 and 4 (aligned with LEDs 5:16) contained glucose sensor sheets made from composite sheet #19 (table 4.1). The chamber undergoes a

series of fluid exchanges that include 400, 290, 180, 72 and 18 mg/dl glucose solutions followed by 1x PBS respectively. The calibration is performed with a continuous injection of 76 mmHg O_2.

The results show that the oxygens reference sensor sheets detect a constant level of oxygen throughout the experiment (LEDs= 2,3) while the glucose sensor sheets located on rows 2-4 (LEDs 5:16) show a step change in their average lifetime values. This step change is correlated to the changes in glucose levels during the calibrations. During which the enzymatic bioreaction is consuming oxygen and the local oxygen concentrations at the sensor sheets increase with a decrease in analyte levels and the reaction rate. This local oxygen increase results in decrease of lifetime values in the oxygen sensitive dye. To quantitatively analyze the average lifetime values obtained from each sensor at different analyte concentrations a custom made MATLAB code was developed to find the fluid change timepoints. Red dots in Fig. 4.8 represent the time of each fluid exchange.

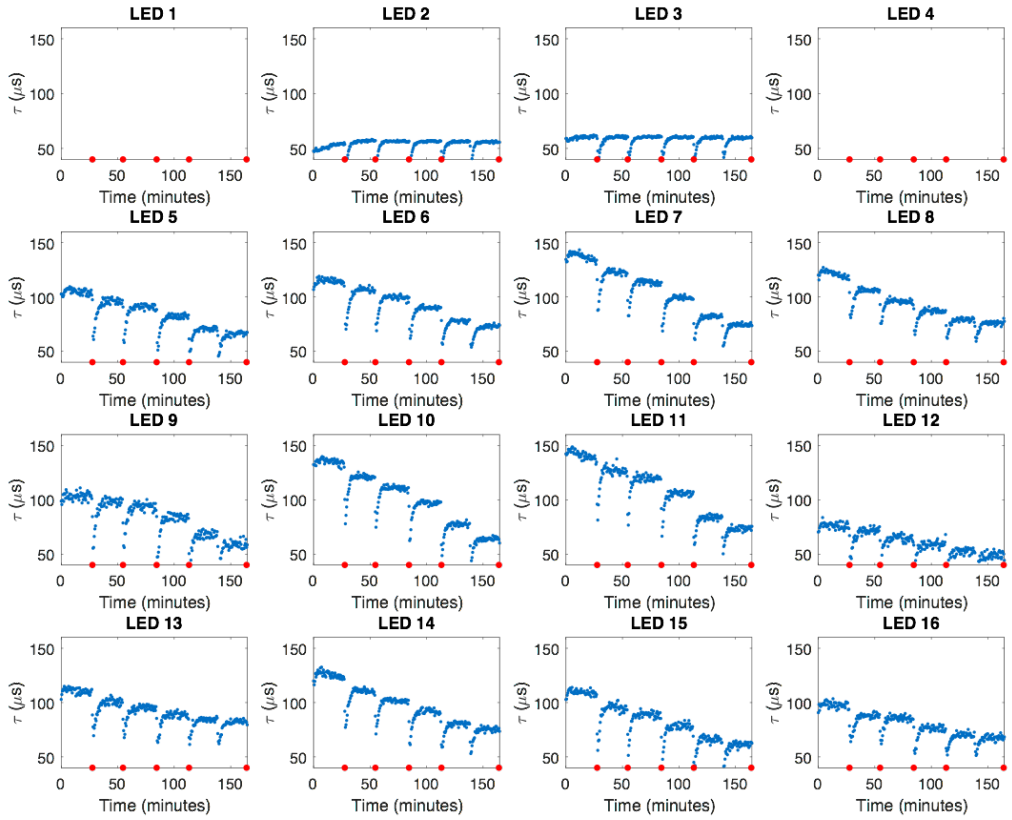

Figure 4.8: Glucose calibration of a chamber containing 16 sensors. Different solutions are injected into the chamber is sequence. These solutions are 400, 290, 180, 72, 18 mg/dl glucose followed by 1x PBS. The calibration is performed with a constant injection of 76 mmHg O_2. The first row (LEDs 1:4) contains oxygen reference sensor sheets made from 25 µm electrospun PTFE and PdTPTBP dye. Rows 2, 3 and 4 contain glucose sensor sheets made from composite sheet #19 (table 4.1). Note that LEDs 1 and 4 were not operating during the experiment.

The developed MATLAB code averages all the lifetime values obtained from the sensors and uses the first derivative of lifetime over time ($\delta\tau/\delta t$) to find the rapid changes (Fig. 4.9A). These rapid changes in lifetime (τ) are because of the fluid exchange. The fluid within the chamber contains the injected 76 mmHg pO_2 while the newly injected fluid contains room air oxygen concentration (160 mmHg). Further, to analyze the changes of lifetime due to the enzymatic reaction at the sensor, the lifetime values obtained from operating reference oxygen sensors (LEDs 2 and 3 here for example) are averaged at each timepoint and subtracted from the corresponding lifetime value of analyte sensors The values calculated after the reference

subtraction is called $\Delta\tau$. Fig. 4.9B shows the average value of 30 $\Delta\tau$ measurements at each plateau (analyte) level for sensor 8 (aligned with LED 8) graphed versus the corresponding analyte concentrations. The average values calculated with the method can then be used to find the relationship between the lifetime values and analyte concentrations.

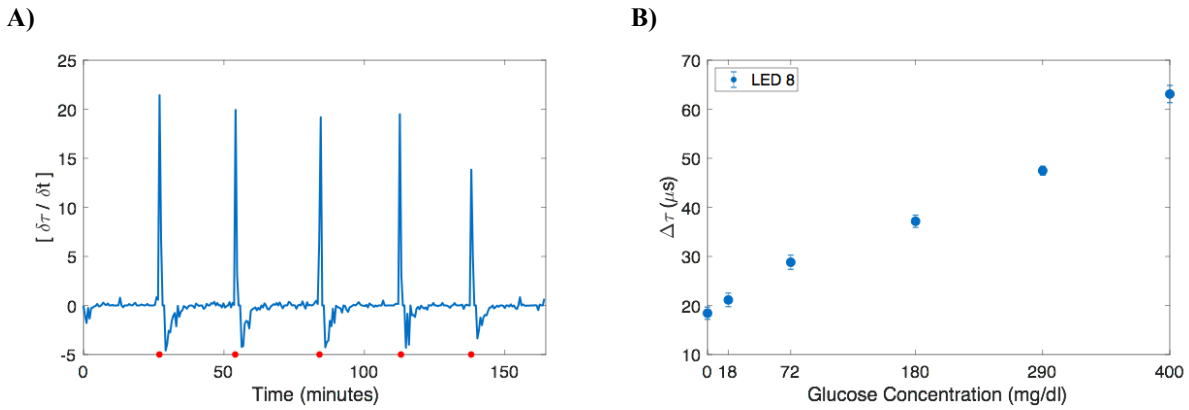

Figure 4.9: (A) shows the first derivative of lifetime over time ($\delta\tau/\delta t$), the peaks are found using a developed MATLAB code and they indicate fluid exchange timepoints. (B) Shows a typical analysis on sensor 8 from the calibrated chamber, in which the lifetime values are subtracted from the corresponding reference lifetime values over the period of the calibration to find the $\Delta\tau$. Average $\Delta\tau$ at each analyte concentration is then calculated by using the fluid exchange timepoints and finding plateau levels at each analyte concentration (averaging 30 consecutive values are reported in the graph).

To study the response of different sensors made from the same composite sheet and asses the repeatability, four more recent iterations of the formed sheets (composite sheets #17, #18, #19 and #20, table 4.1) were used and from each sheet, 3 chambers were made. Each such chamber contained one row of oxygen reference sheet sensors (aligned with LEDs 1:4) and three rows of composite sheet sensors (aligned with LEDs 5:16). All chambers were injected with 1x PBS and incubated for two days at 37℃ prior to calibrations. All calibrations were performed with a continuous injection of 76 mmHg O_2. The glucose sensors (composite sheets #18 & #19, table 4.1) underwent fluid changes of 400, 290, 180, 72 and 18 mg/dl glucose followed by 1x PBS. The lactate sensors (composite sheets #15 & #20, table 4.1) underwent solution changes of 22, 16, 10, 4 and 1 mM lactate followed by 1x PBS. The analyte levels as well as the

concentration of the oxygen gas inserted were chosen to simulate the physiological conditions. A step change decrease in lifetime values of the analyte sensors was observed in all calibrations. To analyze the calibration data the calculated lifetime values of the analyte sensors were subtracted by the corresponding reference oxygen lifetime values to obtain $\Delta\tau$. Afterwards average $\Delta\tau$ at each analyte concentration is calculated (average of 30 values). The average values for each analyte concentration is then subtracted by its average $\Delta\tau$ at 1x PBS to normalize the calibrations. The final value reported is named *Normalized* τ.

Figure 4.10 shows the analyzed results from a typical glucose sensor made from composite sheet #19 and a typical lactate sensor made from composite sheet # 20 (table 4.1). The results are obtained from chamber calibrations. In the analysis, *Normalized* τ values at each analyte level is graphed versus the analyte concentration. The results show that sensors are sensitive within the physiological ranges of the analyte concentrations. Additionally, it is observed that a correlation between *Normalized* τ and analyte concentration (polynomial level 2) exists in all sensors. The repeated chamber calibrations successfully showed 30 working sensors from each four composite sheets.

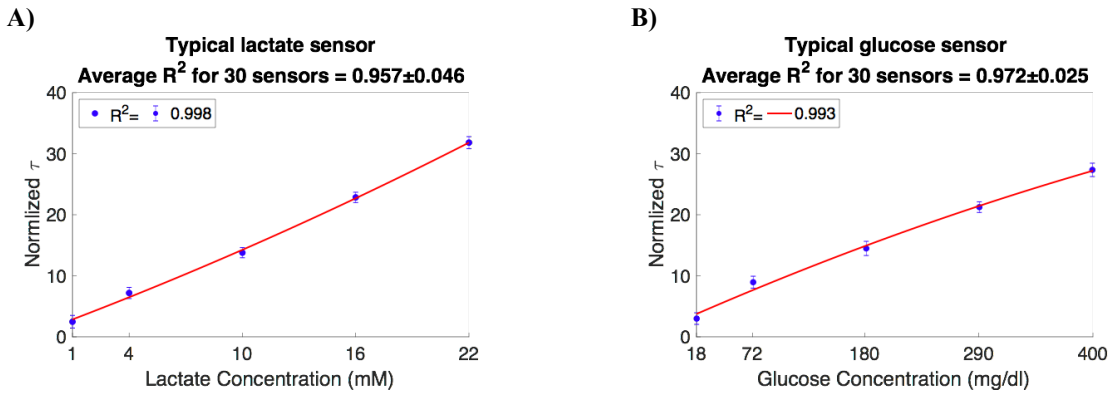

Figure 4.10: Shows *Normalized* τ values at different concentration of analytes for (A) a typical glucose sensor and (B) a lactate sensor made from composite sheets #19 and #20 (table 4.1). The data is fit into a polynomial level 2 equation. These results are obtained from multiple chamber calibrations in which data was analyzed for at least 30 working sensors per composite sheet. The average R^2 values for glucose sensors made from composite sheet #19 was 0.957 +- 0.046 and for the lactate sensor made from composite sheet #20 was 0.972 +- 0.025

4.3.4 Evaluating storage life and pilot animal study

The fabricated composite sheets are stored dry, in room conditions. This storage method is chosen to represent the storage of a final product used by patients. Storage time studies up until today, shows that the sensors have been maintaining their activity as well as sensitivity over a period of 13 months. To quantitatively analyze the functionality of the composite sheets after the storage period, flexible circuit sensors were made comprising a composite analyte sensor sheet and an oxygen reference sensor sheet (process explained in *4.2.2*). Fig. 11A shows calibration of a glucose sensor made from composite sheet #2 after 13 months of dry storage (table 4.1). Calibration is performed with continuous injection of 76 mmHg O_2. Tip of the flex circuit is inserted into a cylindrical tube and solutions containing 400, 180, 72 and 18 mg/dl glucose followed by 1X PBS are inserted. The oxygen reference shows similar lifetime values throughout the experiment while step changes in lifetime values of the glucose sensor corresponds to changes in analyte concentration. Fig. 4.11B-C show the analyzed results of calibrations performed on multiple glucose and lactate sensors made from fabricated sheets that were stored dry for 13 months (composite sheets #2 and #4, table 4.1). All calibration are performed with continuous injection of 76 mmHg O_2. As described previously (*4.3.3*), for the analysis *Normalized* τ was calculated and correlated to analyte level concentrations.

Note that all the calibrated sensors shown in Figure 4.11 were put together from composite sheets made with first iterations of the fabrication process. The technique used was later on advanced to a finalized protocol which was explained in *4.3.3*. Because of the preliminary method of fabrication used, the calibrated sensors show some degree of variability, nevertheless they prove to be active and sensitive within the physiological ranges, further validating the success of the developed technique to create long lasting biosensors.

A)

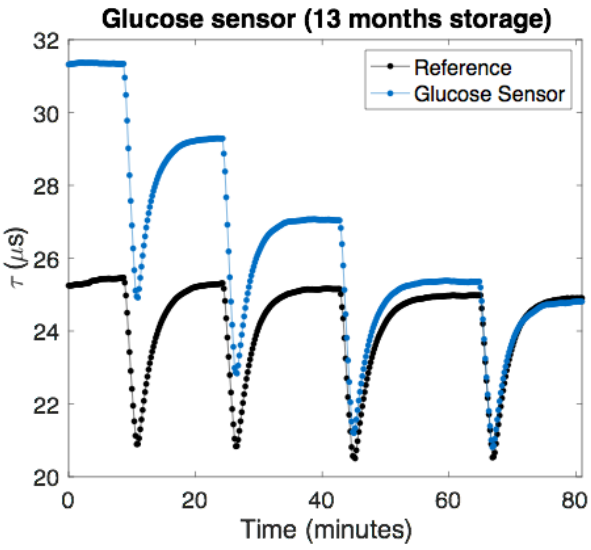

B)

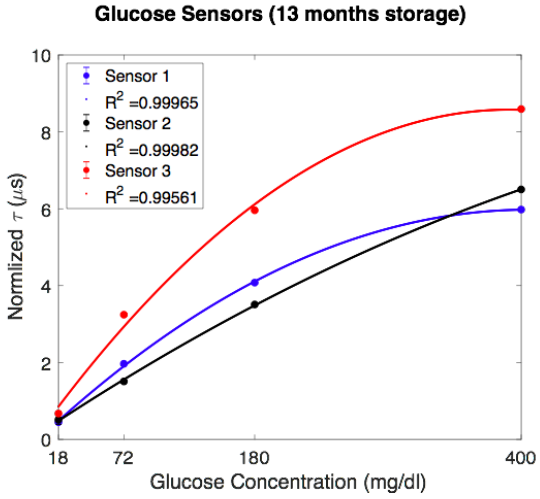

C)

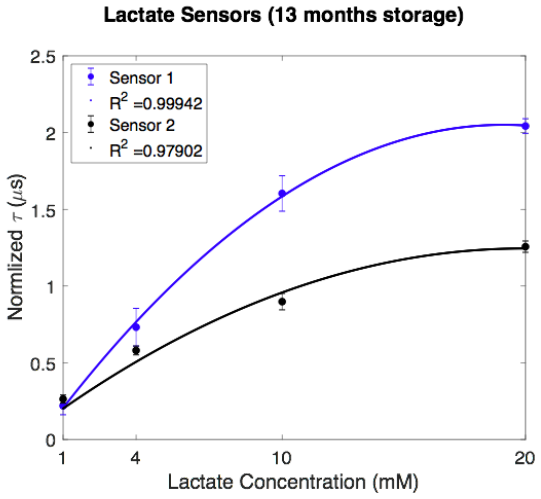

Figure 4.11: Calibration of sensors made from composite sheets that were stored dry for 13 month. All calibration are performed with continuous injection of 76 mmHg O_2 to simulate tissue oxygenation conditions. (A) Calibration of a typical glucose sensor made from composite sheet # 2 (table 4.1) at 400, 180, 72, 18 mg/dl glucose followed by 1x PBS. The step changes in τ in the glucose sensor sheet accompanied by the constant average τ value reported from the reference oxygen sensor shows the functionality of the sensors. (B-C) Multiple glucose and lactate sensors made from composite sheets #2 and #4 are calibrated (table 4.1). Analyzed results show a polynomial level 2 correlation between the *Normalized* τ and different analyte concentrations.

Successful proof of concept, repeatable results as well as a long storage time showed potential for the developed biosensors to be tested *in vivo*. For the pilot *in vivo* experiment a rabbit cyanide poisoning model was used (explained in *4.2.5*) in which the animal is poisoned

with a lethal dose of cyanide. Cyanide is known to increase lactate build up through impairing tissue ability to utilize oxygen by binding to cytochrome c oxidase [121]. A lactate sensor fabricated from composite sheet #20 (table 4.1) was used for this *in vivo* experiment. The tip of the sensor was inserted underneath the skin and the photodetector receiver was placed directly above the skin. After 10 minutes of collecting data, cyanide injection started. Cyanide was continuously infused for a duration of 30 minutes. Figure 4.12 shows continuous data collected after the cyanide insertion was stopped (40 minutes into the experiment). $\Delta\tau$ is calculated by subtraction of lactate sensor sheet lifetime values from the corresponding oxygen reference lifetime values (Fig. 4.12B). The continuous lactate monitor shows an overall increase in the calculated $\Delta\tau$ values. This rise in $\Delta\tau$ may correspond to the changes in lactate level as shown by the reference blood lactate measurements (red circles). Although no conclusion can be drawn from a pilot animal study, the results show few important validating observations. First, the lactate sensor used in this study was fabricated from 25 µm PTFE sheet and PdTPTBP dye. The results show that although the thin PTFE has lower surface area for containing the dye and that the dye used has an inherently low emission intensity [76], the created sensors are capable of providing adequate recordable emission light that can pass through the skin and reach the photodetector. Additionally, the enzymatic reaction in the sensor did not cause a complete depletion of the oxygen, showing the composite formulation contains a level of enzyme/gel ratio which can continuously detect high levels of tissue lactate *in vivo*.

A)

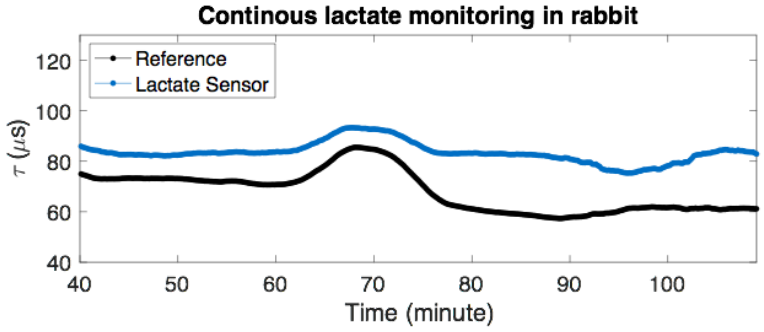

B)

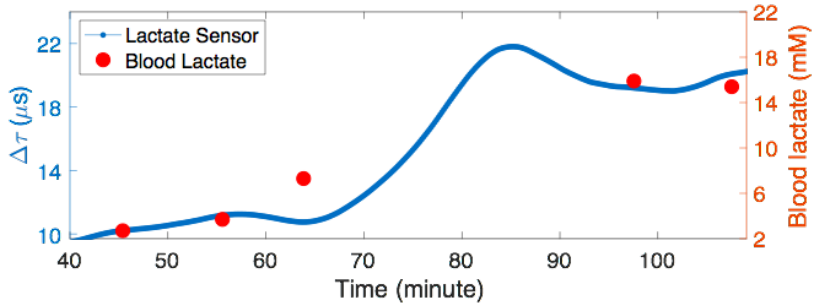

Figure 4.12: Pilot *in vivo* study of cyanide poisoning in a rabbit model to increase blood lactate levels. Cyanide injection starts 10 minutes into the experiment and lasts for 30 minutes (40 minutes after). The collected lactate sensor data after the cyanide injection is showed is shown in the figure. (A) Lifetime values collected from a subcutaneously inserted continuous lactate sensor made from composite sheet #20 (table 4.1). (B) An increasing trend in continuous calculated $\Delta\tau$ may indicate the rise of lactate, which is also confirmed by reference blood lactate measurements (shown with red circles) .

4.4 Discussion

Analyte sensors are used to detect and measure the levels of analytes in biological fluids and tissues. Examples of such sensors include enzymatic oxidase-based continuous glucose and lactate monitors. For diabetic patients, measurement of both such analytes in subcutaneous space can result in a better understanding of the metabolic pathways and prediction of glucose changes, especially during and following periods of intense physical activity. The combined data can lead to a more accurate dosing of insulin and better glycemic control. Additionally, continuous measurement of lactate can act as a reliable indicator of shock for critically ill patients.

This chapter addresses limitations in the biosensing technology and introduces new methods to create lactate and glucose biosensors. In the current state of technology, analyte biosensors that utilize enzymatic oxygen consuming reactions, are typically constructed by having an oxygen sensitive dye volume juxtaposed to an enzyme volume. The enzyme and dye are layered next to each other onto a platform responsible for excitation and detection of the light. In this methodology, only the dye particles directly in contact with the enzyme molecules emit a light signal which reports the level of analytes or products of the enzymatic reaction. The remaining volume of the dye is typically insensitive to the reaction, nevertheless emitting light. As a consequence of this geometry, the addition of more dye does not increase the signal amplitude as related to analyte monitoring, but instead only contributes to an unwanted background. Alternatively, in other methodologies, the enzyme and dye may be incorporated into a hydrogel. This introduces a challenge because the dye particles and enzyme molecules are often non co-soluble in the water phase of the hydrogel and thus it is difficult to uniformly distribute them within the gel. Further, hydrogels are characteristically soft and fragile, and thus they typically must be formed on the device itself, as opposed to being formed in large scale using a second process and then placed onto a sensing device. Additionally, adhesion of such a hydrogel to a second surface presents challenges, particularly, hydrogels tend to swell or contract away from a surface they are deposited onto during hydration and polymerization. Such second surfaces may have characteristic lengths of several to hundreds of microns, further inhibiting reliable and repeatable placement of the hydrogels over thousands of units in manufacturing scale. There is need for improved materials and strategies for co-immobilizing dyes and enzymes, assuring their uniform distribution within their embedding matrix. Additionally, it is

needed to advance the sensor material characteristics in such a way that they become manufacturable on large scales and can be precisely placed onto small second surfaces.

The describes invention in this chapter is a new class of biosensing material, a composite that contains necessary components to detect and measure the level of analytes. The composite material comprises a porous matrix (mesh) which acts as a reinforcement constituent, a luminescent substance, such as an oxygen-sensitive dye, formulated to coat the surface area of the porous matrix, and a hydrogel filling the porous matrix, where the hydrogel contains at least one additional substance, such as a catalyst, for example enzyme, or a binding protein. This composite's structure of interpenetrating dye coated fibers and hydrogel enzyme mixture affords several key advantages for the biosensors. First, in the composite matrix, high activity of the enzyme molecules is maintained by the methods of entrapment, as compared to the method of covalent attachment to a substrate. Second, the composite material can be directly adhered to a light source resulting in greater sensor mechanical stability and higher signals. Third, due to the interpenetrating nature of the porous mesh, the surface area of hydrogel-dye contact is very large as compared to a system utilizing a non porous matrix which is limited to a layered geometry between the hydrogel phase and the dye coated matrix. As a result, the invented composite can achieve a targeted surface area of dye to hydrogel contact, within much smaller size as compared to the layered geometry. Fourth, the composite is much stronger than a hydrogel alone, and thus for a thin geometry, the composite can be mechanically manipulated with forces consistent with manufacturing processes. Because of this, composite material can be fabricated in large sheets or films, cut into appropriate sizes for a sensor and then picked up from the sheet and deposited onto the sensor. Fifth, lower diffusion rates through the composite due to the porous mesh, possessing a tortuous path, allows for longer diffusion paths without increasing bulk dimensions.

Moreover even with the thin geometry, the diffusion characteristics of the composite can be further altered by changes to the hydrogel phase. This is important in the case of the oxidase-based sensors, where the diffusion constant of the analyte within the hydrogel phase of the composite can be optimized for a desired measurable range of analyte concentration. Lastly, the dimensions of the matrix, or reinforcement constituent, of the composite can be tuned to optimize factors such as mechanical strength, total dye mass (and thus brightness), analyte diffusion path lengths, and response time to changes in bulk analyte concentration.

The results of this study show the glucose and lactate sensors fabricated with the described composite sheets have met certain targeted criteria which indicates they can potentially be used in clinical trials and further on by patients. For example, the size of the composite sheet containing all the components necessary for analyte detection can be minimized to as low as 30 μm in thickness (or thinner), thereby making the analyte sensor overall thinner and insertion into the subcutaneous space less painful. Importantly, the glucose and lactate sensors made from the composite sheets show sensitivity in tissue oxygen levels and within physiological ranges of analyte concentrations, which is 40-400 mg/dl for glucose and 1-15 mM for lactate [111, 123]. Additionally, the fabricated sensors have shown fast response time to analyte changes, this can be very important for continuous measurement of lactate and glucose in diabetic patients to help prevent occurrence of hypoglycemia or hyperglycemia. Furthermore, the fabricated sensors have shown to maintain activity and sensitivity over a long period of shelf storage. Lastly, sensors made from composite sheets have demonstrated repeatable results in activity and sensitivity. This repeatability as well ease of fabrication and assembly can lead to lower manufacturing costs.

None of the presently known prior references or work have the unique inventive technical features of the described invented composite. Application of the described technology in biosensing can results in development of long lasting, biocompatible and sensitive glucose and lactate sensors that can be used in an Artificial Pancreas system. This application can advance the predictions of blood glucose changes and insulin administrations, and result in achieving better glycemic control in diabetic patients.

CHAPTER 5: Conclusion

The advancement in biomedical engineering and materials science promises a future in which diseases can be cured and metabolic changes controlled. That level of advancement may be achieved in decades, nevertheless the path to arrive is clear. Understanding the current state of technology, implementing changes to overcome limitations and building on new findings. This dissertation explores current methods aiming to treat and control diabetes. A condition considered epidemic, remaining the seventh cause of death with total costs more than three hundred billion dollars per year in United States [124]. In three chapters, different approaches aiming to lead to a cure were discussed.

Tissue engineering, although still in early states of developments holds great promise to achieve insulin independence in diabetic patients, especially in type 1 diabetics. This approach aims to replace the non functional cells with newly implanted exogenous insulin producing pancreatic islet cells. Attempts in implementing this approach however have largely failed. The lack of success is because of known limitations, which can be overcome. A primary reason that the newly implanted cells fail is the active host immune system. To protect the implanted cells, they can be encapsulated in a membrane that blocks the passage of the antibodies while providing passage to secreted hormones, importantly insulin. This method is discussed in *Chapter II* by exploring the characteristics of alginate hydrogel, a material commonly used for cell encapsulations. As was discussed, success of a cellular implant that uses such hydrogel to provide cell protection requires detailed understanding of the structural properties of the membrane material. The discussed observations, show that such implants undergo polymeric changes in their inner structure that results in volume fluctuations, both during the polymerization process and after incubation in physiological conditions, importantly for example

in a patient's body. These changes in volume can result in cell protrusion, in case of material contraction, and pore size increase in case of volume expansion. In this work use of confocal microscopy imaging, a new method to understand the structural changes in alginate hydrogel is introduced. By monitoring diffusion of fluorescently tagged molecules of different sizes, it was determined that physiological conditions can result in an increase in pore sizes and therefore compromise the immunoisolating properties of the implant. Knowing this information, preliminary studies prior to an implantation can potentially tune the structure to account for the upcoming *in vivo* changes, therefore creating a protective membrane that reaches its targeted material properties subsequent to implantation. Such methodology can also be used in different applications including drug delivery, in which kinetics of drug release can be predefined.

Cellular encapsulation, however faces serious challenges which may not be solved by changing the material characteristics. These challenges stem from the fact that the newly implanted encapsulated cells are not close to vasculature, meaning they are not in close proximity to oxygen and nutrients, necessary for their function and survival. In *Chapter III* a more advanced approach is discussed, in which potential devices act as small organs to house and protect the transplanted cells. The goal of using such devices instead of cell encapsulation is to provide a prevascularization phase, prior to tissue transplantation. In this method, the devices have a design that can allow vasculature to enter their volume. Such devices are implanted subcutaneously and after a period of time, new vasculature enters their geometry. The key to this approach is to insert the pancreatic islet cells into the implanted devices, only after they are well vascularized. This strategy aims to provide ample oxygenation and abundance of nutrients to the transplanted cells, promising their survival. The success of this method however, relies on the assessment of the state of vasculature growth within the device and correct timing of cell

insertion. In the discussed chapter, a new method of monitoring the state of oxygenation and vasculature growth within such implanted devices is introduced. In this technique, the space allocated for housing the pancreatic cells is initially filled with developed retrievable photonic oxygen sensitive implants. Afterwards the devices are subcutaneously implanted. Photonic signal can then be monitored non-invasively and provide information on oxygenation within the devices as well as the rate of its changes. This non-invasive monitoring can serve as a metric to assess the state of vessel growth and readiness of the devices for cell insertion. At the determined time, the oxygen sensitive implants can be retrieved and then pancreatic islets be inserted into the device. This strategy can have multiple applications in tissue engineering and drug delivery systems in which shorter diffusional distances to the vasculature can be beneficial.

The discussed tissue engineering approaches to provide insulin independence to diabetic patients by transplantation of pancreatic islet cells show great potential. However these technologies are possibly many clinical trials and years away from entering the medical device market to be used safely by patients. Considering that only within United States more than one million people are diagnosed with diabetes every year, there is a need for a more developed technology that can provide glycemic control to diabetic patients. This need could be addressed by Artificial Pancreas (AP), a system that monitors the level of glucose by using a continuous glucose monitor, and is able to predict glycemic changes and administer insulin accordingly. The accuracy of glycemic change predictions and subsequent insulin dosing in AP requires mathematical calculations of multiple input variables. The current state of AP technology utilizes limited input information of continuous glucose levels and food intake. This can lead to imperfect glycemic change prediction especially during and after physical activity. This limitation in accurate prediction can result in incorrect insulin dosing and perversely changing

the blood glucose level, as a result discouraging the patient from regular exercise and in time leading to further health complications.

Chapter IV describes invention of a composite material that can advance the biosensing technology. This material can be used to create different type of biosensors. Important to advancing AP, this composite material was used to create glucose and lactate sensors. Addition of lactate sensor aims to indicate the physical activity and its intensity in diabetic patients. This added information to an AP system can help with better prediction of glycemic changes and insulin dosing. The invented composite comprises a porous matrix that acts as a reinforcing constituents, is coated with a layer oxygen sensitive dye and filled with an enzyme-hydrogel mixture. The embedded enzymes undergo a biochemical reaction that consumes oxygen when they are exposed to analytes. The rate of this oxygen consumption can be monitored through light signal recorded from the oxygen sensitive dye constituent, and then be used to measure the surrounding analyte concentration. This composite material is adhered to small LEDs that are placed on a flexible circuit. The tip of the flexible circuit can be inserted under the skin to continuously measure the analyte levels. The structure of this material can be tuned to have different diffusion characteristics and therefore sensitivities to analytes. Importantly, the structure is designed to immobilized enzymes inside a porous matrix instead of covalently bonding them, this as a result increases the activity, storage life as well as response time to analyte changes. Additionally, using a porous geometry to contain both the luminescence reporting particles and enzymes, it is possible to decrease the size and thickness of this composite to few tens of microns, therefore resulting in painless subcutaneous insertion of the sensors. This developed material can be used in creating biosensors to advance artificial pancreas

and insulin administration. It can also be used in other applications, for example continuous measurements of lactate can be act as reliable indicator of shock in critical injury.

The discussed tissue engineering and biosensing approaches hold promise in achieving insulin independence, providing better glycemic control and importantly help with diabetes management. They may also be used in many different applications within the medical field. In the future, tissue engineering will be able to provide immunoisolation without compromising oxygen and nutrient availability to the cells, this will probably happen through material modification and advancement in implant geometry. Moreover, biosensing may be used to monitor the state of cellular implants and guide the therapy. In a few decades, biosensors will possibly become minimally invasive, for example sensors may be implanted and functional for years at a time, providing continuous stream of data on multiple different metrics. Such collected data over populations can then possibly predict and even prevent diseases, leading to extended human longevity.

References

1. American Diabetes Association. Economic Costs of Diabetes in the U.S. in 2007. Diabetes Care. 2008;31: 596–615.

2. Tuomilehto J. The emerging global epidemic of type 1 diabetes. Curr Diab Rep. 2013;13: 795–804.

3. World Health Organization. Global Report on Diabetes. 2016.

4. James Shapiro AM, Shaw JAM. Islet Transplantation and Beta Cell Replacement Therapy. CRC Press; 2007.

5. Yoon J-W, Jun H-S. Autoimmune Destruction of Pancreatic B Cells. Am J Ther. 2005;12: 580–591.

6. Gillard P, Keymeulen B, Mathieu C. Beta-cell transplantation in type 1 diabetic patients: a work in progress to cure. Verh K Acad Geneeskd Belg. 2010;72: 71–98.

7. Kennedy L, Leahy JL. Intensive Diabetes Treatment and Cardiovascular Disease in Patients with Type 1 Diabetes. Yearbook of Endocrinology. 2007;2007: xvii–xxiii.

8. LeRoith D, Taylor SI, Olefsky JM. Diabetes Mellitus: A Fundamental and Clinical Text. Lippincott Williams & Wilkins; 2004.

9. Shapiro AM, Lakey JR, Ryan EA, Korbutt GS, Toth E, Warnock GL, et al. Islet transplantation in seven patients with type 1 diabetes mellitus using a glucocorticoid-free immunosuppressive regimen. N Engl J Med. 2000;343: 230–238.

10. Brissová M, Lacík I, Powers AC, Anilkumar AV, Wang T. Control and measurement of permeability for design of microcapsule cell delivery system. J Biomed Mater Res. 1998;39: 61–70.

11. Colton CK, Avgoustiniatos ES. Bioengineering in development of the hybrid artificial pancreas. J Biomech Eng. 1991;113: 152–170.

12. Lanza RP, Sullivan SJ, Chick WL. Perspectives in diabetes. Islet transplantation with immunoisolation. Diabetes. 1992;41: 1503–1510.

13. Chang TM. Hybrid artificial cells: microencapsulation of living cells. ASAIO J. 1992;38: 128–130.

14. Maki T, Mullon CJ, Solomon BA, Monaco AP. Novel delivery of pancreatic islet cells to treat insulin-dependent diabetes mellitus. Clin Pharmacokinet. 1995;28: 471–482.

15. O'Shea GM, Goosen MF, Sun AM. Prolonged survival of transplanted islets of Langerhans encapsulated in a biocompatible membrane. Biochim Biophys Acta. 1984;804: 133–136.

16. Lim F, Sun A. Microencapsulated islets as bioartificial endocrine pancreas. Science. 1980;210: 908–910.

17. Wang T, Taylor W, Igor L, Marcela B, Anilkumar AV, Ales P, et al. An encapsulation system for the immunoisolation of pancreatic islets. Nat Biotechnol. 1997;15: 358–362.

18. Langer RS, Vacanti JP. Tissue Engineering: The Challenges Ahead. Sci Am. 1999;280: 86–89.

19. Andrade JD. Hydrogels for Medical and Related Applications: A Symposium. 1976.

20. Juang JH, Bonner-Weir S, Ogawa Y, Vacanti JP, Weir GC. Outcome of subcutaneous islet transplantation improved by polymer device. Transplantation. 1996;61: 1557–1561.

21. Pileggi A, Damaris Molano R, Ricordi C, Zahr E, Collins J, Valdes R, et al. Reversal of Diabetes by Pancreatic Islet Transplantation into a Subcutaneous, Neovascularized Device. Transplantation. 2006;81: 1318–1324.

22. de Vos P, Hamel AF, Tatarkiewicz K. Considerations for successful transplantation of encapsulated pancreatic islets. Diabetologia. 2002;45: 159–173.

23. Najdahmadi A, Lakey JRT, Botvinick E. Structural Characteristics and Diffusion Coefficient of Alginate Hydrogels Used for Cell Based Drug Delivery. MRS Advances. 2018;3: 2399–2408.

24. Najdahmadi A, Lakey J, Botvinick E. Diffusion coefficient of alginate microcapsules used in pancreatic islet transplantation, a method to cure type 1 diabetes. Nanoscale Imaging, Sensing, and Actuation for Biomedical Applications XV. 2018. doi:10.1117/12.2318565

25. de Vos P, Spasojevic M, Faas MM. Treatment of Diabetes with Encapsulated Islets. Advances in Experimental Medicine and Biology. 2010. pp. 38–53.

26. Sakata N, Aoki T, Yoshimatsu G, Tsuchiya H, Hata T, Katayose Y, et al. Strategy for clinical setting in intramuscular and subcutaneous islet transplantation. Diabetes Metab Res Rev. 2014;30: 1–10.

27. Pepper AR, Pawlick R, Gala-Lopez B, MacGillivary A, Mazzuca DM, White DJG, et al. Diabetes Is Reversed in a Murine Model by Marginal Mass Syngeneic Islet Transplantation Using a Subcutaneous Cell Pouch Device. Transplantation. 2015;99: 2294–2300.

28. Shimizu S, Eguchi Y, Kamiike W, Itoh Y, Hasegawa J, Yamabe K, et al. Induction of apoptosis as well as necrosis by hypoxia and predominant prevention of apoptosis by Bcl-2 and Bcl-XL. Cancer Res. 1996;56: 2161–2166.

29. Ratner BD. A pore way to heal and regenerate: 21st century thinking on biocompatibility. Regenerative Biomaterials. 2016;3: 107–110.

30. Phelps EA, Templeman KL, Thulé PM, García AJ. Engineered VEGF-releasing PEG–MAL hydrogel for pancreatic islet vascularization. Drug Deliv Transl Res. 2013;5: 125–136.

31. Lovett M, Lee K, Edwards A, Kaplan DL. Vascularization strategies for tissue engineering. Tissue Eng Part B Rev. 2009;15: 353–370.

32. Kaplan AV, Baim DS, Smith JJ, Feigal DA, Simons M, Jefferys D, et al. Medical device development: from prototype to regulatory approval. Circulation. 2004;109: 3068–3072.

33. Niimi S. Practice of Regulatory Science (Development of Medical Devices). Yakugaku Zasshi. 2017;137: 431–437.

34. Marks JB. The Forgotten Complication. Clin Diabetes. 2005;23: 3–4.

35. Hanazaki K, Munekage M, Kitagawa H, Yatabe T, Munekage E, Shiga M, et al. Current topics in glycemic control by wearable artificial pancreas or bedside artificial pancreas with closed-loop system. J Artif Organs. 2016;19: 209–218.

36. Bussau VA, Ferreira LD, Jones TW, Fournier PA. A 10-s sprint performed prior to moderate-intensity exercise prevents early post-exercise fall in glycaemia in individuals with type 1 diabetes. Diabetologia. 2007;50: 1815–1818.

37. Billat LV, Véronique Billat L. Use of Blood Lactate Measurements for Prediction of Exercise Performance and for Control of Training. Sports Med. 1996;22: 157–175.

38. Augst AD, Kong HJ, Mooney DJ. Alginate Hydrogels as Biomaterials. Macromol Biosci. 2006;6: 623–633.

39. Najdahmadi A, Zarei-Hanzaki A, Farghadani E. Mechanical properties enhancement in Ti–29Nb–13Ta–4.6Zr alloy via heat treatment with no detrimental effect on its biocompatibility. Mater Des. 2014;54: 786–791.

40. Lutolf MP, Hubbell JA. Synthetic biomaterials as instructive extracellular microenvironments for morphogenesis in tissue engineering. Nat Biotechnol. 2005;23: 47–55.

41. Beris AE, Lykissas MG, Papageorgiou CD, Georgoulis AD. Advances in articular cartilage repair. Injury. 2005;36: S14–S23.

42. Tønnesen HH, Karlsen J. Alginate in Drug Delivery Systems. Drug Dev Ind Pharm. 2002;28: 621–630.

43. Kuo CK, Ma PX. Ionically crosslinked alginate hydrogels as scaffolds for tissue engineering: part 1. Structure, gelation rate and mechanical properties. Biomaterials. 2001;22: 511–521.

44. Mørch YA, Donati I, Strand BL, Skjåk-Braek G. Effect of Ca2+, Ba2+, and Sr2+ on alginate microbeads. Biomacromolecules. 2006;7: 1471–1480.

45. Okay O. General Properties of Hydrogels. Springer Series on Chemical Sensors and Biosensors. 2009. pp. 1–14.

46. Mazué G, Newman AJ, Scampini G, Della Torre P, Hard GC, Iatropoulos MJ, et al. The

Histopathology of Kidney Changes in Rats and Monkeys Following Intravenous Administration of Massive Doses of FCE 26184, Human Basic Fibroblast Growth Factor. Toxicol Pathol. 1993;21: 490–501.

47. Bouhadir KH, Alsberg E, Mooney DJ. Hydrogels for combination delivery of antineoplastic agents. Biomaterials. 2001;22: 2625–2633.

48. Peters MC, Isenberg BC, Rowley JA, Mooney DJ. Release from alginate enhances the biological activity of vascular endothelial growth factor. J Biomater Sci Polym Ed. 1998;9: 1267–1278.

49. Whalen GF, Shing Y, Folkman J. The Fate of Intravenously Administered bFGF and the Effect of Heparin. Growth Factors. 1989;1: 157–164.

50. Zimmermann H, Shirley SG, Zimmermann U. Alginate-based encapsulation of cells: past, present, and future. Curr Diab Rep. 2007;7: 314–320.

51. Grimmer JF, Fredrik Grimmer J, Gunnlaugsson CB, Alsberg E, Murphy HS, Kong HJ, et al. Tracheal Reconstruction Using Tissue-Engineered Cartilage. Archives of Otolaryngology–Head & Neck Surgery. 2004;130: 1191.

52. Calafiore R. Alginate microcapsules for pancreatic islet cell graft immunoprotection: struggle and progress towards the final cure for type 1 diabetes mellitus. Expert Opin Biol Ther. 2003;3: 201–205.

53. de Vos P, Faas MM, Strand B, Calafiore R. Alginate-based microcapsules for immunoisolation of pancreatic islets. Biomaterials. 2006;27: 5603–5617.

54. Kummerfeld G, Krishnan R, Najdahmadi A, Botvinick E, Lakey JRT. Alginate Composition and Temperature Influence Microcapsule Permeability. Royan International Twin Congress 11th Congress on Stem Cell Biology and Technology. 2015. pp. 19–20 Volume 17, Supplement 1.

55. Goosen MF, O'Shea GM, Gharapetian HM, Chou S, Sun AM. Optimization of microencapsulation parameters: Semipermeable microcapsules as a bioartificial pancreas. Biotechnol Bioeng. 1985;27: 146–150.

56. Weidling J, Sameni S, Lakey JRT, Botvinick E. Method measuring oxygen tension and transport within subcutaneous devices. J Biomed Opt. 2014;19: 087006.

57. Najdahmadi A, Gurlin RE, Weidling J, White S, Shergill B, Lakey JRT, Botvinick E. Non invasive study of oxygen tension and vascularization in subcutaneously implanted medical devices. Proc SPIE. 2018;10488: P. 048847.

58. Crank J. The Mathematics of Diffusion. Oxford University Press; 1979.

59. Goosen MF, O'Shea GM, Gharapetian HM, Chou S, Sun AM. Optimization of microencapsulation parameters: Semipermeable microcapsules as a bioartificial pancreas. Biotechnol Bioeng. 1985;27: 146–150.

60. de Vos P, Hoogmoed CG, Busscher HJ. Chemistry and biocompatibility of alginate-PLL capsules for immunoprotection of mammalian cells. J Biomed Mater Res. 2002;60: 252–259.

61. Serp D, Mueller M, Von Stockar U, Marison IW. Low-temperature electron microscopy for the study of polysaccharide ultrastructures in hydrogels. II. Effect of temperature on the structure of Ca2+-alginate beads. Biotechnol Bioeng. 2002;79: 253–259.

62. DiBartola SP. Fluid, Electrolyte, and Acid-Base Disorders in Small Animal Practice. Elsevier Health Sciences; 2011.

63. Dholakia S, Oskrochi Y, Easton G, Papalois V. Advances in pancreas transplantation. J R Soc Med. 2016;109: 141–146.

64. Hering BJ. Achieving and Maintaining Insulin Independence in Human Islet Transplant Recipients. Transplantation. 2005;79: 1296–1297.

65. Froud T, Ricordi C, Baidal DA, Hafiz MM, Ponte G, Cure P, et al. Islet transplantation in type 1 diabetes mellitus using cultured islets and steroid-free immunosuppression: Miami experience. Am J Transplant. 2005;5: 2037–2046.

66. Smink AM, de Haan BJ, Lakey JRT, de Vos P. Polymer scaffolds for pancreatic islet transplantation - Progress and challenges. Am J Transplant. 2018;18: 2113–2119.

67. Shen H-M, Vandenabeele P. Necrotic Cell Death. Springer Science & Business Media; 2014.

68. Kumar S. Apoptosis: Mechanisms and Role in Disease. Springer Science & Business Media; 2013.

69. Pedraza E, Brady A-C, Fraker CA, Molano RD, Sukert S, Berman DM, et al. Macroporous three-dimensional PDMS scaffolds for extrahepatic islet transplantation. Cell Transplant. 2013;22: 1123–1135.

70. Dufour JM, Rajotte RV, Zimmerman M, Rezania A, Kin T, Dixon DE, et al. Development of an ectopic site for islet transplantation, using biodegradable scaffolds. Tissue Eng. 2005;11: 1323–1331.

71. Smink AM, Li S, Hertsig DT, de Haan BJ, Schwab L, van Apeldoorn AA, et al. The Efficacy of a Prevascularized, Retrievable Poly(D,L,-lactide-co-ε-caprolactone) Subcutaneous Scaffold as Transplantation Site for Pancreatic Islets. Transplantation. 2017;101: e112–e119.

72. Abe K, Kimura H. The possible role of hydrogen sulfide as an endogenous neuromodulator. J Neurosci. 1996;16: 1066–1071.

73. Kanagy NL, Szabo C, Papapetropoulos A. Vascular biology of hydrogen sulfide. American Journal of Physiology-Cell Physiology. 2017;312: C537–C549.

74. Cai W-J, Wang M-J, Moore PK, Jin H-M, Yao T, Zhu Y-C. The novel proangiogenic effect of hydrogen sulfide is dependent on Akt phosphorylation. Cardiovasc Res. 2007;76: 29–40.

75. Gurlin RE, Keating MT, Li S, Lakey JR, de Feraudy S, Shergill BS, et al. Vascularization and innervation of slits within polydimethylsiloxane sheets in the subcutaneous space of athymic nude mice. J Tissue Eng. 2017;8: 2041731417691645.

76. Borisov SM, Michela Q, Ingo K. Indicators for optical oxygen sensors. Advances in Chemical Bioanalysis. 2012. pp. 1–70.

77. Luttikhuizen DT, Harmsen MC, Van Luyn MJA. Cellular and molecular dynamics in the foreign body reaction. Tissue Eng. 2006;12: 1955–1970.

78. Wynn TA. Common and unique mechanisms regulate fibrosis in various fibroproliferative diseases. J Clin Invest. 2007;117: 524–529.

79. Morais JM, Papadimitrakopoulos F, Burgess DJ. Biomaterials/tissue interactions: possible solutions to overcome foreign body response. AAPS J. 2010;12: 188–196.

80. Campos PP, Andrade SP, Moro L, Ferreira MAND, Vasconcelos AC. Cellular proliferation, differentiation and apoptosis in polyether-polyurethane sponge implant model in mice. Histol Histopathol. 2006;21: 1263–1270.

81. Mendes JB, Rocha MA, Araújo FA, Moura SAL, Ferreira MAND, Andrade SP. Differential effects of rolipram on chronic subcutaneous inflammatory angiogenesis and on peritoneal adhesion in mice. Microvasc Res. 2009;78: 265–271.

82. Anderson JM, Rodriguez A, Chang DT. Foreign body reaction to biomaterials. Semin Immunol. 2008;20: 86–100.

83. Michiels C. Physiological and Pathological Responses to Hypoxia. Am J Pathol. 2004;164: 1875–1882.

84. Xiao X, Wang W, Liu D, Zhang H, Gao P, Geng L, et al. The promotion of angiogenesis induced by three-dimensional porous beta-tricalcium phosphate scaffold with different interconnection sizes via activation of PI3K/Akt pathways. Sci Rep. 2015;5: 9409.

85. Laschke MW, Strohe A, Scheuer C, Eglin D, Verrier S, Alini M, et al. In vivo biocompatibility and vascularization of biodegradable porous polyurethane scaffolds for tissue engineering. Acta Biomater. 2009;5: 1991–2001.

86. Druecke D, Langer S, Lamme E, Pieper J, Ugarkovic M, Steinau HU, et al. Neovascularization of poly(ether ester) block-copolymer scaffolds in vivo: long-term investigations using intravital fluorescent microscopy. J Biomed Mater Res A. 2004;68: 10–18.

87. Mastrogiacomo M, Scaglione S, Martinetti R, Dolcini L, Beltrame F, Cancedda R, et al. Role of scaffold internal structure on in vivo bone formation in macroporous calcium phosphate bioceramics. Biomaterials. 2006;27: 3230–3237.

88. Smink AM, Hertsig DT, Schwab L, van Apeldoorn AA, de Koning E, Faas MM, et al. A Retrievable, Efficacious Polymeric Scaffold for Subcutaneous Transplantation of Rat Pancreatic Islets. Ann Surg. 2017;266: 149–157.

89. Dufton N, Natividad J, Verdu EF, Wallace JL. Hydrogen sulfide and resolution of acute inflammation: A comparative study utilizing a novel fluorescent probe. Sci Rep. 2012;2: 499.

90. Turner APF. BIOCHEMISTRY: Biosensors-Sense and Sensitivity. Science. 2000;290: 1315–1317.

91. Clark LC Jr, Lyons C. Electrode systems for continuous monitoring in cardiovascular surgery. Ann N Y Acad Sci. 1962;102: 29–45.

92. Updike SJ, Hicks GP. The Enzyme Electrode. Nature. 1967;214: 986–988.

93. Chambers JP, Arulanandam BP, Matta LL, Weis A, Valdes JJ. Biosensor recognition elements. Curr Issues Mol Biol. 2008;10: 1–12.

94. Iqbal SS, Mayo MW, Bruno JG, Bronk BV, Batt CA, Chambers JP. A review of molecular recognition technologies for detection of biological threat agents. Biosens Bioelectron. 2000;15: 549–578.

95. Deiss D, Bolinder J, -P. Riveline J, Battelino T, Bosi E, Tubiana-Rufi N, et al. Improved Glycemic Control in Poorly Controlled Patients with Type 1 Diabetes Using Real-Time Continuous Glucose Monitoring. Diabetes Care. 2006;29: 2730–2732.

96. Breton M, Farret A, Bruttomesso D, Anderson S, Magni L, Patek S, et al. Fully Integrated Artificial Pancreas in Type 1 Diabetes: Modular Closed-Loop Glucose Control Maintains Near Normoglycemia. Diabetes. 2012;61: 2230–2237.

97. Coggan AR, Raguso CA, Gastaldelli A, Williams BD, Wolfe RR. Regulation of glucose production during exercise at 80% of VO2peak in untrained humans. American Journal of Physiology-Endocrinology and Metabolism. 1997;273: E348–E354.

98. Robertson K, Adolfsson P, Scheiner G, Hanas R, Riddell MC. Exercise in children and adolescents with diabetes. Pediatr Diabetes. 2009;10: 154–168.

99. Wasserman DH, Cherrington AD. Hepatic fuel metabolism during muscular work: role and regulation. American Journal of Physiology-Endocrinology and Metabolism. 1991;260: E811–E824.

100. Felig P, Cherif A, Minagawa A, Wahren J. Hypoglycemia during prolonged exercise in normal men. N Engl J Med. 1982;306: 895–900.

101. Galassetti P, Riddell MC. Exercise and Type 1 Diabetes (T1DM). Comprehensive Physiology. 2013.

102. Weijers R. Membrane Flexibility and Exercise: A Guide to Type 2 Diabetes Mellitus. J

Diabetes Metab. 2013;01. doi:10.4172/2155-6156.s10-003

103. Sigal RJ, Fisher S, Halter JB, Vranic M, Marliss EB. The roles of catecholamines in glucoregulation in intense exercise as defined by the islet cell clamp technique. Diabetes. 1996;45: 148–156.

104. Wasserman K, Whipp BJ, Koyl SN, Beaver WL. Anaerobic threshold and respiratory gas exchange during exercise. J Appl Physiol. 1973;35: 236–243.

105. Brazeau A-S, Rabasa-Lhoret R, Strychar I, Mircescu H. Barriers to physical activity among patients with type 1 diabetes. Diabetes Care. 2008;31: 2108–2109.

106. Borghouts LB, Keizer HA. Exercise and insulin sensitivity: a review. Int J Sports Med. 2000;21: 1–12.

107. Pyöräla K. Relationship of glucose tolerance and plasma insulin to the incidence of coronary heart disease: results from two population studies in Finland. Diabetes Care. 1979;2: 131–141.

108. Fagard RH. Exercise characteristics and the blood pressure response to dynamic physical training. Med Sci Sports Exerc. 2001;33: S484–92; discussion S493–4.

109. Riddell MC, Zaharieva DP, Yavelberg L, Cinar A, Jamnik VK. Exercise and the Development of the Artificial Pancreas: One of the More Difficult Series of Hurdles. J Diabetes Sci Technol. 2015;9: 1217–1226.

110. Ostrowski K, Schjerling P, Pedersen BK. Physical activity and plasma interleukin-6 in humans--effect of intensity of exercise. Eur J Appl Physiol. 2000;83: 512–515.

111. Jacobs I. Blood Lactate. Sports Med. 1986;3: 10–25.

112. Marcinek DJ, Kushmerick MJ, Conley KE. Lactic acidosis in vivo: testing the link between lactate generation and H accumulation in ischemic mouse muscle. J Appl Physiol. 2010;108: 1479–1486.

113. Relation Between Plasma Lactate Concentration and Fat Oxidation Rates Over a Wide Range of Exercise Intensities. Int J Sports Med. 2004;25: 32–37.

114. Martinowitz U, Michaelson M, THE ISRAELI MULTIDISCIPLINARY rFVIIa TASK FORCE. Guidelines for the use of recombinant activated factor VII (rFVIIa) in uncontrolled bleeding: a report by the Israeli Multidisciplinary rFVIIa Task Force. J Thromb Haemost. 2005;3: 640–648.

115. Bakker J, Gris P, Coffernils M, Kahn RJ, Vincent JL. Serial blood lactate levels can predict the development of multiple organ failure following septic shock. Am J Surg. 1996;171: 221–226.

116. Vitek V, Cowley RA. Blood Lactate in the Prognosis of Various Forms of Shock. Ann Surg. 1971;173: 308–313.

117. Weil MH, Afifi AA. Experimental and Clinical Studies on Lactate and Pyruvate as Indicators of the Severity of Acute Circulatory Failure (Shock). Circulation. 1970;41: 989–1001.

118. Wong CM, Wong KH, Chen XD. Glucose oxidase: natural occurrence, function, properties and industrial applications. Appl Microbiol Biotechnol. 2008;78: 927–938.

119. Rathee K, Dhull V, Dhull R, Singh S. Biosensors based on electrochemical lactate detection: A comprehensive review. Biochem Biophys Rep. 2016;5: 35–54.

120. Botvinick E, Weidling J, White S. Continuous analyte sensor. US Patent. 20170238856A1.

121. Brenner M, Azer SM, Oh K-J, Han CH, Lee J, Mahon SB, et al. Oral Glycine and Sodium Thiosulfate for Lethal Cyanide Ingestion. J Clin Toxicol. 2017;7. doi:10.4172/2167-7972.1000355

122. Tarhan L. Use of immobilised catalase to remove H2O2 used in the sterilisation of milk. Process Biochem. 1995;30: 623–628.

123. Kulkarni T, Slaughter G. Self-powered glucose biosensor operating under physiological conditions. 2016 IEEE SENSORS. 2016. doi:10.1109/icsens.2016.7808798

124. Mathers CD, Loncar D. Projections of global mortality and burden of disease from 2002 to 2030. PLoS Med. 2006;3: e442.